



University of
Massachusetts
Amherst

PROTEIN-NANOPARTICLE CO-ENGINEERING: SELF-ASSEMBLY, INTRACELLULAR PROTEIN DELIVERY, AND CRISPR/CAS9-BASED GENE EDITING

Item Type	Dissertation (Open Access)
Authors	Mout, Rubul
DOI	10.7275/10275569.0
Download date	2026-05-17 03:10:42
Link to Item	https://hdl.handle.net/20.500.14394/17296

PROTEIN-NANOPARTICLE CO-ENGINEERING: SELF-
ASSEMBLY, INTRACELLULAR PROTEIN DELIVERY, AND
CRISPR/CAS9-BASED GENE EDITING

A Dissertation Presented

By

RUBUL MOUT

Submitted to the Graduate School of the
University of Massachusetts Amherst in partial fulfillment
of the requirements for the degree of

DOCTOR OF PHILOSOPHY

September 2017

Chemistry

© Copyright by Rubul Mout 2017
All Right Reserved

PROTEIN-NANOPARTICLE CO-ENGINEERING: SELF-
ASSEMBLY, INTRACELLULAR PROTEIN DELIVERY, AND
CRISPR/CAS9-BASED GENE EDITING

A Dissertation Presented

By

RUBUL MOUT

Approved as to style and content by:

Vincent M. Rotello, Chair

Min Chen, Member

Michael J. Maroney, Member

Scott C. Garman, Member

Richard W. Vachet, Head
Department of Chemistry

DEDICATION

To my father who dreamed for this day, but could not see.

ACKNOWLEDGEMENTS

My sincerest gratitude is towards my research advisor, Prof. Vincent M Rotello, for his constant guidance, and allowing me to pursue a career in science in his laboratory. He not only guided me in the right direction, but also allowed me to explore research in new fields. Throughout my PhD, I learned a great deal in critical thinking and writing from him. I will be always indebted to him for his efforts and guidance to improve my scientific writing skills. I am very fortunate that I had a chance to work with him.

I am deeply grateful to my thesis committee members Prof. Michael J. Maroney, Prof. Min Chen, and Prof. Scott C. Garman for their invaluable suggestions during my PhD period. I would also like to take this opportunity to thank Prof. Joseph D. Jerry who always helped me for any scientific suggestions whenever I needed. I thank Dr. James Chambers, whose assistance in microscopy greatly helped my research.

My PhD work is the result of many collaborative efforts within the group, and outside. It would have been unrealistic for me to write this thesis without the valuable contribution from my collaborators. I thank all of my coworkers, especially, Gulen, Moumita, Bill, Tristan, Kanae, and Dave.

I am very fortunate to have wonderful friends and their support during my PhD. I am thankful to all past and present members of the Rotello group. Additionally, administrative and technical support from—Carol, Deirdre, JMS, Carrie, Bob (Sabola), Chris, Kay—have been so kind and generous to me. I am especially indebted to all the funding sources that allowed me to perform my research.

Finally, I am greatly thankful to my family members whose constant sacrifices made my dreams come true. My parents and siblings lifted me high so that I could fly, even

in the days of deepest trouble. Without their contributions, I would not have stood here today. I am also thankful to my in-laws and everyone back in *Assam* who contributed in my journey. And at last, though no words are enough to explain, I thank my wife, Alee—for her love, sacrifice, and taking care of me and our son. And to my son, Advik: you will always encourage me to go to a greater height!

Thank you all.

ABSTRACT

PROTEIN-NANOPARTICLE CO-ENGINEERING: SELF-ASSEMBLY, INTRACELLULAR PROTEIN DELIVERY, AND CRISPR/CAS9-BASED GENE EDITING

SEPTEMBER 2017

RUBUL MOUT

B.Sc., TINSUKIA COLLEGE, DIBRUGARH UNIVERSITY

M.Sc., GAUHATI UNIVERSITY

Ph.D., UNIVERSITY OF MASSACHUSETTS AMHERST

Directed by: Professor Vincent M. Rotello

Direct cytoplasmic delivery of gene editing nucleases such CRISPR/Cas9 systems and therapeutic proteins provides enormous opportunities in curing human genetic diseases, and assist research in basic cell biology. One approach to attain such a goal is through engineering nanotechnological tools to mimic naturally existing intra- and extracellular protein delivery/transport systems. Nature builds transport systems for proteins and other biomolecules through evolution-derived sophisticated molecular engineering. Inspired by such natural assemblies, I employed molecular engineering approaches to fabricate self-assembled nanostructures to use as intracellular protein delivery tools. Briefly, proteins and gold nanoparticles were co-engineered to carry complementary electrostatic recognition elements. When these materials were mixed together, they formed highly sophisticated, multi-layered, and hierarchical self-assembled nanostructures of few hundred-nanometer size. These structures carried a large number of

engineered proteins, got fused to cell membrane upon incubation, and delivered the encapsulated protein content directly into cell cytoplasm. Using this technology, we delivered a wide range of proteins, and CRISPR/Cas9-ribonucleoprotein that resulted high efficient gene editing.

TABLE OF CONTENTS

	Page
ACKNOWLEDGEMENTS.....	v
ABSTRACT.....	vii
LIST OF TABLES.....	xi
LIST OF FIGURES.....	xii
CHAPTER	
1. NANOTECHNOLOGY FOR THERAPEUTIC PROTEIN AND CRISPR/CAS9 DELIVERY.....	1
1.1. Protein therapeutics and challenges in intracellular protein delivery.....	1
1.2. CRISPR/Cas9 delivery for therapeutic gene editing.....	3
1.3. Current CRISPR/Cas9 delivery strategies.....	6
1.3.1. Viral delivery of CRISPR/Cas9.....	6
1.3.2. Non-viral delivery of CRISPR/Cas9.....	7
1.4. Challenges in CRISPR/Cas9 delivery.....	8
1.4.1. Packaging challenges.....	8
1.4.2. Targeted delivery.....	9
1.4.3. Delivery and editing efficiency.....	9
1.4.4. Off-target effect.....	9
1.4.5. Immunogenicity.....	9
1.4.6. Insertional mutagenesis.....	10
1.5. Self-assembled nanostructures for intracellular protein delivery.....	10
1.5.1. Self-assemblies.....	10
1.5.2. Gold nanoparticles.....	11
1.5.3. Self-assembled protein-nanoparticle structures.....	12
1.5.4. Protein-nanoparticle co-engineering for fabricating self-assemblies.....	12
1.6. Dissertation overview.....	13
1.7. References.....	17
2. ENVIRONMENTALLY RESPONSIVE HISTIDINE-CARBOXYLATE ZIPPER FORMATION BETWEEN PROTEINS AND NANOPARTICLES.....	23
2.1. Introduction.....	23
2.2. Results.....	25
2.3. Conclusions.....	31

2.4. Experimental section.....	31
2.5. Supporting figures.....	34
2.6. References.....	35
3. PROGRAMMED SELF-ASSEMBLY OF HIERARCHICAL NANOSTRUCTURES THROUGH PROTEIN-NANOPARTICLE CO-ENGINEERING	38
3.1. Introduction.....	38
3.2. Results.....	40
3.3. Conclusions.....	47
3.4. Discussions	47
3.5. Experimental section.....	51
3.6. Supporting figures.....	55
3.7. References.....	62
4. A GENERAL STRATEGY FOR DIRECT CYTOPLASMIC PROTEIN DELIVERY VIA PROTEIN-NANOPARTICLE COENGINEERING	66
4.1. Introduction.....	66
4.2. Results.....	67
4.3. Conclusions.....	74
4.4. Experimental section.....	75
4.5. Supporting figures.....	78
4.6. References.....	85
5. DIRECT CYTOSOLIC DELIVERY OF CRISPR/CAS9-RIBONUCLEOPROTEIN FOR EFFICIENT GENE EDITING	88
5.1. Introduction.....	88
5.2. Results.....	89
5.3. Conclusions.....	97
5.4. Experimental section.....	97
5.5. Supporting figures.....	103
5.6. References.....	110
BIBLIOGRAPHY	113

LIST OF TABLES

Table	Page
1.1. Comparison, and pros/cons of CRISPR/Cas9 delivery in different formats.....	6

LIST OF FIGURES

Figure	Page
1. 1. Protein therapeutics.....	2
1. 2. CRISPR delivery strategies.....	5
1. 3. Structure of gold nanoparticles (AuNPs) used in this thesis work	12
1. 4. Thesis overview	15
2. 1. Zipper formation between AuNP-COOH and N-terminus oligohistidine-tagged GFPs through carboxylate-histidine interaction.....	24
2. 2. The interaction of AuNP-COOH with His-tagged GFP variants.....	26
2. 3. Responsiveness of the carboxylate-histidine zipper towards pH and salt concentration.....	29
2. 4. Reversible carboxylate-histidine zipper formation.....	30
2. 5. Characterization of AuNP-COOH	34
3. 1. Hierarchical organization of engineered proteins and nanoparticles into complex superstructures.. ..	39
3. 2. Superstructure evolution triggered by environmental ionic strength.....	44
3. 3. Dynamic reorganization of the superstructure components.....	46
3. 4. Schemes for the synthesis of ArgNPs	56
3. 5. Characterization of ArgNPs and GFP-E10:ArgNP assemblies.	57
3. 6. Titration of GFP-En with ArgNPs	58
3. 7. ‘Precursor’ based growth dynamics (evolution) of superstructures	59
3. 8. Small angle X-ray scattering (SAXS) investigation of superstructure formation	60
3. 9. Superstructure formation by different E-tagged proteins	61
3. 10. 3D visualization of the GFP-E10:ArgNPs superstructures.....	61

4. 1. Co-engineering of E-tagged proteins and nanoparticles for direct cytoplasmic protein delivery	67
4. 2. Nanoassembly mediated cytoplasmic delivery of E-tagged GFP.....	68
4. 3. A fusion-like mechanism for nanoassembly-mediated direct cytosolic protein delivery	70
4. 4. Direct cytoplasmic delivery of multiple E-tagged proteins	71
4. 5. Nanoassembly-mediated Cre-E10 delivery results efficient gene recombination ...	72
4. 6. Nanoassembly-mediated delivery of functional Granzyme A-E10 (GzmA-E10) effectively killed HeLa cells	74
4. 7. Characterization of nanoassemblies.....	78
4. 8. E-tag length determines GFP-En delivery efficiency	79
4. 9. [ArgNP]/[GFP-E10] ratio determines delivery efficiency.....	79
4. 10. Confocal microscopy Z-stacking images showing thorough cytosolic/nuclear delivery of GFP-E10.....	80
4. 11. Comparison of protein delivery using various delivery strategies.....	81
4. 12. 3D reconstruction of cells from z-stacking confocal images showing GFP-E10 delivery into the whole cell in different cell lines	82
4. 13. A membrane fusion like mechanism is involved in protein delivery..	83
4. 14. Membrane fusion, but not membrane puncture is involved in nanoassembly-mediated protein delivery.	83
4. 15. Delivered GzmA-E10 kills cells in a caspase 3/7 independent manner	84
5. 1. Rational engineering of Cas9 protein and arginine nanoparticles (ArgNPs) for intracellular delivery of Cas9 protein or Cas9-RNP via membrane fusion	90
5. 2. Nanoassembly formation between ArgNPs and Cas9En or Cas9En-RNP	91
5. 3. Endosomal entrapment-free direct cytoplasmic/nuclear delivery of engineered Cas9En or Cas9En-RNP is dictated by E-tag length	94
5. 4. A cholesterol dependent membrane fusion-like delivery mechanism	95

5. 5. Efficient gene editing resulted from Cas9En-RNP delivery.....	96
5. 6. TEM and DLS characterization of nanoparticles, Cas9 and sgRNA.....	103
5. 7. E-tag length determines cytoplasmic/nuclear delivery of Cas9En	104
5. 8. Confocal z-stacking images of delivered FITC labelled Cas9E20 revealing cytoplasmic/nuclear distribution of delivered Cas9	105
5. 9. Lifetime of delivered Cas9En	106
5. 10. Cas9En protein alone get trapped in the endosomes	107
5. 11. Delivery of Cas9E20 into cultured cells	108
5. 12. Time-lapse video imaging of Cas9E20 delivery process.....	108
5. 13. Gene editing in HEK-293T and Raw 264.7 cells	109

CHAPTER 1

NANOTECHNOLOGY FOR THERAPEUTIC PROTEIN AND CRISPR/CAS9 DELIVERY

1.1. Protein therapeutics and challenges in intracellular protein delivery

There are approximately 10,000 human diseases of which only 500 have any cure, according to an information provided by National Institute of Health (NIH).¹ In the past century and so, small molecule therapeutics have revolutionized human medicine curing many major diseases.² Most of the small molecule therapeutics target endogenous proteins, resulting in perturbation or activation of protein functions.³ However, as indicated by NIH information, we are still far away from the complete curing of human diseases.

In 1922, at the beginning of twentieth century protein was directly used as therapeutics for the first time. A Canadian surgeon, Dr. Frederick Banting, and his associates isolated insulin from cows and injected into human patients to cure hitherto incurable Diabetes.⁴ It was the beginning of a new class of therapeutics, named ‘biological therapeutics’ or ‘biologics’ or ‘biopharmaceuticals’.⁵ The idea was to use biological large molecules such as proteins, DNA, and RNA directly to cure various diseases. Although promising, this class of therapeutics had very limited success in the last 95 years. Despite a tremendous effort to use biologics to cure human diseases, only 246 such therapeutics have been approved worldwide till 2014.⁵ Among these, most of the protein therapeutics function in blood or extracellularly in tissues. For example, while insulin, monoclonal antibodies, and growth hormones bind to cell surface receptor for their therapeutic effect, blood factors, anticoagulants and thrombolytics function in the blood. Only a small number

of these protein therapies (10 out of 246) work as intracellular therapy (Figure 1.1). Interestingly, all these 10 intracellular protein therapies are used as enzyme replacement therapy for lysosomal disorders. No approved protein therapies have crossed endo/lysosomal barrier so far to reach other intracellular organelles.

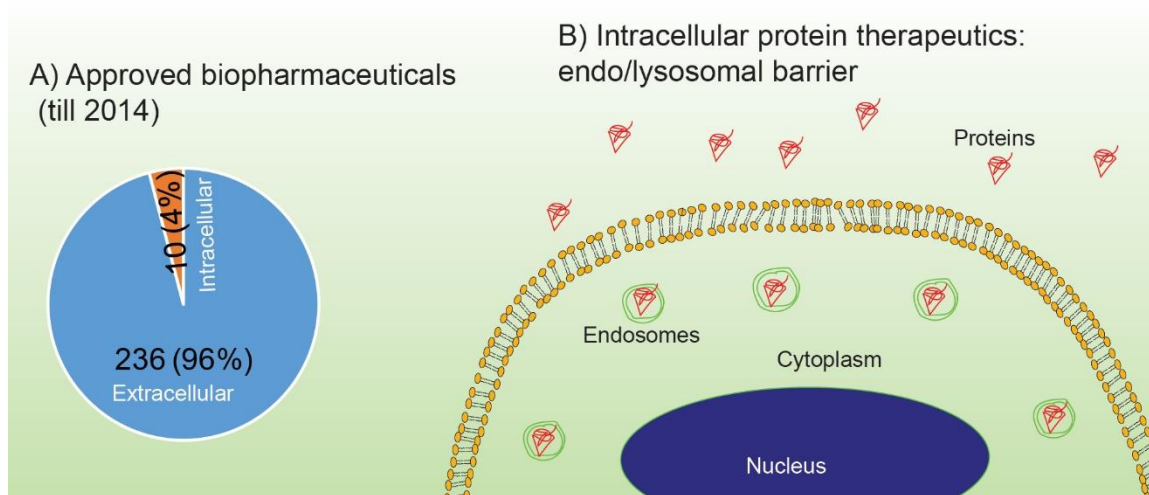


Figure 1. 1. Protein therapeutics. A) Out of 246 biopharmaceuticals approved so far, only 10 (4%) work intracellularly. B) Delivered protein therapeutics get trapped in the endosomes, and thus no protein therapeutics have been approved so far that have the capability to cross the endo/lysosomal barrier.

Designing vehicles to deliver therapeutic proteins that can escape the endo/lysosomal barrier have been a long-standing goal in biomedical research.⁶ A search in 'Pubmed' or 'Scifinder' with a key phrase 'intracellular protein delivery' shows 6,000-11,000 published research articles, indicating an enormous number of ongoing research activities towards designing better intracellular protein delivery methods. Despite such efforts, majority of these delivery strategies suffer from endosomal entrapment of cargos that ultimately undergo degradation.⁷ Only a small fraction of the entrapped protein cargo (~1%) escape from the endosomes, making these strategies highly inefficient.⁸

There have been three broad categories of intracellular protein delivery strategies: a carrier based delivery method, covalent modification of cargo proteins, and mechanical

methods.⁶ Carrier based protein delivery methods employ various nanocarriers such as polymers, lipid and inorganic nanoparticles to transport proteins across cell membranes.⁹ Protein cargos can also be covalently modified with different cell penetrating peptides and proteins providing a carrier-free delivery approach.¹⁰ However, both of these strategies suffer from endosomal entrapment of cargos, a major drawback that hinders the ultimate use of these approaches for therapeutic intracellular protein delivery.⁹ Mechanical distortion methods such as electroporation¹¹ and microneedle injection¹² can achieve efficient cytoplasmic protein delivery, however these techniques are disruptive and less practical for *in vivo* therapeutic applications.⁷

Recently, our laboratory engineered a nanocarrier system to deliver proteins directly into cell cytoplasm, thus avoiding cellular endocytosis.¹³⁻¹⁵ In our system, arginine functionalized gold nanoparticles and native proteins self-assembled on the surface of oil droplets to form Nanoparticle-stabilized capsules (NPSCs).¹⁶ These NPSCs provided a strategy for high efficient direct cytoplasmic protein delivery, however, limited to proteins that have native pI values below 7.0.¹⁷ Therefore, a general strategy that can deliver any protein directly in to cell cytosol, and avoiding endosomal entrapment, is in great demand for protein therapeutics.

1.2. CRISPR/Cas9 delivery for therapeutic gene editing

Off 10,000 human diseases reported by NIH, many thousand diseases are caused by genetic alterations in the human genome.¹ Therefore, a more practical approach to cure these diseases is by fixing the altered gene itself, rather than delivering a functional protein to replace the abnormal protein. Recently invented gene editing technology CRISPR/Cas9

systems (Clustered Regularly Interspaced Short Palindromic Repeat) to manipulate mammalian genomes presents enormous opportunities for curing human diseases.¹⁸⁻²⁰ CRISPR technology enables correcting such genetic alterations, making a large number of these diseases therapeutic targets.

Bacterial CRISPR/Cas9 system is composed of two elements: a nuclease protein Cas9 that cuts double-stranded DNA, and a guide RNA molecule (sgRNA) that guides the Cas9 protein to a specific DNA sequence (Figure 1.2).²¹⁻²⁵ This system (Cas9 protein and the sgRNA, together called CRISPR/Cas9) has been harnessed in mammalian cells to specifically cut target genes, followed by repairing of the target gene *via* host cell repair machinery. The repair can occur through two main mechanisms.²⁶ (1) Non-Homologous End Joining (NHEJ): this mechanism allows the cell to randomly insert or delete nucleotides at the CRISPR-mediated double-stranded DNA break site, resulting in gene coding sequence disruption. (2) Homology-Directed Repair (HDR): this mechanism provides insertion of a template DNA to correct mutations at the DNA break site.

For therapeutic use the CRISPR components need to be delivered into mammalian cells to enable gene modification in the host cell. Once delivered, the CRISPR/Cas9 system can manipulate host cell genome in numerous ways. Depending on the desired genetic manipulation, various components of CRISPR/Cas9 are delivered: (a) a minimal Cas9/sgRNA pair for gene disruption/mutation, (b) Cas9/sgRNA, and a 'spare' template DNA for gene correction, (c) Cas9/sgRNA, and a desired gene for gene insertion, and (d) Cas9 and two sgRNAs for the complete deletion of a gene (or a portion of a gene) (Figure 1.2). In its simplest implementation Cas9/sgRNA pair is sufficient for gene disruption (*i.e.*

knockout), however, the delivery of an additional piece of DNA is required for advanced functions such as gene repair or insertion (knock-in).

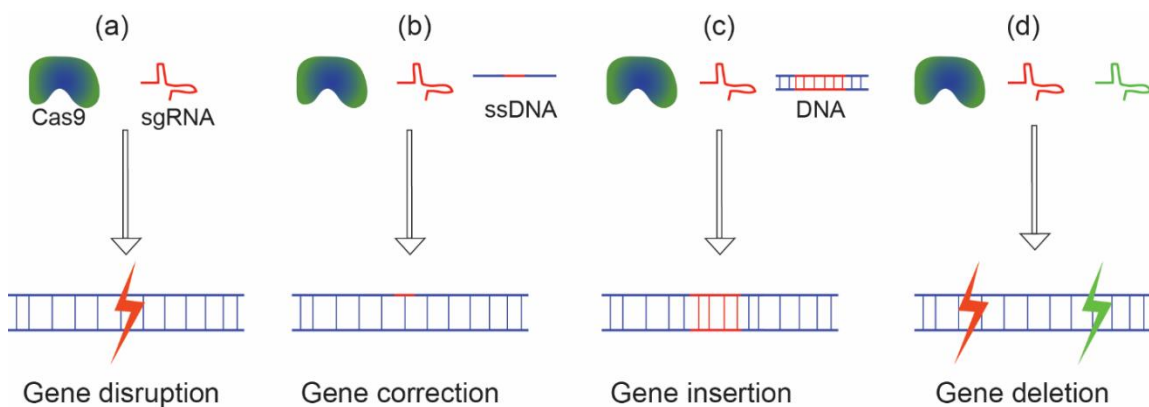


Figure 1. 2. CRISPR delivery strategies. Multiple components of CRISPR/Cas9 system are delivered into cells to achieve a specific function. (a) Cas9 and sgRNA for gene disruption (knock-out), (b) Cas9, sgRNA, and a template ssDNA for mutation correction, (c) Cas9, sgRNA, and a template DNA for gene insertion (knock-in), and (d) Cas9 and two sgRNAs for gene deletion.²⁷

In addition, the CRISPR/Cas9 components can be delivered into cells in different formats: plasmids or viral vectors that carrying Cas9 and sgRNA genes in gene-based delivery; Cas9 mRNA and a synthetic sgRNA in RNA-based delivery; Cas9 protein and a synthetic sgRNA in protein-based delivery (Table 1.1).²⁸ Thus far, Cas9 protein delivery has many advantages over gene or RNA delivery methods. Protein delivery is transient and therefore is less immunogenic. Moreover, unlike gene delivery, protein delivery does not have the issue of permanently integrating CRISPR genes into the host genome (Table 1.1). Although a number of CRISPR delivery platform has been designed so far, the effective delivery of multiple CRISPR components *in vivo* into host cells still remains a major challenge.

Table 1.1. Comparison, and pros/cons of CRISPR/Cas9 delivery in different formats. Compared to other format of delivery, Cas9-RNP delivery has the most advantage as it offers no insertional mutagenesis, high editing efficiency, low off-target, and low immunogenicity.²⁷

Cas9 delivery in different formats				
	Viral	Plasmid	RNA	Protein
Insertional mutagenesis	High	Moderate	No	No
Editing efficiency	High	Moderate	Moderate	High
Off-target	High	Moderate	Moderate	Low
Immunogenicity	High	Moderate	Moderate	Low

1.3. Current CRISPR/Cas9 delivery strategies

A wide variety of intracellular delivery vehicles for CRISPR/Cas9 has been designed so far, intending to deliver CRISPR components in all formats described above. Broadly, the delivery vehicles can be classified into viral and non-viral.²⁸ Non-viral vehicles can be further classified into synthetic and mechanical methods. Viral delivery methods are usually restricted to CRISPR gene delivery, whereas non-viral methods can deliver CRISPR in the form of plasmid DNA, Cas9 mRNA or Cas9 protein along with *in vitro* transcribed sgRNA.²⁷

1.3.1. Viral delivery of CRISPR/Cas9. Both lentiviral as well as adenoviral vectors have been widely used for CRISPR/Cas9 gene delivery.²⁸ Lentiviral vectors provide a non-specific high efficient integration of delivered gene into host genome and therefore is suitable for *in vitro* research. Adeno-associated viruses (AAV) provide controlled integration of delivered CRISPR genes into AAVS1 locus in mammalian cell systems, both

in dividing and non-dividing cells, and therefore this method is more appropriate for *in vivo* delivery that avoids toxicity arising from random integration.²⁹⁻³² Additionally, AAV is the most widely used among the viral vectors due to its non-immunogenicity and its specificity towards a vast range of serotypes.³³ Recently, many studies have used this vector to deliver CRISPR elements into mice to correct mutated dystrophin gene in Duchenne muscular dystrophy (*Dmd*) disease.^{34,35} However, one major drawback of AAV vector is that this vector can package genes only up to the size of ~4.7 kbp.⁴³ Therefore, Cas9 gene and sgRNA were delivered separately using two different AAV-vectors in these studies, as the size of Cas9 gene itself is 4.3 kbp. To overcome the problem of packaging limit, smaller CRISPR/Cas systems were discovered (SaCas9) that allowed the packaging both the SaCas9 gene and the sgRNA into a single AAV vector.³⁶

1.3.2. Non-viral delivery of CRISPR/Cas9. Non-viral synthetic delivery strategies are used for all formats of CRISPR delivery. Cas9 protein alongside sgRNA delivery (Cas9-ribonucleoprotein or Cas9-RNP) is the most attractive format for non-viral delivery due to the low-risk associated with this format.²⁷ In *in vitro* systems, various methods of delivering Cas9-RNP include—lipid nanoparticles,³⁷ cell penetrating peptide based delivery,³⁸ electroporation,^{39,40} and mechanical deformation⁴¹—which resulted efficient gene editing. The delivery efficiency for these methods, however, has not been reported. In *in vivo* systems, only a few Cas9-RNP delivery methods are reported so far. Lipid-mediated (RNAiMAX) delivery of Cas9-RNP in mouse inner ear has demonstrated efficient genome modification at the injection site.³⁷ Other studies of *in vivo* Cas9-RNP delivery include the use of DNA nanoclews (yarn-like DNA nanoparticles) and engineered Cas9 protein with multiple cell penetrating peptides.⁴²

1.4. Challenges in CRISPR/Cas9 delivery

While a few delivery systems have achieved some level of therapeutic gene editing, efficient editing remains a challenge. Different challenges associated with efficient therapeutic gene editing are discussed below.

1.4.1. Packaging challenges. Packaging of CRISPR components into a single vector is a major challenge for therapeutic applications. As stated above, multiple components of CRISPR system are required to utilize the system. The packaging challenge is present in all the formats of delivery strategy *i.e.* gene, RNA, or protein-based delivery. For gene-based delivery through AAV, the size limit of a cargo gene is ~4.7-kilo base pair (kbp).⁴³⁻⁴⁵ However, the size of SpCas9 gene alone is ~4.3 kbp. Thus, inserting additional CRISPR components such as sgRNA, spare oligonucleotide or extra genes is challenging for single AAV vector-based CRISPR gene delivery.⁴⁵ To overcome this problem, splitting Cas9 into two AAV vectors,⁴⁶ or a smaller sized Cas9 has been demonstrated (SaCas9),⁴⁷ however, their versatility for genome engineering applications remains to be investigated.

Although most attractive, protein-based CRISPR delivery poses other challenges: while SpCas9 protein is a large protein (160 kDa, ~7.5 nm hydrodynamic diameter) with a net positive surface charge, sgRNA (~31 kDa, 5.5 nm hydrodynamic diameter) is negatively charged (~100 PO₃⁻ groups).⁴⁸ Thus, packaging these elements through supramolecular chemistry may be a major limitation for designing delivery vehicles. Moreover, incorporation of additional spare DNA (of size in kbp) for multiple applications may further complicate the vector design.

1.4.2. Targeted delivery. Viral vectors can be used for targeted CRISPR/Cas9 delivery, as these vectors provide tissue tropism.⁴⁹ However, non-viral delivery of CRISPR components will require targeting moieties such as peptides or antibodies.⁵⁰ This targeting is particularly difficult to achieve, as incorporation of additional biomolecules to a delivery vector alongside the CRISPR components complicates the packaging.

1.4.3. Delivery and editing efficiency. CRISPR/Cas9 editing efficiency is determined by the delivery efficiency of the system. Low editing efficiency may be enough for alleviating certain diseases (e.g. muscular dystrophy, liver tyrosinemia), however, other diseases such as cancer may require as high as 100% editing efficiency. Unfortunately, in majority of the recently published CRISPR/Cas9 delivery research papers they did not mention the delivery efficiency.

1.4.4. Off-target effect. One of the major limitations of CRISPR-based genome editing is its off-target effect.^{51,52} Even though the sgRNA is designed to target a specific gene of interest, often a significant number of non-specific genes are targeted by the same Cas9/sgRNA. In gene-based CRISPR delivery, the long-term constitutive expression of Cas9/sgRNA further makes the problem worse: repeated exposure of Cas9/sgRNA to non-specific genes can lead to large off-target effects. Different methods have been designed to reduce off-target effect including engineering high specificity Cas9 protein.^{53,54} Protein-based CRISPR delivery, on the other hand, offers transient exposure of the host genome to the Cas9/sgRNA, that may result in reduced off-targeting events.³⁸

1.4.5. Immunogenicity. Since Cas9 or other CRISPR-based genome editing proteins are derived from bacteria, these systems are expected to elicit host immune response. Specially, gene-based delivery of CRISPR elements can permanently integrate Cas9 gene

into host cells. The constitutive expression of foreign Cas9 protein in the host cell will engage the MHC class I immune response which may result in the elimination of Cas9 expressing cells in the host.⁵⁵ Indeed, a recent study showed that AAV-based CRISPR delivery *in vivo* elicits a strong immune response against Cas9 protein but not against the vector itself.⁴⁶ On the other hand, protein based CRISPR delivery system may offer minimal potential immunogenicity as delivered Cas9 protein will transiently present in the host cell (Table 1.1).

1.4.6. Insertional mutagenesis. Many viral vectors are incorporated into random locations in the genome causing mutagenesis of essential genes. Gene therapy trials with retroviruses to treat SCID (Severe combined immunodeficiency) led to leukemic transformation after integration of the virus into the host genome.⁵⁶ Insertional mutagenesis due to the integration of genes near a protooncogene may lead to tumorigenesis, illustrating the danger of gene-based CRISPR therapy. Protein/RNA delivery based CRISPR therapy, on the other hand, avoids this problem and thus is an attractive alternative to gene therapy (Table 1.1).

1.5. Self-assembled nanostructures for intracellular protein delivery

1.5.1. Self-assemblies. In biological systems proteins and other biomolecules are often trafficked in ‘tiny’ nanocontainers called vesicles.⁵⁷ Both intracellular and extracellular protein transport is carried out through these exquisitely designed delivery vehicles.⁵⁸ Likewise, viruses carry their nucleic acids inside a container composed of capsid proteins.⁵⁹ These natural delivery systems are the result of molecular self-assembly of proteins and other biomolecular building blocks.⁶⁰ Inspired by these naturally existing systems, a variety

of hierarchical self-assembled structures have been fabricated in recent years. Most of these materials were based on DNA,^{61,62} polymers,⁶³ and inorganic nanoparticle building blocks⁶⁴. Designing similar self-assembled hierarchical structures for any protein of interest with hybrid nanomaterials is challenging; as such an effort will require manipulating physiochemical properties of proteins (such as charges). Nonetheless, such structures with a desired protein may provide novel emergent functions including in intracellular protein delivery, enzymatic catalysis and photosynthetic energy harvesting.

1.5.2. Gold nanoparticles. Gold nanoparticles (AuNPs) provide attractive building blocks for fabricating self-assembled functional structures. Monolayer protected AuNPs have particularly been employed in material science through the control of their surface functionality.⁶⁵ The structure of AuNPs can be divided into two parts: a gold core, and a monolayer of organic ligands covering the core (Figure 1.3).⁶⁶ This monolayer feature a hydrophobic chain to confer stability, a non-interacting oligo (ethylene glycol) moiety, and the surface interacting head-groups (Figure 1.3). The size of both the core and the surface monolayer can precisely be controlled, often to commensurate biological large molecules such as proteins and DNA.⁶⁷ In addition, AuNPs exhibit a number of unique physical and chemical properties including their enormous surface area, oriented functionalities, and a functionalized surface with desired molecules. Such properties of AuNPs make them attractive building blocks for material fabrications, optical devices, chemical and biological sensor platforms, cellular imaging, and as drug delivery vehicles.⁶⁸

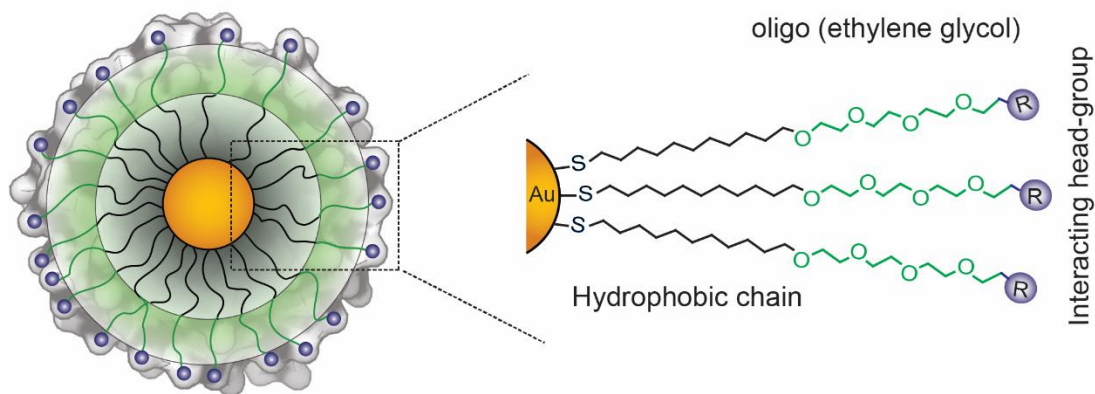


Figure 1. 3. Structure of gold nanoparticles (AuNPs) used in this thesis work. AuNPs feature a 2-nm gold core (yellow), and a surface organic monolayer comprising a hydrophobic chain, oligo (ethylene glycol) moiety, and a surface interacting head-group.

1.5.3. Self-assembled protein-nanoparticle structures. AuNPs and proteins serve as attractive complementary building blocks for fabricating complex structures, allowing the incorporation of bio-functionality into the structures. Recently, various kinds of protein-nanoparticle assemblies were constructed including protein-nanoparticle discrete assemblies,⁶⁹ superstructures,⁷⁰ and corona-like co-assemblies.⁷¹ These co-assemblies were either built based on self-templating proteins such as the viral capsid proteins,⁷² or relied on naturally existing complementary supramolecular interactions. Thus, these systems are restricted to a relatively narrow range of proteins; incorporation of any protein into a desired structure may require further engineering of the protein.

1.5.4. Protein-nanoparticle co-engineering for fabricating self-assemblies. AuNPs can be easily engineered by functionalizing with a desired surface ligand. The surface ligand dictates the function of nanoparticles. A wide variety of chemical entities such hydrophobic, electrostatic, π - π interacting, and polar head groups can be placed on the

surface of a AuNP.⁷³ As counterparts of these functionalized nanoparticles, proteins can be engineered with appropriate modifications. Both site-directed-mutagenesis to create specific mutations, as well as attaching a peptide sequence to one end of a protein provide means of engineering proteins. Once the proteins and nanoparticles are co-engineered with appropriate complementarity, we hypothesize that a wide variety of self-assembled nanostructures can be fabricated with emergent functions including for intracellular protein delivery.

1.6. Dissertation overview

The main goal of this thesis is to engineer biomimetic self-assemblies for intracellular delivery of proteins and CRISPR/Cas9 elements for therapeutic purpose. Molecular details of materials in nanoscale dictate their function in cell biology at macroscopic scale. Therefore, the rational design of the self-assemblies and their function as delivery vehicle for cell biology is thoroughly studied in this thesis. First two chapters (Chapter 2&3) will describe designing principle of self-assembled protein-nanoparticle materials, and rational co-engineering proteins and nanoparticles based on such principles to build higher order complex self-assemblies (Figure 1.4). In the last two chapters (Chapter 4&5), these nanoassemblies will be used to investigate their interactions with cell membrane, and delivery of protein and CRISPR/Cas9-RNP cargo into cells (Figure 1.4).

Interfacing proteins and nanoparticles to build self-assemblies require finding recognition elements that can bring these two materials together. In chapter 2, we reported the creation of a reversible multivalent supramolecular "zipper" recognition motif between gold nanoparticles and proteins. In this assembly, carboxylate-functionalized nanoparticles

interact strongly with oligohistidine tags. This interaction was tuned through His-tag length, and offered unique binding profiles based on the pH and electrolyte concentration of the medium.

Hierarchical organization of macromolecules through self-assembly is a prominent feature in biological systems. Synthetic fabrication of such structures provides materials with emergent functions such as intracellular protein delivery. In chapter 3, we reported the fabrication of self-assembled superstructures through co-engineering of recombinant proteins and nanoparticles. These structures featured a highly-sophisticated level of multi-layered hierarchical organization of the components: individual proteins and nanoparticles co-assembled to form discrete assemblies that collapsed to form granules, which then further self-organized to generate superstructures of hundreds of nanometer size. The components within these superstructures are dynamic and spatially reorganize in response to environmental influences. The precise control over the molecular organization of building blocks imparted by this protein-nanoparticle co-engineering strategy provided strategy for creating hierarchical hybrid materials and formed the foundation for the cell biological application the following chapters.

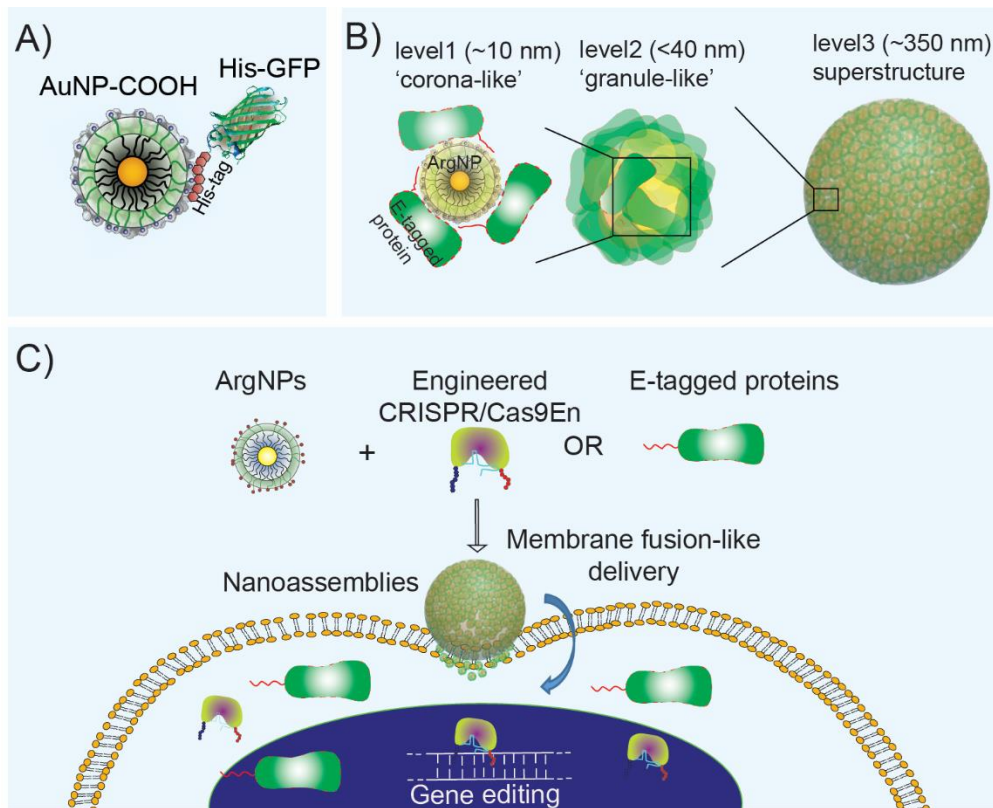


Figure 1. 4. Thesis overview. Chapter 2 and 3 includes engineering molecular recognition elements between proteins and gold nanoparticles (AuNPs) for fabricating (A) simple, and (B) complex self-assemblies. Chapter 4 &5 will describe the use these assemblies for direct cytoplasmic delivery of therapeutic proteins and CRISPR/Cas9 systems for gene editing (C).

The applicability of our nanoassemblies reported in chapter 3 was tested in chapter 4. Access to the cytosol is crucial for many protein-based therapeutic strategies, making endosomal entrapment a key challenge. We used our nanoassemblies to deliver proteins directly into cell cytosol. These assemblies fused with cell membranes, releasing the E-tag proteins directly into the cytosol. Five different proteins with diverse charges, sizes, and functions were effectively delivered into cells, demonstrating the generality of our method. Significantly, the engineered proteins retained activity after cytosolic delivery as demonstrated through the delivery of active Cre recombinase and Granzyme A to kill cancer cells.

Genome editing through the delivery of CRISPR/Cas9 system provides tremendous opportunity in curing human genetic diseases. Delivery of CRISPR elements in protein format (Cas9-ribonucleoprotein or Cas9-RNP) reduces unwanted gene targeting and avoids integrational mutagenesis that can occur through gene delivery strategies. Direct and efficient delivery of Cas9-RNP into the cytosol followed by translocation to the nucleus remains a major challenge in realizing the potential of CRISPR/Cas9 in human medicine. In chapter 5, we reported a remarkably high efficient (~90%) direct cytoplasmic/nuclear delivery of Cas9 protein through the co-engineering of Cas9 protein and carrier nanoparticles. This construct provided effective (~30%) gene editing efficiency and opened up opportunities in studying genome dynamics.

1.7. References

- (1) <https://ncats.nih.gov/files/NCATS-factsheet>
- (2) Drews J. Drug Discovery: A Historical Perspective. *Science* **2000**, 287, 1960-1964.
- (3) Drews, J.; Ryser, S. Classic Drug Targets. *Nat. Biotechnol.* **1997**, 15, 1350.
- (4) Quianzon, C. C.; Cheikh, I. History of Insulin. *J. Community Hosp. Intern. Med. Perspect.* **2012**, 2.
- (5) Walsh, G. Biopharmaceutical Benchmarks 2014. *Nat. Biotechnol.* **2014**, 32, 992-1000.
- (6) Fu, A.; Tang, R.; Hardie, J.; Farkas, M. E.; Rotello, V. M. Promises and Pitfalls of Intracellular Delivery of Proteins. *Bioconjug. Chem.* **2014**, 25, 1602-1608.
- (7) Stewart, M. P.; Sharei, A.; Ding, X.; Sahay, G.; Langer, R.; Jensen, K. F. *In Vitro* and *Ex Vivo* Strategies for Intracellular Delivery. *Nature* **2016**, 538, 183-192.
- (8) Gilleron, J.; Querbes, W.; Zeigerer, A.; Borodovsky, A.; Marsico, G.; Schubert, U.; Manyoats, K.; Seifert, S.; Andree, C.; Stöter, M.; Epstein-Barash, H.; Zhang, L.; Koteliansky, V.; Fitzgerald, K.; Fava, E.; Bickle, M.; Kalaidzidis, Y.; Akinc, A.; Maier, M.; Zerial, M. Image-Based Analysis of Lipid Nanoparticle-Mediated siRNA Delivery, Intracellular Trafficking and Endosomal Escape. *Nat. Biotechnol.* **2013**, 31, 638-646.
- (9) Ray, M.; Lee, Y.-W.; Scaletti, F.; Yu, R.; Rotello, V. M. Intracellular Delivery of Proteins by Nanocarriers. *Nanomedicine (Lond)*. **2017**, 12, 941-952.
- (10) Dinca, A.; Chien, W. M.; Chin, M. T. Intracellular Delivery of Proteins with Cell-Penetrating Peptides for Therapeutic Uses in Human Disease. *Int. J. Mol. Sci.* **2016**, 17, 263.
- (11) Deora, A. A.; Diaz, F.; Schreiner, R.; Rodriguez-Boulan, E. Efficient Electroporation of DNA and Protein into Confluent and Differentiated Epithelial Cells in Culture. *Traffic* **2007**, 8, 1304-1312.
- (12) Choi, S. O.; Kim, Y. C.; Lee, J. W.; Park, J. H.; Prausnitz, M. R.; Allen, M. G. Intracellular Protein Delivery and Gene Transfection by Electroporation using a Microneedle Electrode Array. *Small* **2012**, 8, 1081-1091.
- (13) Tang, R.; Kim, C. S.; Solfiell, D. J.; Rana, S.; Mout, R.; Velázquez-Delgado, E. M.; Chompoosor, A.; Jeong, Y.; Yan, B.; Zhu, Z. J.; Kim, C.; Hardy, J. A.; Rotello, V. M. Direct Delivery of Functional Proteins and Enzymes to the Cytosol using Nanoparticle-Stabilized Nanocapsules. *ACS Nano* **2013**, 7, 6667-6673.
- (14) Ray, M.; Tang, R.; Jiang, Z.; Rotello, V. M. Quantitative Tracking of Protein Trafficking to the Nucleus using Cytosolic Protein Delivery by Nanoparticle-Stabilized Nanocapsules. *Bioconjug. Chem.* **2015**, 26, 1004-1007.

- (15) Tang, R.; Jiang, Z.; Ray, M.; Hou, S.; Rotello, V. M. Cytosolic Delivery of Large Proteins using Nanoparticle-Stabilized Nanocapsules. *Nanoscale* **2016**, *8*, 18038-18041.
- (16) Yang, X. C.; Samanta, B.; Agasti, S. S.; Jeong, Y.; Zhu, Z. J.; Rana, S.; Miranda, O. R.; Rotello, V. M. Drug Delivery Using Nanoparticle-Stabilized Nanocapsules. *Angew. Chem. Int. Ed.* **2011**, *50*, 477-481.
- (17) Mout, R.; Ray, M.; Tay, T.; Sasaki, K.; Tonga, G. Y.; Rotello, V. M. A General Strategy for Direct Cytoplasmic Protein Delivery. *Submitted manuscript*.
- (18) Doudna, J. A.; Charpentier, E. The New Frontier of Genome Engineering with CRISPR-Cas9. *Science* **2014**, *346*, 1258096.
- (19) Hsu, P. D.; Lander, E. S.; Zhang, F. Development and Applications of CRISPR-Cas9 for Genome Engineering. *Cell* **2014**, *157*, 1262-1278.
- (20) Cox, D. B.; Platt, R. J.; Zhang, F. Therapeutic Genome Editing: Prospects and Challenges. *Nat. Med.* **2015**, *21*, 121-131.
- (21) Gasiunas, G.; Barrangou, R.; Horvath, P.; Siksnys, V. Cas9-crRNA Ribonucleoprotein Complex Mediates Specific DNA Cleavage for Adaptive Immunity in Bacteria. *Proc. Natl. Acad. Sci. U S A.* **2012**, *109*, E2579-86.
- (22) Jinek, M.; Chylinski, K.; Fonfara, I.; Hauer, M.; Doudna, J. A.; Charpentier, E. A Programmable Dual-RNA-Guided DNA Endonuclease in Adaptive Bacterial Immunity. *Science* **2012**, *337*, 816-821.
- (23) Cong, L.; Ran, F. A.; Cox, D.; Lin, S.; Barretto, R.; Habib, N.; Hsu, P. D.; Wu, X.; Jiang, W.; Marraffini, L. A.; Zhang, F. Multiplex Genome Engineering Using CRISPR/Cas Systems. *Science* **2013**, *339*, 819-823.
- (24) Mali, P.; Yang, L.; Esvelt, K. M.; Aach, J.; Guell, M.; DiCarlo, J. E.; Norville, J. E.; Church, G. M. RNA-Guided Human Genome Engineering via Cas9. *Science* **2013**, *339*, 823-826.
- (25) Cho, S. W.; Kim, S.; Kim, J. M.; Kim, J. S. Targeted Genome Engineering in Human Cells with the Cas9 RNA-Guided Endonuclease. *Nat. Biotechnol.* **2013**, *31*, 230-232.
- (26) Sander, J. D.; Joung, J. K. CRISPR-Cas Systems for Editing, Regulating and Targeting Genomes. *Nat. Biotechnol.* **2014**, *32*, 347-355.
- (27) Mout, R.; Ray, M.; Lee, Y.W.; Scaletti, F.; Rotello, V. M. *In Vivo* Delivery of CRISPR/Cas9 for Therapeutic Gene Editing: Progress and Challenges. *Bioconjug. Chem.* **2017**, *28*, 880-884.
- (28) Komor, A. C.; Badran, A. H.; Liu, D. R. CRISPR-Based Technologies for the Manipulation of Eukaryotic Genomes. *Cell* **2017**, *168*, 20-36.

- (29) Wang, A. Y.; Peng, P. D.; Ehrhardt, A.; Storm, T. A.; Kay, M. A. Comparison of Adenoviral and Adeno-Associated Viral Vectors for Pancreatic Gene Delivery *in vivo*. *Hum. Gene Ther.* **2004**, *15*, 405-413.
- (30) Gori, J. L.; Hsu, P. D.; Maeder, M. L.; Shen, S.; Welstead, G. G.; Bumcrot, D. Delivery and Specificity of CRISPR/Cas9 Genome Editing Technologies for Human Gene Therapy. *Hum. Gene Ther.* **2015**, *26*, 443-451.
- (31) Cheng, R.; Peng, J.; Yan, Y.; Cao, P.; Wang, J.; Qiu, C.; Tang, L.; Liu, D.; Tang, L.; Jin, J.; Huang, X.; He, F.; Zhang, P. Efficient Gene Editing in Adult Mouse Livers *via* Adenoviral Delivery of CRISPR/Cas9. *FEBS Lett.* **2014**, *588*, 3954-3958.
- (32) Ding, Q.; Strong, A.; Patel, K. M.; Ng, S.-L.; Gosis, B. S.; Regan, S. N.; Rader, D. J.; Musunuru, K. Permanent Alteration of PCSK9 with *in vivo* CRISPR-Cas9 Genome Editing. *Circ. Res.* **2014**, *115*, 488-492.
- (33) Nelson, C. E.; Gersbach, C. A. Engineering Delivery Vehicles for Genome Editing. *Annu. Rev. Chem. Biomol. Eng.* **2016**, *7*, 637-662.
- (34) Long, C.; Amoasii, L.; Mireault, A. A.; McAnally, J. R.; Li, H.; Sanchez-Ortiz, E.; Bhattacharyya, S.; Shelton, J. M.; Bassel-Duby, R.; Olson, E. N. Postnatal Genome Editing Partially Restores Dystrophin Expression in a Mouse Model of Muscular Dystrophy. *Science* **2016**, *351*, 400-403.
- (35) Tabebordbar, M.; Zhu, K.; Cheng, J. K. W.; Chew, W. L.; Widrick, J. J.; Yan, W. X.; Maesner, C.; Wu, E. Y.; Xiao, R.; Ran, F. A.; Cong, L.; Zhang, F.; Vandenberghe, L. H.; Church, G. M.; Wagers, A. J. *In vivo* Gene Editing in Dystrophic Mouse Muscle and Muscle Stem Cells. *Science* **2016**, *351*, 407-411.
- (36) Nelson, C. E.; Hakim, C. H.; Ousterout, D. G.; Thakore, P. I.; Moreb, E. A.; Rivera, R. M. C.; Madhavan, S.; Pan, X.; Ran, F. A.; Yan, W. X.; Asokan, A.; Zhang, F.; Duan, D.; Gersbach, C. A. *In vivo* Genome Editing Improves Muscle Function in a Mouse Model of Duchenne Muscular Dystrophy. *Science* **2015**, *351*, 403-407.
- (37) Zuris, J. A.; Thompson, D. B.; Shu, Y.; Guilinger, J. P.; Bessen, J. L.; Hu, J. H.; Maeder, M. L.; Joung, J. K.; Chen, Z.-Y.; Liu, D. R. Cationic Lipid-Mediated Delivery of Proteins Enables Efficient Protein-Based Genome Editing *in vitro* and *in vivo*. *Nat. Biotechnol.* **2015**, *33*, 73-80.
- (38) Ramakrishna, S.; Kwaku Dad, A.-B.; Beloor, J.; Gopalappa, R.; Lee, S.-K.; Kim, H. Gene Disruption by Cell-Penetrating Peptide-Mediated Delivery of Cas9 Protein and Guide RNA. *Genome Res.* **2014**, *24*, 1020-1027.
- (39) Kim, S.; Kim, D.; Cho, S. W.; Kim, J.; Kim, J.-S. Highly Efficient RNA-Guided Genome Editing in Human Cells *via* Delivery of Purified Cas9 Ribonucleoproteins. *Genome Res.* **2014**, *24*, 1012-1019.
- (40) Schumann, K.; Lin, S.; Boyer, E.; Simeonov, D. R.; Subramaniam, M.; Gate, R. E.; Haliburton, G. E.; Ye, C. J.; Bluestone, J. A.; Doudna, J. A.; Marson, A. Generation of

Knock-In Primary Human T Cells using Cas9 Ribonucleoproteins. *Proc. Natl. Acad. Sci. U. S. A.* **2015**, *112*, 10437-10442.

(41) Han, X.; Liu, Z.; Jo, M. c.; Zhang, K.; Li, Y.; Zeng, Z.; Li, N.; Zu, Y.; Qin, L. CRISPR-Cas9 Delivery to Hard-to-Transfect Cells *via* Membrane Deformation. *Sci. Adv.* **2015**, *1*, e1500454.

(42) Sun, W.; Ji, W.; Hall, J. M.; Hu, Q.; Wang, C.; Beisel, C. L.; Gu, Z. Self-Assembled DNA Nanoclews for the Efficient Delivery of CRISPR–Cas9 for Genome Editing. *Angew. Chem. Int. Ed.* **2015**, *54*, 12029-12033.

(43) Wu, Z.; Yang, H.; Colosi, P. Effect of Genome Size on AAV Vector Packaging. *Mol. Ther.* **2010**, *18*, 80-86.

(44) Dong, B.; Nakai, H.; Xiao, W. Characterization of Genome Integrity for Oversized Recombinant AAV Vector. *Mol. Ther.* **2010**, *18*, 87-92.

(45) Senís, E.; Fatouros, C.; Große, S.; Wiedtke, E.; Niopek, D.; Mueller, A. K.; Börner, K.; Grimm, D. CRISPR/Cas9-Mediated Genome Engineering: An Adeno-Associated Viral (AAV) Vector Toolbox. *Biotechnol. J.* **2014**, *9*, 1402-1412.

(46) Chew, W. L.; Tabebordbar, M.; Cheng, J. K.; Mali, P.; Wu, E. Y.; Ng, A. H.; Zhu, K.; Wagers, A. J.; Church, G. M. A Multifunctional AAV-CRISPR-Cas9 and its Host Response. *Nat. Methods* **2016**, *13*, 868-874.

(47) Ran, F. A.; Cong, L.; Yan, W. X.; Scott, D. A.; Gootenberg, J. S.; Kriz, A. J.; Zetsche, B.; Shalem, O.; Wu, X.; Makarova, K. S.; Koonin, E. V.; Sharp, P. A.; Zhang, F. *In vivo* Genome Editing using Staphylococcus Aureus Cas9. *Nature* **2015**, *520*, 186-191.

(48) Mout, R.; Ray, M.; Tonga, G. Y.; Lee, Y.-W.; Tay, T.; Sasaki, K.; Rotello, V. M. Direct Cytosolic Delivery of CRISPR/Cas9-Ribonucleoprotein for Efficient Gene Editing. *ACS Nano* **2017**, *11*, 2452-2458.

(49) Zincarelli, C.; Soltys, S.; Rengo, G.; Rabinowitz, J. E. Analysis of AAV Serotypes 1-9 Mediated Gene Expression and Tropism in Mice After Systemic Injection. *Mol. Ther.* **2008**, *16*, 1073-1080.

(50) Peer, D.; Karp, J. M.; Hong, S.; Farokhzad, O. C.; Margalit, R.; Langer, R. Nanocarriers as an Emerging Platform for Cancer Therapy. *Nat. Nanotechnol.* **2007**, *2*, 751-760.

(51) Cho, S. W.; Kim, S.; Kim, Y.; Kweon, J.; Kim, H. S.; Bae, S.; Kim, J. S. Analysis of Off-Target Effects of CRISPR/Cas-Derived RNA-Guided Endonucleases and Nickases. *Genome Res.* **2014**, *24*, 132-141.

(52) Fu, Y.; Foden, J. A.; Khayter, C.; Maeder, M. L.; Reyon, D.; Joung, J. K.; Sander, J. D. High-Frequency Off-Target Mutagenesis Induced by CRISPR-Cas Nucleases in Human Cells. *Nat. Biotechnol.* **2013**, *31*, 822-826.

- (53) Kleinstiver, B. P.; Pattanayak, V.; Prew, M. S.; Tsai, S. Q.; Nguyen, N. T.; Zheng, Z.; Joung, J. K. High-Fidelity CRISPR-Cas9 Nucleases with no Detectable Genome-Wide Off-Target Effects. *Nature* **2016**, *529*, 490-495.
- (54) Slaymaker, I. M.; Gao, L.; Zetsche, B.; Scott, D. A.; Yan, W. X.; Zhang, F. Rationally Engineered Cas9 Nucleases with Improved Specificity. *Science* **2016**, *351*, 84-88.
- (55) Neefjes, J.; Jongsma, M. L.; Paul, P.; Bakke, O. Towards a Systems Understanding of MHC Class I and MHC Class II Antigen Presentation. *Nat. Rev. Immunol.* **2011**, *11*, 823-836.
- (56) Hacein-Bey-Abina, S.; Garrigue, A.; Wang, G. P.; Soulier, J.; Lim, A.; Morillon, E.; Clappier, E.; Caccavelli, L.; Delabesse, E.; Beldjord, K. *et al.* Insertional Oncogenesis in 4 Patients After Retrovirus-Mediated Gene Therapy of SCID-X1. *J. Clin. Invest.* **2008**, *118*, 3132-3142.
- (57) Alberts, B.; Johnson, A.; Lewis, J.; *et al.*, Intracellular Vesicular Traffic. *Molecular Biology of the Cell* **2002**, 4th edition, New York: Garland Science.
- (58) <https://www.ncbi.nlm.nih.gov/books/NBK7286/>
- (59) Mateu, M. G. Assembly, Stability and Dynamics of Virus Capsids. *Arch. Biochem. Biophys.* **2013**, *531*, 65-79.
- (60) Kushner, D. J. Self-Assembly of Biological Structures. *Bacteriol. Rev.* **1969**, *33*, 302-345.
- (61) Han, D.; Pal, S.; Yang, Y.; Jiang, S.; Nangreave, J.; Liu, Y.; Yan, H. DNA Gridiron Nanostructures Based on Four-Arm Junctions. *Science* **2013**, *339*, 1412-1415.
- (62) Inuma, R.; Ke, Y.; Jungmann, R.; Schlichthaerle, T.; Woehrstein, J. B.; Yin, P. Polyhedra Self-Assembled from DNA Tripods and Characterized with 3D DNA-PAINT. *Science* **2014**, *344*, 65-69.
- (63) Qiu, H.; Hudson, Z. M.; Winnik, M. A.; Manners, I. Multidimensional Hierarchical Self-Assembly of Amphiphilic Cylindrical Block Comicelles. *Science* **2015**, *347*, 1329-1332.
- (64) Singh, G.; Chan, H.; Baskin, A.; Gelman, E.; Repnin, N.; Král, P.; Klajn, R. Self-Assembly of Magnetite Nanocubes into Helical Superstructures. *Science* **2014**, *345*, 1149-1153.
- (65) Rana, S.; Bajaj, A.; Mout, R.; Rotello, V. M. Monolayer Coated Gold Nanoparticles for Delivery Applications. *Adv. Drug. Deliv. Rev.* **2012**, *64*, 200-216.
- (66) Saha, K. Understanding Structure-Property Relationships at the Nano-Bio Interface for Delivery Applications. *Doctoral Dissertations* **2014**.
- (67) De, M.; Ghosh, P. S.; Rotello, V. M. Applications of Nanoparticles in Biology. *Adv. Mater.* **2008**, *20*, 4225-4241.

- (68) Salata, O. V. Applications of Nanoparticles in Biology and Medicine. *J. Nanobiotechnology* **2004**, 2, 3.
- (69) Kostianen, M. A.; Hiekkataipale, P.; Laiho, A.; Lemieux, V.; Seitsonen, J.; Ruokolainen, J.; Ceci, P. Electrostatic Assembly of Binary Nanoparticle Superlattices Using Protein Cages. *Nat. Nanotechnol.* **2013**, 8, 52-56.
- (70) Park, J. I.; Nguyen, T. D.; de Queirós Silveira, G.; Bahng, J. H.; Srivastava, S.; Zhao, G.; Sun, K.; Zhang, P.; Glotzer, S. C.; Kotov, N. A. Terminal Supraparticle Assemblies from Similarly Charged Protein Molecules and Nanoparticles. *Nat. Commun.* **2014**, 5, 3593.
- (71) Bayraktar, H.; You, C. C.; Rotello, V. M.; Knapp, M. J. Facial Control of Nanoparticle Binding to Cytochrome C. *J. Am. Chem. Soc.* **2007**, 129, 2732-2733.
- (72) Douglas, T.; Young, M. Viruses: Making Friends with Old Foes. *Science* **2006**, 312, 873-875.
- (73) Mout, R.; Moyano, D. F.; Rana, S.; Rotello, V. M. Surface Functionalization of Nanoparticles for Nanomedicine. *Chem. Soc. Rev.* **2012**, 41, 2539-2544.

CHAPTER 2

ENVIRONMENTALLY RESPONSIVE HISTIDINE-CARBOXYLATE ZIPPER FORMATION BETWEEN PROTEINS AND NANOPARTICLES

2.1. Introduction

Tailoring molecular recognition between synthetic materials and biomolecules provides a versatile strategy for creating bioconjugate systems.¹ A variety of supramolecular approaches have been devised to interface synthetic and biological systems for diverse applications.² However, using these systems in physiological environments such as serum is challenging, where high concentrations of proteins and other biomolecules compete for interaction.

Co-engineering of biomolecules and synthetic materials provides a strategy for generating high affinity and reversible molecular interactions.³ Inspiration for this co-design can be obtained from Nature: naturally occurring molecular zippers, including duplex DNA⁴ and leucine zippers⁵ exhibit robust multivalent reversible interactions in intracellular conditions. Microtubules polymerize and de-polymerize through the formation of specific molecular zippers.⁶ This multivalent motif⁷ has been used to create synthetic molecular duplexes⁸ through non-covalent interactions including electrostatic interactions,⁹ hydrogen bonding,¹⁰ π - π interactions,¹¹ and van der Waals forces to generate zippers.¹²

Multivalency is a key structural prerequisite for zipper motifs. Nanomaterials offer molecular scaffolds that can be engineered to present multivalent recognition elements.¹³

Gold nanoparticles (AuNPs) provide a particularly versatile platform for biomolecular recognition,¹⁴ and have been interfaced with proteins for a wide variety of applications.¹⁵ The AuNP surface can be readily engineered to feature recognition elements. Additionally, AuNPs can be generated with sizes commensurate to proteins, providing surface complementarity for recognition while maintaining effective biological function.¹⁶

The metal ion-mediated oligohistidine-nitrilotriacetate recognition motif has been widely employed to capture proteins using nanomaterials.¹⁷ We hypothesized that the oligohistidine cationic tail¹⁸ used in this strategy could be employed as a zipper component for interaction with nanomaterials. In this report, we demonstrate a reversible molecular zipper between His-tagged proteins and carboxylate functionalized AuNPs. This zipper exhibits high affinity binding in physiologically relevant environments, including serum conditions. The system is also environmentally responsive, with binding dictated by solution pH. This new recognition motif presents opportunities for engineering specific molecular interactions between synthetic and biomolecules.

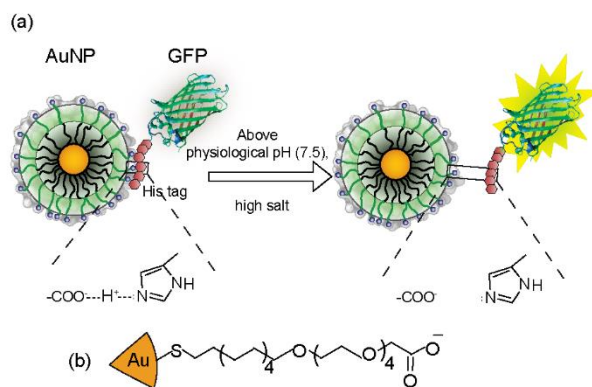


Figure 2. 1. (a) Zipper formation between AuNP-COOH and N-terminus oligohistidine-tagged GFPs through carboxylate-histidine interaction (b) The chemical structure of 2 nm gold core nanoparticle AuNP-COOH.

2.2. Results

The host nanoparticle was provided by AuNPs (2nm core diameter) functionalized with anionic ligands (AuNP-COOH) that can interact with proteins without denaturation.¹⁹ We next explored the interaction of these inherently multivalent carboxylate particles with a family of His-tagged green fluorescent proteins (GFP)²⁰ (Figure 2.1). We cloned and purified three eGFP²¹ variants carrying different length of N-terminal His-tags: one His (1xHis-GFP), six His (6xHis-GFP), and twelve His (12xHis-GFP) to determine the required number of interactions. These proteins were all anionic, with predicted pI values of 5.8, 6.1, and 6.5, respectively.

The binding efficiency of AuNP-COOH with the His-tagged GFPs was quantified through fluorescence titration,²² utilizing the quenching properties of the AuNP.²³ At low ionic strength (5 mM phosphate buffer, PB) AuNP-COOH bound both 12xHis-GFP and 6xHis-GFP with high affinity (Figure 2.2a). The binding constant (K_s) values for 12xHis-GFP ($K_s = 2.95 \pm 0.6 \times 10^7 \text{ M}^{-1}$) was ~3-fold higher than that of 6xHis-GFP ($K_s = 7.8 \pm 0.38 \times 10^6 \text{ M}^{-1}$), indicating that multivalency is crucial for zipper formation. Interestingly, more GFPs bound to each nanoparticle for 12xHis-GFP ($n = 11.6 \pm 0.8$) than for 6xHis-GFP ($n = 4.7 \pm 1$), potentially due to decreased secondary repulsion between the anionic GFPs.²⁴ No significant binding was observed with 1xHis-GFP within the nanoparticles concentration that were chosen for the study, demonstrating that specific zipper formation was required for interaction.

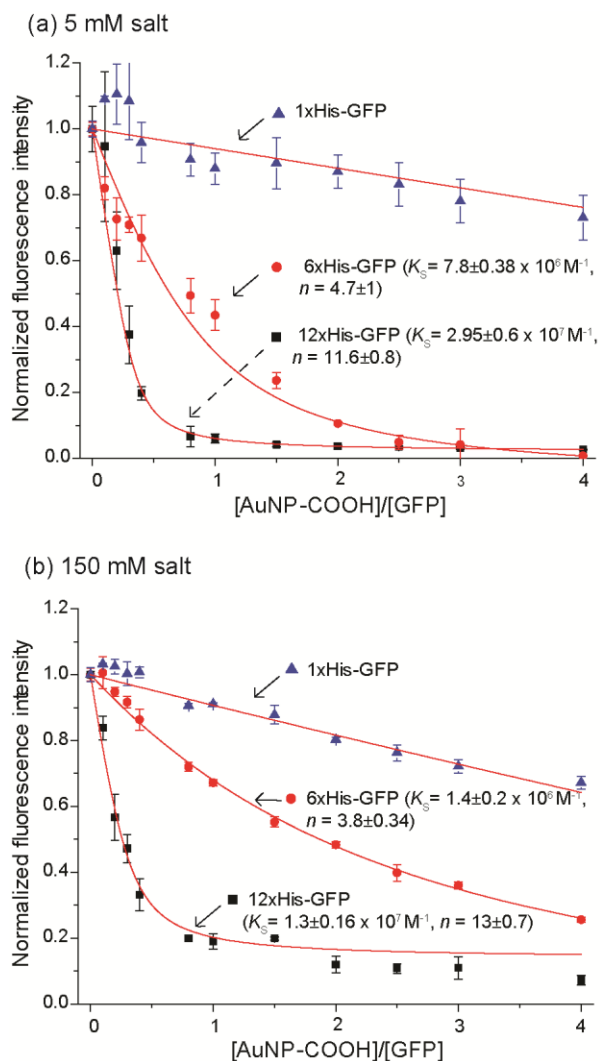


Figure 2. 2. The interaction of AuNP-COOH with His-tagged GFP variants. Fluorescence ($\lambda_{ex}=475 \text{ nm}$, $\lambda_{em}=510 \text{ nm}$) titrations between nanoparticles and GFPs (100 nM) in (a) 5 mM phosphate buffer (PB), and (b) PBS buffer (150 mM NaCl in 5 mM PB) at pH 7.4. The complex association constant (K_S) and the binding stoichiometry (n) were determined using previously reported method.²²

The pragmatic use of non-covalent bioconjugates requires high affinity interactions at physiological ionic strength. In previous studies, electrostatic interactions between nanoparticles and proteins were fully disrupted at quite low salt concentrations, typically 10-50 mM salt.²⁵ In contrast, high binding affinities were observed between AuNP-COOH and both 12xHis-GFP ($K_S = 1.3 \pm 0.16 \times 10^7 \text{ M}^{-1}$), and 6xHis-GFP ($K_S = 1.4 \pm 0.2 \times 10^6 \text{ M}^{-1}$)

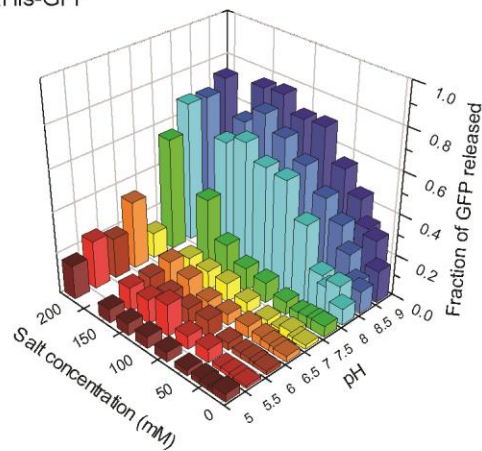
in PBS buffer (150 mM NaCl in 5 mM PB, pH 7.4) (Figure 2.2b). Notably, a larger n value was observed for 12xHis-GFP compared to 6xHis-GFP, similar to the trend observed at low (5 mM) electrolyte concentration.

Reversible zipper formation at physiologically relevant conditions. One of the key advantages of supramolecular bioconjugates is their ability to respond to environmental changes. pH is an important biological parameter. For example, normal tissues have a pH of 7.4, while tumor tissues have lower pH (~6 to 7).²⁶ Additionally, pH decreases through the endosomal/lysosomal pathways inside cells, reaching a pH of ~4.8.²⁷ In our system, the histidine tag in GFPs offers a potentially pH-switchable recognition scaffold. To explore this possibility, we investigated the pH and ionic strength dependent reversibility of the carboxylate-histidine zipper formation. Both 12xHis-GFP and 6xHis-GFP interacted strongly with AuNP-COOH below pH ~7.5 at physiological salt concentration (PBS). Significantly, above pH ~7.5 the carboxylate-histidine zipper disassembled, releasing the GFP from the nanoparticles surface (Figure 2.3a and 2.3b). As expected, 1xHis-GFP did not interact with nanoparticles at any condition (Figure 2.3c). Taken together, these studies demonstrated the pH response of the zipper motif.

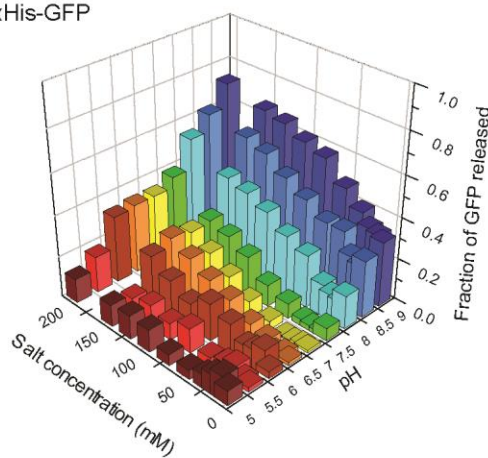
Reversible zipper formation in serum conditions. *In vivo* applications including protein and gene delivery require specific and reversible interactions between synthetic carrier materials and the cargo molecules in serum.²⁸ Serum presents a complex competitive chemical environment featuring a high (~1 mM) concentration of protein,²⁹ making it challenging to engineer effective recognition motifs. We parametrically investigated the serum concentration and pH dependent reversibility of the carboxylate-histidine zipper. At pH <7.5 and at 10% serum (cell culture condition), 12xHis-GFP

exhibited a high affinity binding towards AuNP-COOH (Figure 2.4a). Significantly, in 55% serum condition (*in vivo* condition) at pH 7.5 there was substantial binding between AuNP-COOH and 12xHis-GFP (Figure 2.4c). While the binding isotherm is complex, considerable binding was observed at high nanomolar concentrations. In contrast, 6xHis-GFP did not bind with AuNP-COOH at any serum condition under investigation (Figure 2.4b), indicating that a high degree of multivalency is crucial for carboxylate-histidine zipper formation in complex biological environments.

(a) 12xHis-GFP



(b) 6xHis-GFP



(c) 1xHis-GFP

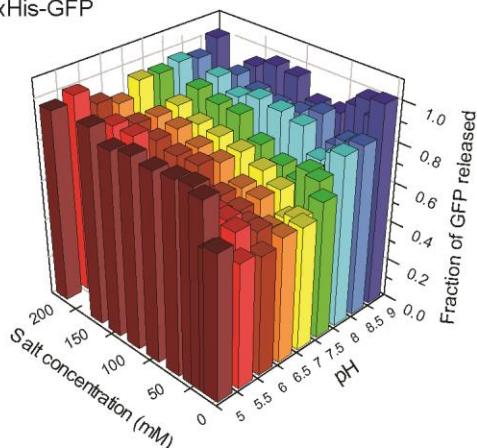


Figure 2. 3. Responsiveness of the carboxylate-histidine zipper towards pH and salt concentration. Fluorescence titrations between 400 nM of AuNP-COOH and 100 nM of (a) 12xHis-GFP, (b) 6xHis-GFP, and (c) 1xHis-GFP were performed parametrically varied pH and salt (NaCl) concentrations in 5 mM PB. The intensity of GFP released from nanoparticles was normalized against the intensity of free GFP.

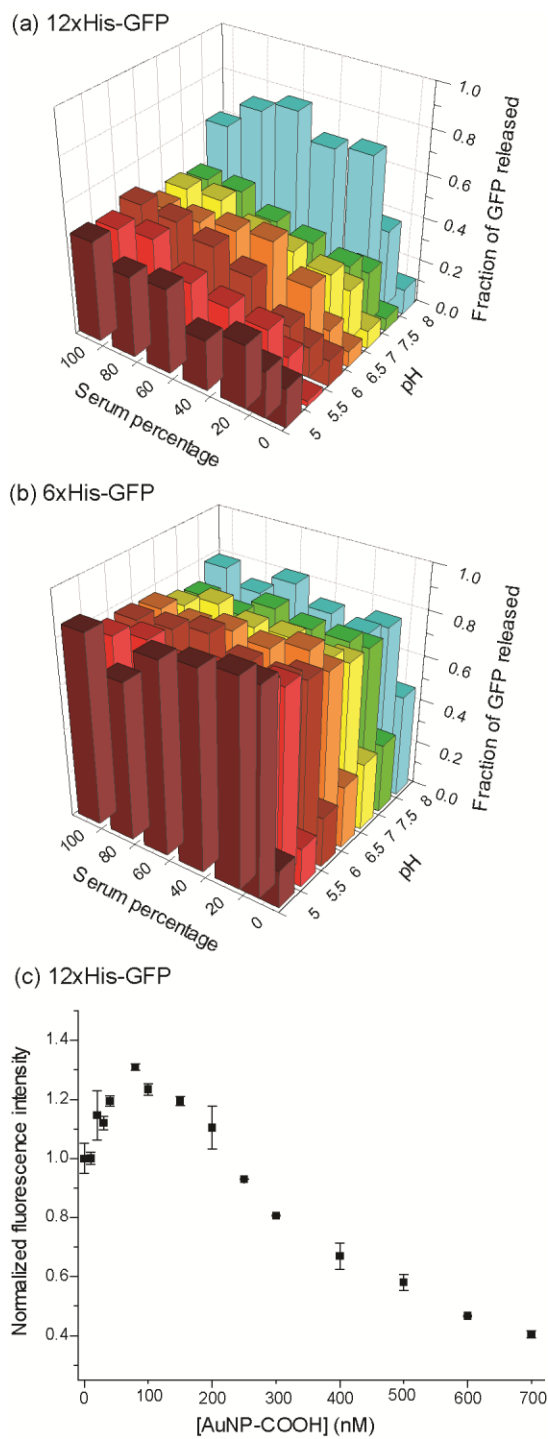


Figure 2. 4. Reversible carboxylate-histidine zipper formation between AuNP-COOH and (a) 12xHis-GFP, and (b) 6xHis-GFP at serum conditions. 400 nM of AuNP-COOH was titrated against 100 nM of His-tagged GFPs varying the serum percentage and pH at 150 mM salt (1xPBS) concentration. (c) Fluorescence titrations between AuNP-COOH and 12xHis-GFP (100 nM) at 55% serum condition, pH 7.4.

2.3. Conclusions

In summary, we have tailored a molecular zipper based on multivalent carboxylate-histidine interactions through co-engineering of the AuNP surface and proteins. The carboxylate-histidine zipper exhibited high affinity interactions under physiologically relevant conditions that were pH responsive, making these systems attractive starting points for delivery and imaging applications. In a broader context, these studies demonstrate how co-engineering of biomolecules and nanoparticles can be used to generate bioconjugates with new and useful properties.

2.4. Experimental section

Cloning and over expression of green fluorescent proteins (GFPs). Genetic engineering manipulation and protein expression were done according to standard protocols. (a) To generate 1xHis-GFP, a constitutive expression vector (pUCCB-ntH6-eGFP) was purchased from Addgene (plasmid id- 32557).³⁰ For the sake of purification, a 6xHis tag was placed on the N-terminus of 1xHis-GFP, upstream of a thrombin cleavage site. (b) 6xHis-GFP expression vector (pET21-d-GFP) was obtained from Novagen. (c) 12xHis-GFP was generated by incorporating twelve histidines in the N-terminus of GFP. Briefly, using GFP as the template, PCR was performed with the following primers. Subsequently, the PCR product was digested (using *Bam*HI and *Hind*III restriction enzymes) and inserted into pQE80 vector, downstream of nucleotides for six histidine tag to construct pQE80-12xHis-GFP expression vector. Successful cloning was confirmed by DNA sequencing.

Forward primer: 5'- ACGATGGATCCCACCATCACCAT -3'

Reverse primer: 5'- GTGACAAGCTTTTACTTGTACAGCTC -3'

To produce recombinant proteins, plasmids carrying 1xHis-GFP, 6xHis-GFP, or 12xHis-GFP was transformed into *Escherichia coli* BL21(DE3) strain. A transformed colony was picked up to grow small cultures in 50 mL 2xYT media at 37 °C for overnight. The following day, 15 mL of grown culture was inoculated into one liter 2xYT media and allowed to grow at 37 °C until OD reaches 0.6. At this point, the protein expression was induced by adding isopropyl-b-D-thiogalactopyranoside (IPTG; 1 mM final concentration) at 25 °C. After 16 hours of induction, the cells were harvested and the pellets were lysed using a microfluidizer. His-tagged fluorescent proteins were purified from the lysed supernatant using HisPur cobalt columns. The integrity and the purity of native protein were determined by 12% SDS-PAGE gel.

1xHis-GFP was cleaved from its 6xHis tag using thrombin-agarose beads (Thrombin CleanCleave™ Kit, Sigma-Aldrich) as described in the instruction manual. After the cleavage, 1xHis-GFP was passed through a HisPur cobalt column to remove the cleaved 6xHis tag. Further, the residual 6xHis was removed by a 10KD-MWCO (molecular weight cut off) filter.

Synthesis and characterization of nanoparticles. Carboxylate functionalized gold nanoparticles (AuNP-COOH) were synthesized according to a previous report.³¹ Briefly, Brust-Schiffrin two-phase synthesis was used to synthesize pentanethiol-coated AuNPs with core diameter ~2 nm.³² The Murray place-exchange method was followed to obtain AuNP-COOH.³³ The monolayer protected nanoparticles were re-dispersed in water. The excess ligand/pentanethiol were removed by dialysis using a 10,000 MWCO snake-skin

membrane. The final concentration was measured by UV spectroscopy at 502 nm. To assess their quality, the nanoparticles were characterized by Zeta potential (surface charge), Dynamic Light Scattering (DLS) (hydrodynamic radius), and Transmission Electron Microscopy (TEM) (core size) as shown in Figure 2.5.

Fluorescence titration. Fluorescence titration experiments between nanoparticles and GFPs were carried out as described previously.³⁴ Briefly, the change of fluorescence intensity of GFPs at 510 nm was measured with an excitation wavelength of 475 nm at various concentrations of nanoparticles from 0 to 400 nM on a Molecular Devices SpectraMax M3 microplate reader (at 25 °C). Quenching of fluorescence intensity arising from 100 nM GFP was observed with increasing nanoparticle concentration. Nonlinear least-squares curve fitting analysis was carried out to estimate the binding constant (K_s) and association stoichiometry (n , $[GFP]/[AuNP-COOH]$) using a one site binding model.²¹

For the pH and salt dependent interactions (fluorescence titrations) between nanoparticles and GFPs, the concentration of GFP chosen was 100 nM for each study. The concentrations of AuNP-COOH used for the titrations were 400 nM. The fluorescence intensity for each study was normalized against the intensity of GFP without nanoparticles at their respective pH and salt (NaCl in 5 mM PB) concentration. The titrations were carried out in triplicates, and repeated at least twice with different batches of nanoparticles.

Similar fluorescence titrations were performed for the serum concentration and pH dependent interactions between AuNP-COOH and His-tagged GFPs. Both the nanoparticle (400 nM) and GFP (100 nM) concentrations were kept fixed, varying the serum percentage and pH of the solutions. In a typical experiment, AuNP-COOH/GFP complexes were made first, incubated at dark for 10 minutes, then the required serum amount was added to the

complexes, followed by immediate shaking for 30 seconds. Fluorescence reading was taken after 30 minutes of incubation.

2.5. Supporting figures

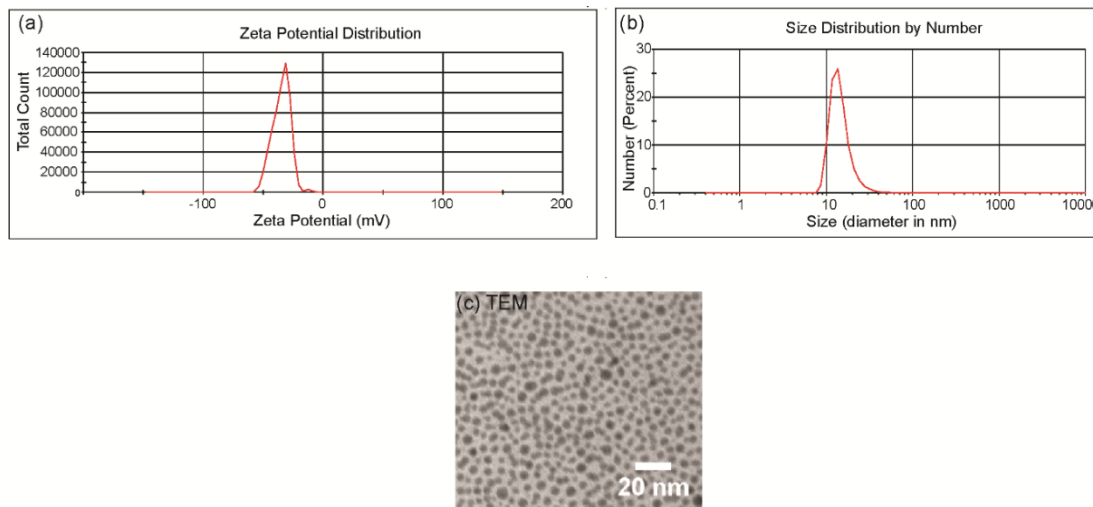


Figure 2. 5. Characterization of AuNP-COOH. (a) Zeta potential (-34.8 ± 3.1 mV, measured at 5 mM PB, pH 7.4), (b) Dynamic light scattering (DLS) diameter (14.1 ± 1.2 nm, measured at 5 mM PB, pH 7.4), and (c) TEM image of AuNP-COOH.

2.6. References

- (1) Lehn, J. M. Toward Self-Organization and Complex Matter. *Science* **2002**, *295*, 2400-2403.
- (2) Mout, R. M.; Moyano, D. F.; Rana S.; Rotello, V. M. Surface Functionalization of Nanoparticles for Nanomedicine. *Chem. Soc. Rev.* **2012**, *41*, 2539-2544.
- (3) Kostianen, M. A.; Hiekkataipale, P.; Laiho, A.; Lemieux, V.; Seitsonen, J.; Ruokolainen, J.; Ceci, P. Electrostatic Assembly of Binary Nanoparticle Superlattices using Protein Cages. *Nat. Nanotechnol.* **2013**, *8*, 52-56.
- (4) Weaver, R. F. *Molecular Biology*, 5th ed; McGraw-Hill, **2011**.
- (5) Nir, E.; Kleinermanns, K.; de Vries, M. S. Pairing of Isolated Nucleic-Acid Bases in the Absence of the DNA Backbone. *Nature* **2000**, *408*, 949-951.
- (6) Sandblad, L.; Busch, K. E.; Tittmann, P.; Gross, H.; Brunner, D.; Hoenger, A. The Schizosaccharomyces Pombe EB1 Homolog Mal3p Binds and Stabilizes the Microtubule Lattice Seam. *Cell* **2006**, *127*, 1415-1424.
- (7) Levine, P. M.; Carberry, T. P.; Holub J. M.; Kirshenbaum, K. Crafting Precise Multivalent Architectures. *Med. Chem. Commun.* **2013**, *4*, 493-509.
- (8) Culik, R. M.; Jo, H.; DeGrado, W. F.; Gai, F. Using Thioamides to Site-Specifically Interrogate the Dynamics of Hydrogen Bond Formation in β -Sheet Folding. *J. Am. Chem. Soc.* **2012**, *134*, 8026-8029.
- (9) Diss, M. L.; Kennan, A. J. Simultaneous Directed Assembly of Three Distinct Heterodimeric Coiled Coils. *Org. Lett.* **2008**, *10*, 3797-3800.
- (10) Spencer, R.; Chen, K. H.; Manuel, G.; Nowick, J. S. Recipe for β -Sheets: Foldamers Containing Amyloidogenic Peptide Sequences. *Eur. J. Org. Chem.* **2013**, 3523-3528.
- (11) Waters, M. L. Aromatic Interactions in Peptides: Impact on Structure and Function. *Biopolymers* **2004**, *76*, 435-445.
- (12) Kim, H. W.; Jung, J.; Han, M.; Lim, S.; Tamada, K.; Hara, M.; Kawai, M.; Kim, Y.; Kuk, Y. One-Dimensional Molecular Zippers. *J. Am. Chem. Soc.* **2011**, *133*, 9236-9238.
- (13) Rana, S.; Bajaj, A.; Mout, R.; Rotello, V. M. Monolayer Coated Gold Nanoparticles for Delivery Applications. *Adv. Drug. Deliv. Rev.* **2012**, *64*, 200-216.

- (14) Daniel, M. C.; Astruc, D. Gold Nanoparticles: Assembly, Supramolecular Chemistry, Quantum-Size-Related Properties, and Applications Toward Biology, Catalysis, and Nanotechnology. *Chem. Rev.* **2004**, *104*, 293-346.
- (15) Mout, R.; Rotello, V. M. Bio and Nano Working Together: Engineering the Protein-Nanoparticle Interface. *Isr. J. Chem.* **2013**, *53*, 521-529.
- (16) Rosi, N. L.; Mirkin, C. A. Nanostructures in Biodiagnostics. *Chem. Rev.* **2005**, *105*, 1547-1562.
- (17) De, M.; Rana, S.; Rotello, V. M. Nickel-Ion-Mediated Control of the Stoichiometry of His-Tagged Protein/Nanoparticle Interactions. *Macromol. Biosci.* **2009**, *9*, 174-178.
- (18) Marti, D. N.; Bosshard, H. R. Electrostatic Interactions in Leucine Zippers: Thermodynamic Analysis of the Contributions of Glu and His Residues and the Effect of Mutating Salt Bridges. *J. Mol. Biol.* **2003**, *330*, 621-637.
- (19) Bayraktar, H.; You, C. C.; Rotello, V. M.; Knapp, M. J. Facial Control of Nanoparticle Binding to Cytochrome C. *J. Am. Chem. Soc.* **2007**, *129*, 2732-2733.
- (20) Tsien, R. Y. The Green Fluorescent Protein. *Annu. Rev. Biochem.* **1998**, *67*, 509-544.
- (21) Cormack, B. P.; Valdivia, R. H.; Falkow, S. FACS-Optimized Mutants of the Green Fluorescent Protein (GFP). *Gene* **1996**, *173*, 33-38.
- (22) You, C. C.; De, M.; Han, G.; Rotello, V. M. Tunable Inhibition and Denaturation of Alpha-Chymotrypsin with Amino Acid-Functionalized Gold Nanoparticles. *J. Am. Chem. Soc.* **2005**, *127*, 12873-12881.
- (23) De, M.; Rana, S.; Akpınar, H.; Miranda, O. R.; Arvizo, R. R.; Bunz, U. H.; Rotello, V. M. Sensing of Proteins in Human Serum using Conjugates of Nanoparticles and Green Fluorescent Protein. *Nat. Chem.* **2009**, *1*, 461-465.
- (24) Torrens, F.; Castellano, G. Protein Negative/Positively Cooperative Binding to Zwitterionic/Anionic Vesicles. *J. Cheminform.* **2010**, *2*(Suppl 1): P12.
- (25) Peng, Z. G.; Hidajat, K.; Uddin, M. S. Adsorption of Bovine Serum Albumin on Nanosized Magnetic Particles. *J. Colloid. Interface Sci.* **2004**, *271*, 277-283.
- (26) Schmaltz, C.; Hardenbergh, P. H.; Wells, A.; Fisher, D. E. Regulation of Proliferation-Survival Decisions During Tumor Cell Hypoxia. *Mol. Cell Biol.* **1998**, *18*, 2845-2854.
- (27) Sorkin, A.; Von Zastrow, M. Signal Transduction and Endocytosis: Close Encounters of Many Kinds. *Nat. Rev. Mol. Cell Biol.* **2002**, *3*, 600-614.

- (28) Tang, R.; Kim, C. S.; Solfiell, D. J.; Rana, S.; Mout, R.; Velázquez-Delgado, E. M.; Chompoosor, A.; Jeong, Y.; Yan, B.; Zhu, Z. J.; Kim, C.; Hardy, J. A.; Rotello, V. M. Direct Delivery of Functional Proteins and Enzymes to the Cytosol using Nanoparticle-Stabilized Nanocapsules. *ACS Nano* **2013**, *7*, 6667-6673.
- (29) Adkins, J. N.; Varnum, S. M.; Auberry, K. J.; Moore, R. J.; Angell, N. H.; Smith, R. D.; Springer, D. L.; Pounds, J. G. Toward a Human Blood Serum Proteome: Analysis by Multidimensional Separation Coupled with Mass Spectrometry. *Mol. Cell Proteomics* **2002**, *1*, 947-955.
- (30) Vick, J. E.; Johnson, E. T.; Choudhary, S.; Bloch, S. E.; Lopez-Gallego, F.; Srivastava, P.; Tikh, I. B.; Wawrzyn, G. T.; Schmidt-Dannert, C. Optimized Compatible set of BioBrick™ Vectors for Metabolic Pathway Engineering. *Appl. Microbiol. Biotechnol.* **2011**, *92*, 1275-1286.
- (31) Hong, R.; Emrick, T.; Rotello, V. M. Monolayer-Controlled Substrate Selectivity using Noncovalent Enzyme-Nanoparticle Conjugates. *J. Am. Chem. Soc.* **2004**, *126*, 13572-13573.
- (32) Kanaras, A. G.; Kamounah, F. S.; Schaumburg, K.; Kiely, C. J.; Brust, M. Thioalkylated Tetraethylene Glycol: a New Ligand for Water Soluble Monolayer Protected Gold Clusters. *Chem. Commun. (Camb)* **2002**, *20*, 2294-2295.
- (33) Templeton, A. C.; Wuelfing, W. P.; Murray, R. W. Monolayer-Protected Cluster Molecules. *Acc. Chem. Res.* **2000**, *33*, 27-36.
- (34) Rana, S.; Singla, A. K.; Bajaj, A.; Elci, S. G.; Miranda, O. R.; Mout, R.; Yan, B.; Jirik, F. R.; Rotello, V. M. Array-Based Sensing of Metastatic Cells and Tissues using Nanoparticle-Fluorescent Protein Conjugates. *ACS Nano* **2012**, *6*, 8233-8240.

CHAPTER 3

PROGRAMMED SELF-ASSEMBLY OF HIERARCHICAL NANOSTRUCTURES THROUGH PROTEIN-NANOPARTICLE CO-ENGINEERING

3.1. Introduction

Complex self-assembled structures observed in Nature are formed through multiple levels of hierarchical organization.¹ The components in these systems are spatially organized to acquire functions,^{2,3} evolving through dynamic reorganization during cellular processes.⁴ Building synthetic structures to mimic these complex dynamic assemblies is challenging.^{5,6} Recent studies have fabricated ordered discrete structures based on self-assembly of DNA,⁷ proteins,^{8,9} and proteins with DNA.¹⁰ These structures mirror the structural complexity of biological systems, however their architectures are ‘fixed’ in lattice arrays, and lack the dynamic behavior of bioassemblies. Synthetic systems including nanoparticles¹¹⁻¹³ and polymers^{5,14,15} have likewise been used to build hierarchical assemblies, however fabrication of dynamically-organized self-assembled hierarchical structures remains elusive.

Nanoparticles and proteins serve as attractive complementary building blocks for fabricating ‘bricks and mortar’ hierarchical structures, allowing the incorporation of bio-functionality into nanostructures. These nanoassemblies include discrete lattices,¹⁶ superstructures,¹⁷ and corona-like co-assemblies.¹⁸ These co-assemblies were either built based on self-templating proteins such as viral capsid proteins,¹⁹ or relied on naturally

existing complementary supramolecular interactions between nanomaterials and wild-type proteins, restricting these systems to a relatively narrow range of proteins.

We report here a protein-nanoparticle co-engineering approach that provides programmed self-assembly of dynamic superstructures. These assemblies exhibit multiple layers of structural hierarchy, with an organizational complexity similar to that of membrane-free intracellular assemblies (Figure 3.1). Our initial co-engineered system uses a green fluorescent protein (GFP) bearing a genetically incorporated glutamic acid peptide chain (E-tags). This engineered protein self-assembles with 2 nm core gold nanoparticles carrying arginine-terminated ligands (ArgNP)²⁰ through carboxylate-guanidinium interactions²¹ to generate hierarchical nanostructures guided by electrostatic self-assembly. This assembly process is quite general, as demonstrated through the use of multiple proteins (Figure 3.1e-g).

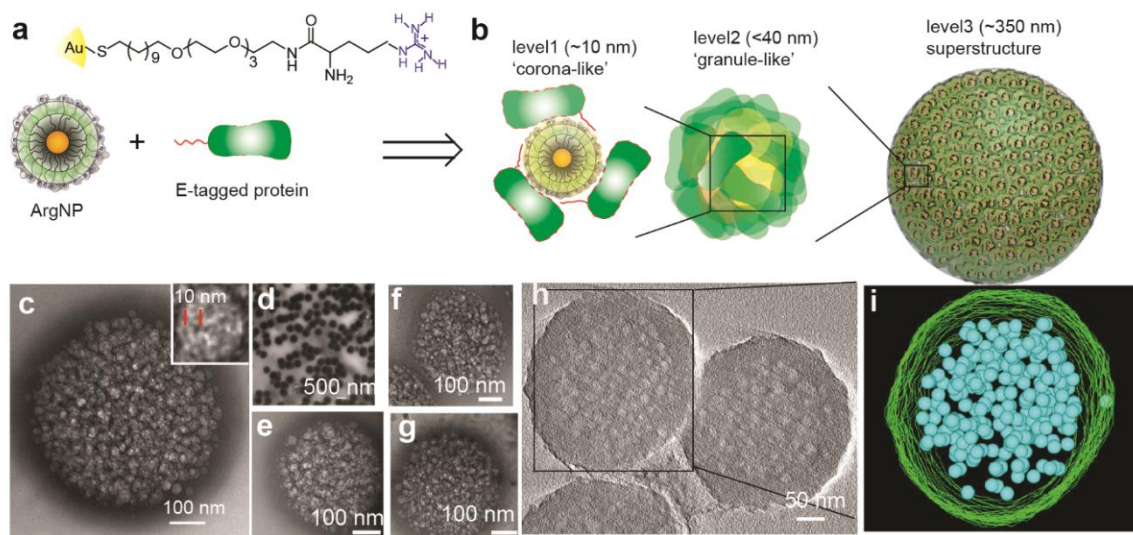


Figure 3. 1. Hierarchical organization of engineered proteins and nanoparticles into complex superstructures. (a) Chemical structure of the arginine functionalized gold nanoparticles ArgNPs, and b, schematic representation of different layers of protein-nanoparticle hierarchical organizations observed in a superstructure. (c) high, and (d) low magnification transmission electron microscopy (TEM) images of the superstructures. Inset in c is TEM image of a single granule in a superstructure, where black and white patches represent ArgNPs and GFP-E10 respectively; red lines represent interparticle center-to-center distance. (e-g) Hierarchical

organization of different proteins with ArgNPs: Histone 2A-E10 (e), Cre recombinase E10 (f), and single chain antibody fragment scFv(ErbB2)-E10 (g). h, A tilt-section of a tomogram; and i, the 3D visualization of a reconstructed superstructure of GFP-E10:ArgNPs in (h), showing the surface (green) and the inner granules (blue).

3.2. Results

Fabrication of hierarchically organized protein-nanoparticle superstructures. In natural systems, controlled multivalency plays an important role in driving self-assembly and in the organization of molecules into higher ordered structures.²² We provided analogous control over our self-assembly process by engineering GFP with a series of different lengths of E-tags (GFP-En, where n= 0 to 20) at the C-terminus of the protein, a technique we previously used to facilitate local interaction between engineered proteins and nanoparticles.³⁸ We initially performed fluorescence titration experiments between GFP-En and ArgNPs at physiologically relevant pH values (PBS, pH 7.4) to find the appropriate GFP variants for effective and dynamic interactions with ArgNPs. As expected, due to its negative overall charge, GFP-E0 exhibits weak binding with ArgNPs, while binding increased as the length of E-tag was increased to E10 (Figure 3.6). GFP-E15 and GFP-E20 were bound poorly to the nanoparticles as compared to GFP-E10, presumably due to non-specific aggregate formation with the higher length of E-tags. We therefore chose GFP-E10 for studying the subsequent assembly formation (Figure 3.6).

Self-organized superstructures were generated by mixing GFP-E10 and ArgNPs at 3:1 (750:250 nM) molar ratio in PBS or in cell culture media (DMEM), and assembling at room temperature for 10 min, followed by a 30-min incubation at 37 °C. The resulting structures were inspected by electron microscopy and small angle X-ray scattering (SAXS)

experiments. Individual nanoparticles (2-nm core diameter) and proteins (ca. 3 nm) co-assembled into large superstructures of ca. 250–350 nm diameter (Figure 3.1c and d). Transmission electron microscopy (TEM) studies at low magnification (Figure 3.1d) showed the formation of uniform superstructures, with higher magnification (Figure 3.1c) revealing magnified structures. Within the superstructures, three distinct layers of hierarchical organization of proteins and nanoparticles were observed. The first layer of hierarchical organization consisted particles surrounded by multiple proteins to produce ‘corona-like’ structures (Figure 3.1b) of ca. 10 nm in overall diameter (Figure 3.1c, inset). These corona-like structures further evolved to produce ‘granule-like’ structures (<40 nm diameter) that comprise the second layer of hierarchical organization (Figure 1c, inset). The average center-to-center particle distance in these granular superstructures is ~10 nm, according to both TEM (Figure 3.1c inset) and SAXS measurements (Figure 3.8). These granular structures then assembled together to produce the final ~250–350 nm diameter superstructures (Figure 3.1b—i). This assembly process is generalizable: E10 tagged proteins featuring different sizes and pI values of the native protein (Histone 2A, pI=10.9, MW=14.1 kDa; Cre recombinase, pI=9.6, MW=38.5 kDa; single chain antibody fragment scFv, pI=8.4, MW=32.3 kDa) all generated hierarchical structures essentially identical to those observed with GFP-E10 (pI=5.9, MW=27 kDa) (Figure 3.1e-g).

Detailed insight into the organized superstructures was obtained using EM tomography. Images of the 3D superstructures were obtained with capture angles from +60° to -60°. Figure 3.10 shows a 3D density map, showing the surface structure of the superstructure. The 3D visualization provided by the reconstructed tomograms showed the packed inner granules (Figure 3.1h—i).

Environmental ionic strength dependent superstructure evolution. We next investigated the mechanism of superstructure formation. Many environmental factors trigger self-organization/re-organization of building blocks in cellular compartments, including pH (*e.g.*, actin polymerization)²³ and ion gradient (*e.g.*, endosomes, neuronal signaling).²⁴ Our system is electrostatic in nature, and is strongly dependent on the concentration of electrolytes in the solution. At low salt concentration (Figure 3.2a, 5 and 10 mM) GFP-E10 and ArgNPs co-assembled to form extended ‘precursor’ clusters, however no superstructure formation was observed. With the increase in salt concentration, these granular precursors continued to evolve and the formation of larger superstructures started appearing at a salt concentration of 20 mM. Complete superstructure formation was observed at 50 mM salt, with no observable free GFP-E10:ArgNPs precursor clusters. The dynamics of the evolution of the assembly can be related to other recently reported assembly formation processes,^{25,26} in which ‘precursor’ clusters, but not individual proteins and particles, serve as the intermediate for the superstructure formation (Figure 3.7). While the morphology of the superstructures remained the same above 50 mM salt solutions, the size increased with increasing salt concentration of the solution (Figure 3.2a). An electrolyte-dependent-assembly evolution process was also supported by SAXS measurements (Figure 3.2b; Figure 3.8). With increasing ionic strength, a gradual increase in the peak intensity at $1/q$ ca. 0.06 \AA was observed, corresponding to the interparticle center-to-center distance ($d_{\text{NP-NP}}$), which resulted from assembly formation. The peak intensity reached saturation at 50 mM salt concentration, indicating complete superstructure formation, consistent with that observed by TEM measurements.

The electrolyte dependence of GFP-E10:ArgNPs superstructure formation can be qualitatively rationalized by electrical double layer formation around GFP-E10:ArgNPs clusters (Figure 3.7 red boxes).^{16,27,28} The magnitude of the electrical double layer is dependent on Debye screening length (κ^{-1}), where κ^{-1} is inversely related to the ionic strength of the solution (Experimental section). When ionic strength increases, κ^{-1} decreases; reducing the electrical double layer repulsion between GFP-E10:ArgNPs precursor clusters. At specific concentrations of salt, the double-layer repulsion becomes minimal, forcing the clusters to collapse to form a superstructure (Figure 3.2d; Discussions). The superstructure formation is further dictated by GFP-E10, as the polyvalency of the counterion is critical for the initial cluster formation (Figure 3.5d)²⁹ (Discussions); this behavior demonstrates the importance of co-engineering of nanoparticles and proteins for building these hierarchical superstructures.

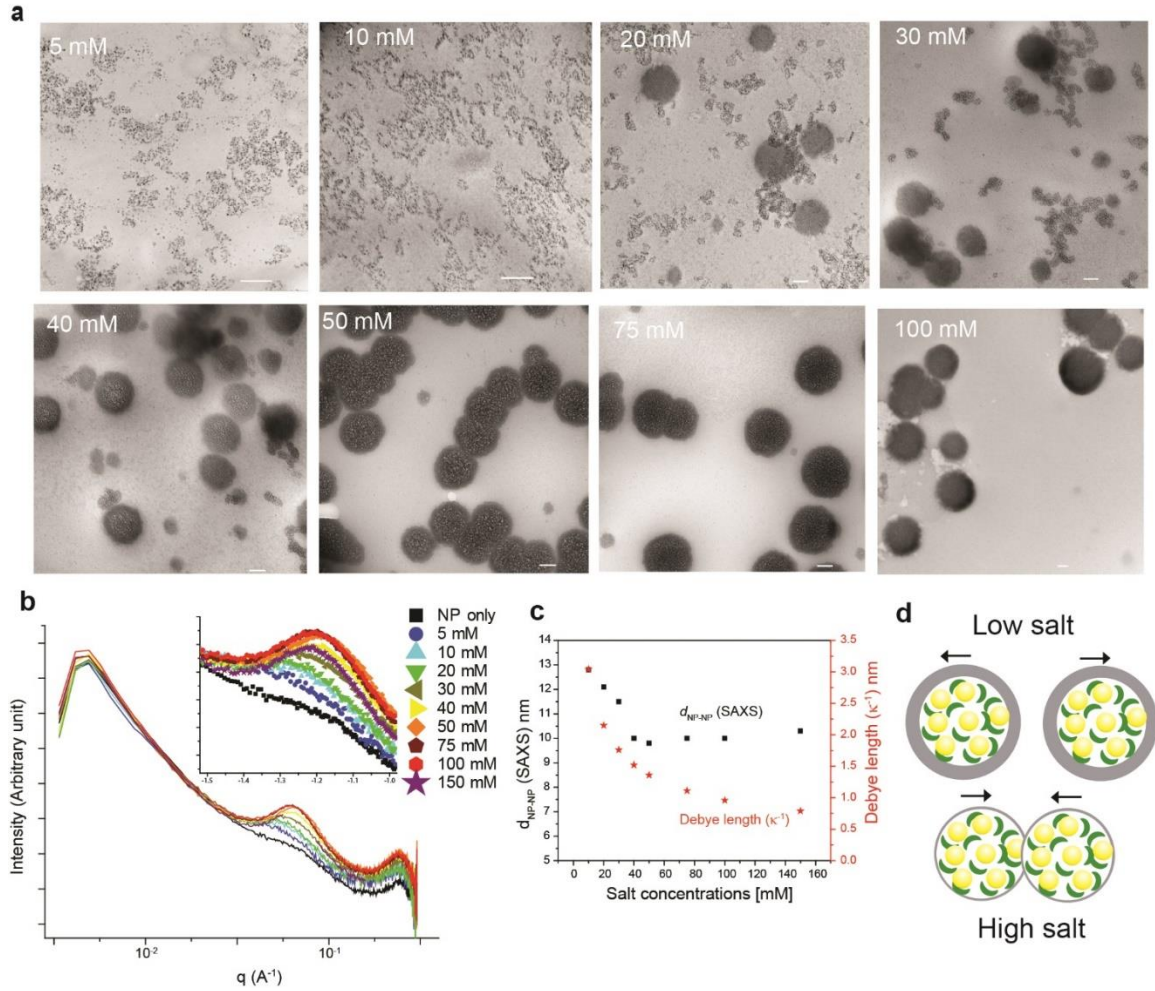


Figure 3. 2. Superstructure evolution triggered by environmental ionic strength. (a) TEM images of salt-induced superstructures between GFP-E10 and ArgNPs. Scale bar: 100 nm. (b) SAXS inspection of superstructure formation at various salt concentrations showing the gradual intensity enhancement and a shift in q value arising from superstructure formation. (c) Comparison of inter-particle distance ($d_{\text{NP-NP}}$) of the assemblies with theoretical Debye length (κ^{-1}) at different salt concentrations. (d) Physical principle governing superstructure formation. Yellow and green at the core are ArgNPs-proteins ‘clusters’ and the gray shell represents the Debye screening layer respectively.

SAXS experiments further provided evidence for the electrolyte dependence of GFP-E10:ArgNPs superstructure formation, as the reduction in κ^{-1} of ArgNPs correlated with increasing electrolyte concentration. As shown in Figure 3.2b (inset), with increasing ionic strength, the peak corresponding to $d_{\text{NP-NP}}$ shifted towards a higher q value, which is indicative of the reduction in κ^{-1} values of ArgNPs. It is noteworthy that higher q value

signifies a decrease in the $d_{\text{NP-NP}}$ distance that is anticipated with the reduction of Debye screening length of the ArgNPs. We measured the $d_{\text{NP-NP}}$ from these SAXS peaks and compared with the theoretical κ^{-1} values as a function of salt concentration (Figure 3.2c; Figure 3.8). As ionic strength increased, $d_{\text{NP-NP}}$ dropped until it reached a saturation point at 50 mM salt concentration. On the contrary, theoretical κ^{-1} values continued to decrease beyond 50 mM salts; this discrepancy is presumably due to the steric "locking in" of the ArgNPs upon completion of superstructure formation (at 50 mM salt concentration). In the resulting assembly, there is no further room for the particles to come closer, a factor not accounted for in theoretical calculations of κ^{-1} . A slight increase in $d_{\text{NP-NP}}$ was observed beyond 50 mM salt concentration, which presumably arises from the molecular reorganization of the building blocks within the superstructure (Figure 3.3). Taken together, these experiments indicate that complementarity and multivalency between building blocks are essential, but not sufficient for the evolution of higher ordered complex assemblies, and that environmental triggers play a decisive role for such processes.

Dynamic and spatial organization of the superstructure components. Electrolytes govern the dynamic and spatial reorganization of the building blocks in these superstructures. As ionic strength was raised beyond 40 mM salt, the components within the superstructures undergo organizational transformation. At 40 mM salt, GFP-E10 and ArgNPs assembled into corona-like structures within the superstructure; these structures represent lower level molecular organization (Figure 3.3a, 40 mM). The size of an individual corona structure is ca. 11 nm in diameter (Figure 3.3b, 40 mM, marked by a red arrow, and in the inset), which suggests a corona composition of one particle at the core surrounded by ~3 proteins. As the salt concentration increased to 75 or 100 mM, multiple

GFP-E10:ArgNPs coronas coalesced to form bigger granular structures of ~20 nm in diameter. When salt concentration was increased to 150 mM, further condensation of GFP-E10:ArgNPs was observed, with the size of these granules increasing to ~40 nm in diameter (Figure 3.3b—c at 150 mM).

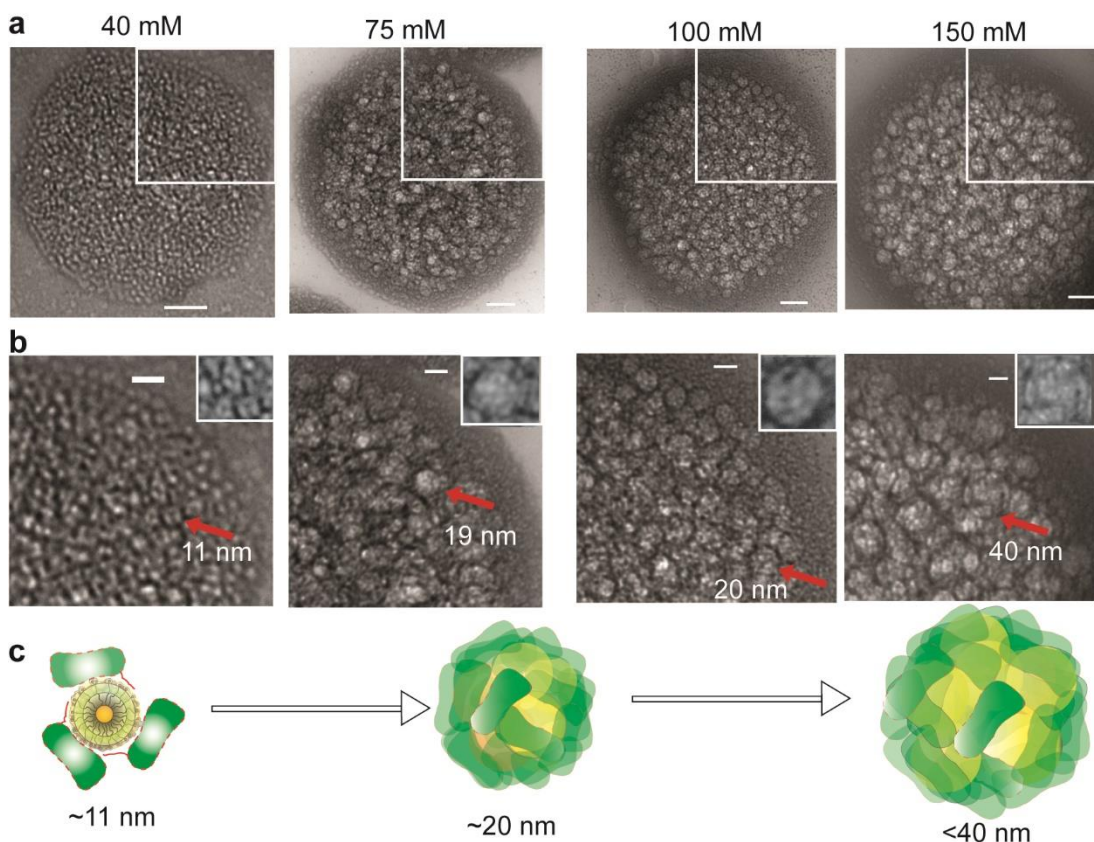


Figure 3. 3. Dynamic reorganization of the superstructure components. (a) High magnification TEM images of superstructures at different salt concentrations Scale bar: 50 nm. (b) A portion of each image from (a) was magnified. Scale bar: 20 nm. Individual nanoparticles (black) were surrounded by about three proteins (white) to form corona or granules as shown by red arrows. Inset showing enlarged corona (40 mM) or granules (75, 100, and 150 mM). (c) Schematics showing the molecular reorganization of the superstructure components as salt concentration increased. Yellow and green represent ArgNPs and GFP-E10, respectively.

3.3. Conclusions

In summary, we have demonstrated that co-engineering of proteins and nanoparticles can be used to generate complex hierarchical assemblies with sophisticated structural and dynamic properties. The dynamic arrangement of the components within the superstructures is highly responsive to environmental stimuli. The ability to fabricate complex structures in this fashion presents systems for studying emergent behavior, as well as pursuing pragmatic applications including therapeutic delivery,³⁰ catalysis, and photosynthetic energy harvesting.³¹

3.4. Discussions

Electrolyte dependent higher order superstructure formation. The stability of colloidal micro particles (μP) in solution can be explained through classical **Derjaguin-Landau-Verwey-Overbeek (DLVO)** theory.³² DLVO theory, in its simplest form, takes account for the electrostatic repulsion and van der Waal's interactions between particles in solution. Briefly, the overall potential of μPs in solution is given by sum of repulsive and attractive forces:

$$V_r = V_{\text{el}} + V_{\text{vdW}}$$

Where V_r is the overall potential at a 'r' center-to-center distance, V_{el} is the electrostatic repulsion, and V_{vdW} is the van der Waals (vdW) attraction between the particles. V_{el} is determined by the Debye electrical double layer around the particles. At low salt concentration, when the Debye screening length is reasonably high, the repulsive and the

attractive forces counterstabilize the particles in solutions. However, when the salt concentration increases, the Debye electrical double layer shrinks and the attractive vdW forces dominate over the electrical double layer repulsion, causing the particles to aggregate in solution. As mentioned, this is the simplest explanation of microparticle stability in solution by DLVO theory. In practice, however, due to complex nature of forces arising from interacting particles, modified DLVO theories are generated (extended-DLVO theory).³³

Although the forces between nanoparticles (NPs) in solution remain same with μ Ps, classical DLVO theory fails to explain NP colloidal stability.²⁸ The repulsive and the attractive forces of DLVO theory (V_E and V_{vdW}) may not be simply ‘added’ to predict the stability of NPs in solution: Kotov and his coworkers described this property as ‘Nonadditivity of nanoparticle interactions’.²⁸ There are numerous assumptions why nonadditivity of NPs interactions exist. For example, when the size of the particles is only a few nanometers, the size of the counterions (solvated ions) in the electrical double layer cannot be considered as point particles which is in the case of DLVO theory. Other reasons of nonadditivity include: a) inorganic NPs are often functionalized with organic ligands to provide an interfacial layer that protect the core NPs. Thus, the inorganic core of the NPs and the surrounding interfacial organic layer cannot be assumed as uniform continua. b) NPs are often made from metals and semiconductors that have high polarizability. Collectively—dimensionality, topology, and polarizability—all contribute towards nonadditivity of NPs interactions.

Several studies have shown that stability of NPs of size 50 nm or larger can be predicted by DLVO theory.^{34,35} Very recently, vdW interaction at ‘nanoscale’ between

complex nanostructures such as proteins and nanowire have been predicted.³⁶ Thus, it is evident that the additive properties of various forces of DLVO theory may not accurately predict NP aggregation, nonetheless, these very forces play major roles in stability or aggregation of these particles. Therefore, the contribution of vdW forces is crucial for NPs assembly. In fact, by increasing the electrolyte concentration to minimize the electrical double layer of nanoparticles Kostiainen *et. al.* has managed to fabricate 2D crystal lattice like structures from these NPs.¹⁶ In another example, Grzybowski and his coworkers fabricated diamond-like lattice structures from oppositely charged binary nanoparticles by manipulating forces at nanoscale.^{27,37}

In the light of above theoretical and experimental background, a partial explanation for higher order nanoparticle aggregation by our system can be provided. As mentioned in the manuscript our ArgNPs have a core size of ~2 nm diameter and ~3-4 nm of interfacial ligands surrounding the core. The dimension and the lack of uniform continua make the ArgNPs deviate from DLVO prediction of colloidal stability. Indeed, when the salt concentration of ArgNP solution was increased to 150 mM to reduce the Debye screening length, the particles were still stable and did not aggregate (Figure 3.5b) in contrary to DLVO prediction for μP . As E-tagged proteins are added to ArgNPs solution at low salt concentration, the binary protein-nanoparticles started forming small aggregates *via* simple electrostatic interactions that we called ‘precursor clusters’. The size of these clusters is ~30-40 nm in diameter (Figure 3.5d; Figure 3.7; 5, 10, and 20 nm; red box). [Note that these clusters may be the basis of the granule structures (2nd level of assembly) that are observed at higher salt concentration. Also, the first layer of hierarchical assembly *i.e.* the corona-like structures are buried within these clusters and they may not exist as

independent entity in our study.] When the salt concentration is increased the electrical double layer around these clusters is expected to shrink, resulting in reduced electrostatic repulsion between the clusters. At this point, the dominating attractive forces (*i.e.* vdW and other undetermined attractive forces, though they do not obey additivity) may trigger the clusters to collapse together to form the superstructures (3rd layer of hierarchical assembly).

We must point out here though is that the explanation we provided for higher order hierarchical assembly formation by our system is a simplistic version. In reality, further theoretical and computational assistance are required to fully understand the aggregation mechanism.

Importance of the ligand on the surface of gold nanoparticles. A single gold nanoparticle (AuNP) accommodates hundreds of arginine-functionalized thiol ligands (HS-C11-TEG-NH-Arginine) on its surface (Figure 3.4). The resultant AuNPs acquires multivalency, prerequisite for a strong supramolecular interaction with E-tagged proteins. In contrast, if only a single ligand (Figure 3.4, compound 7) is used, the interaction with E-tagged proteins will not be strong enough for assembly formation.

Different components of the ligand are also crucial for the stability and function of the particles. As shown in Figure 3.4, the thiol (HS) group pins the ligand to the gold surface, the hydrophobic C11 group stabilizes the nanoparticle, the tetraethylene glycol (TEG) moiety confers biocompatibility on the particle, and the arginine head group dictates the interaction with E-tagged proteins through supramolecular arginine–carboxylate interactions.

Influence of counter ion on superstructure formation- Schulze-Hardy rule.

Coagulation of colloidal particle is driven by the charge state of the oppositely charged counter ions.²⁹

Critical concentration of coagulation (C_{crit}) is given by-

$$C_{crit} \propto \text{Constant}/Z^6$$

where,

Z is the valence state of the counter ion (GFP-E10, in our case).

3.5. Experimental section

Nanoparticle engineering. Arginine-functionalized gold nanoparticles (ArgNPs) were prepared according to our previous methods.²⁰ Briefly, the arginine-functionalized thiol ligand was synthesized first (Figure 3.4a). Nanoparticles were subsequently prepared by conventional place-exchange reaction of 2-nm sized 1-pentanethiol-protected gold nanoparticles (Au-C5) with HS-C11-TEG-NH-Arginine (Compound 7) ligand (Figure 3.4b). The resultant ArgNPs were dissolved in distilled water, purified by dialysis, and characterized (Figure 3.5).

Engineering E-tagged proteins. Engineering of GFP-En (where n is the number of glutamic acids) and protein expression were done according to standard protocols. GFP gene was PCR-amplified and cloned into a bacterial expression vector (pQE80) with 6×His at the N-terminus. The following primers were used to amplify GFP gene:

Forward primer: ACGATGGATCCATGGTGAGCAAGGG

Reverse primers:

GFP-E0: GTGTAAGCTTTTACTTGTACAGCTC

affect the protein expression and purification, and the yield was equivalent to the expression of wild-type GFP.

E10-tagged Histone 2A, Cre recombinase, and single chain antibody fragment scFv (scFv-anti-ErbB2) was similarly cloned and expressed in *E. coli* BL21 Rosetta strain.

Fluorescence titration. Fluorescence titration experiments between nanoparticles and GFP-En were carried out as described previously.³⁸ Briefly, the change of fluorescence intensity of GFP-En at 510 nm was measured with an excitation wavelength of 475 nm at various concentrations of nanoparticles from 0 to 400 nM on a Molecular Devices SpectraMax M3 microplate reader (at 25 °C). Quenching of fluorescence intensity arising from 100 nM GFP-En was observed with increasing nanoparticle concentration. Nonlinear least-squares curve fitting analysis was carried out to estimate the binding constant (K_S) and association stoichiometry (n , $[GFP-En]/[ArgNP]$) by using a one-site binding model.³⁹

Superstructure fabrication. GFP-En:ArgNPs superstructures were prepared through a simple mixing procedure. ArgNPs (50 μ M stock in 5 mM PB, pH 7.4) were added to 100 μ L of 1 \times PBS, followed by adding GFP-En (50 μ M stock in 5 mM PB, pH 7.4) at appropriate molar ratio [usually at 1:3 ratio (ArgNP, 250 nM)/(GFP-En, 750 nM) for most of the applications]. The complex was incubated at room temperature for 10 min. DMEM media (low glucose) or 1 \times PBS (or pure NaCl solution) was added to the complex to make the final volume up to 500 μ L. For the salt concentration-dependent assembly studies proteins and NPs were initially mixed in 5 mM PB, then the salt concentration was gradually adjusted by adding required salt solution. The superstructures were then incubated at 37 °C for 30 min for TEM, and SAXS studies.

Superstructures of other proteins were similarly fabricated using following molar ratios: H2A-E10:ArgNPs (3:1); Cre recombinase-E10:ArgNPs (1:2); and scFv-E10:ArgNPs (1:2).

Transmission electron microscopy (TEM). 10 μ L of the superstructure solution was drop-cast on to a TEM grid (carbon film- 400 mesh copper, electron microscopy sciences) and the sample allowed to dry at room temperature overnight. Superstructures were inspected by using JEOL 2000FX TEM.

TEM Tomography, reconstruction of tomographic tilt series, and 3D modelling. TEM Tomography was performed using JEOL 2200FX TEM. Samples were prepared similarly as for regular TEM in grids (carbon film—150 mesh copper). Tilt series were acquired from -60° to $+60^\circ$. Reconstructed tomograms were generated using IMOD/eTomo interface acquisition systems. For 3D visualization, reconstructed tomograms were further segmented and modelled using 3dmod. The 3D density maps of the corresponding tomograms were generated using UCSF Chimera.⁴⁰

Small angle X-ray scattering (SAXS). GFP-E10:ArgNPs superstructure samples for SAXS experiments were prepared as described above, with slight modifications. Briefly, ArgNPs (50 μ M stock in 5 mM PB, pH 7.4) were added to 20 μ L of PB such that the final concentration of nanoparticles became 2 μ M in 200 μ L volume. Then GFP-E10 (50 μ M stock in 5 mM PB, pH 7.4) was added into the nanoparticle solution (final protein concentration = 6 μ M). Superstructures were allowed to form at room temperature for 10 min; then for 30 min after making up the volume to 200 μ L with appropriate buffer with necessary salt concentration. 75 μ L of each sample was drop-cast on a kapton film and allowed to dry at room temperature. Alternatively, solution samples were prepared by

placing 100–200 μL of the superstructure solution into SAXS sample holder between two mica sheets. Samples were analyzed by using Ganesha SAXS-LAB (Northampton, Massachusetts).

Calculation of Debye screening length (κ^{-1}). κ^{-1} was calculated using following equation.¹⁶

$$\kappa^{-1} = \sqrt{\frac{\epsilon_0 \epsilon_r k_b T}{e^2 \sum_i c_i z_i^2}}$$

where,

κ^{-1} = Debye screening length

ϵ_0 = Vacuum permittivity

ϵ_r = Dielectric constant of solvent (water)

k_b = Boltzmann constant

T = Absolute temperature

e = Elementary charge

c_i = Concentration of electrolyte ions (NaCl)

z_i = Valencies of electrolyte ions

3.6. Supporting figures

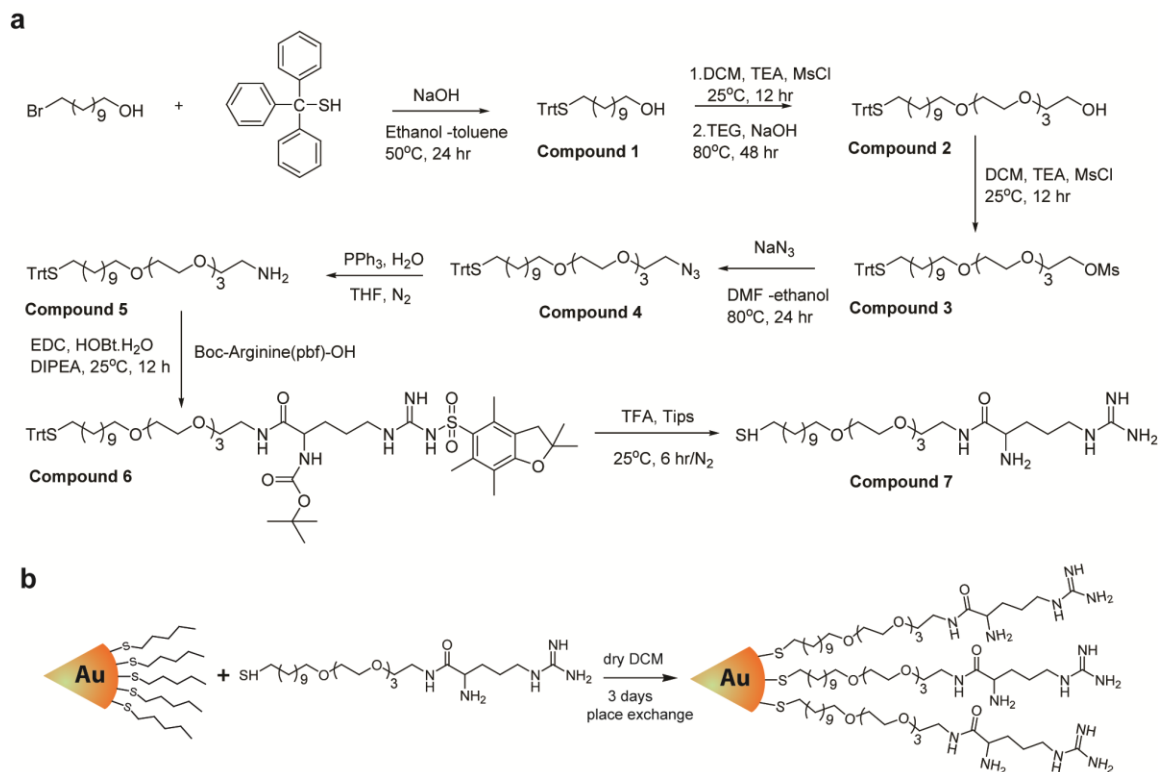


Figure 3. 4. Schemes for the synthesis of ArgNPs. a, the synthesis and the chemical structure of arginine ligand (Compound 7), and b, place exchange for preparing gold nanoparticles (ArgNPs).

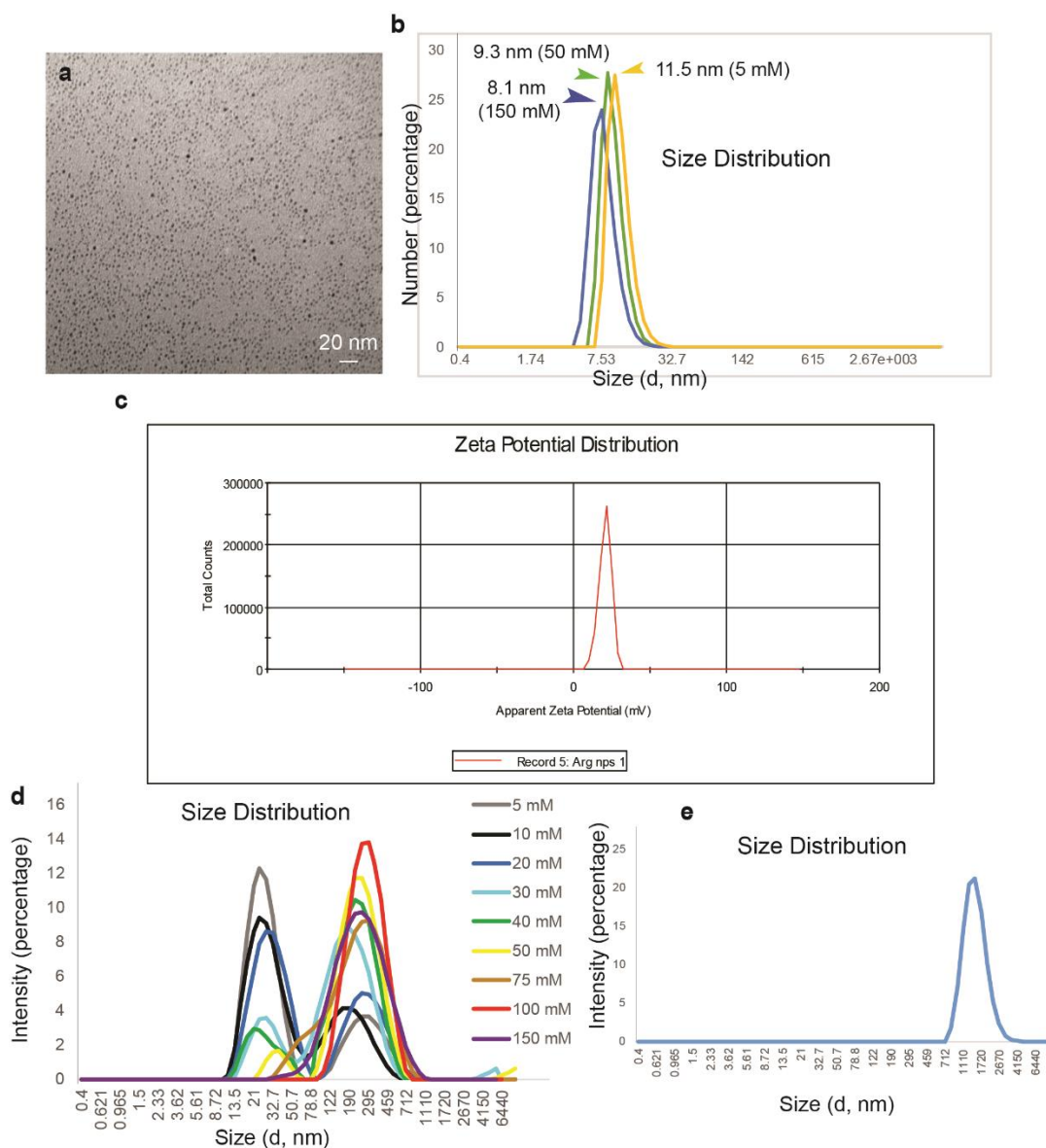


Figure 3. 5. Characterization of ArgNPs and GFP-E10:ArgNP assemblies. a, TEM image of ArgNPs. b, DLS measurement indicating the hydrodynamic size of ArgNPs at various salt concentrations. The hydrodynamic size of nanoparticles decrease as the salt concentration increases due to the reduction of Debye electrical double layer. c, Electrokinetic potential (+20.8 mV) of ArgNPs. d, DLS size distribution of GFP-E10:ArgNPs assembly at various salt concentrations. The gradual formation of superstructures (<300 nm, diameter) from intermediate precursors (~30 nm, diameter) was observed as the salt concentration was increased (also see Figure 3.2). e, DLS size of GFP-E10:ArgNPs assembly at high salt concentration (300 mM) showing large aggregation.

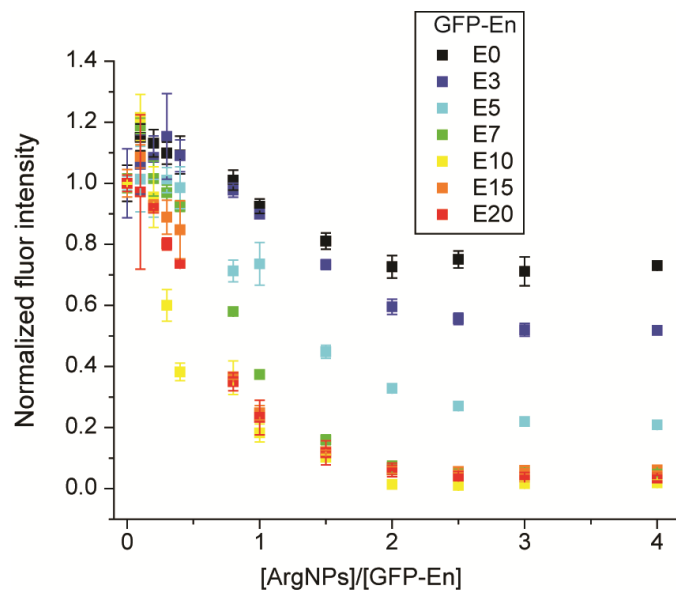


Figure 3. 6. Titration of GFP-En with ArgNPs. Fluorescence titration between GFP-En (100 nM) and ArgNPs (0-400 nM) under physiologically relevant conditions (150 mM salt, pH 7.4). As the length of E-tag on GFP was increased the interaction with ArgNPs increased, reaching a maximum at E10 (GFP-E10). Surprisingly, investigation of binding affinity revealed that GFP-E15 and GFP-E20 bound poorly to nanoparticles compared to GFP-E10, presumably due to the aggregation formation at higher length of E-tag. The binding constant ($K_s=2.4\pm0.2 \times 10^8 \text{ M}^{-1}$) and binding ratio ($n=2.9$) between GFP-E10 and ArgNPs was determined by using an algorithm as described previously.³⁹

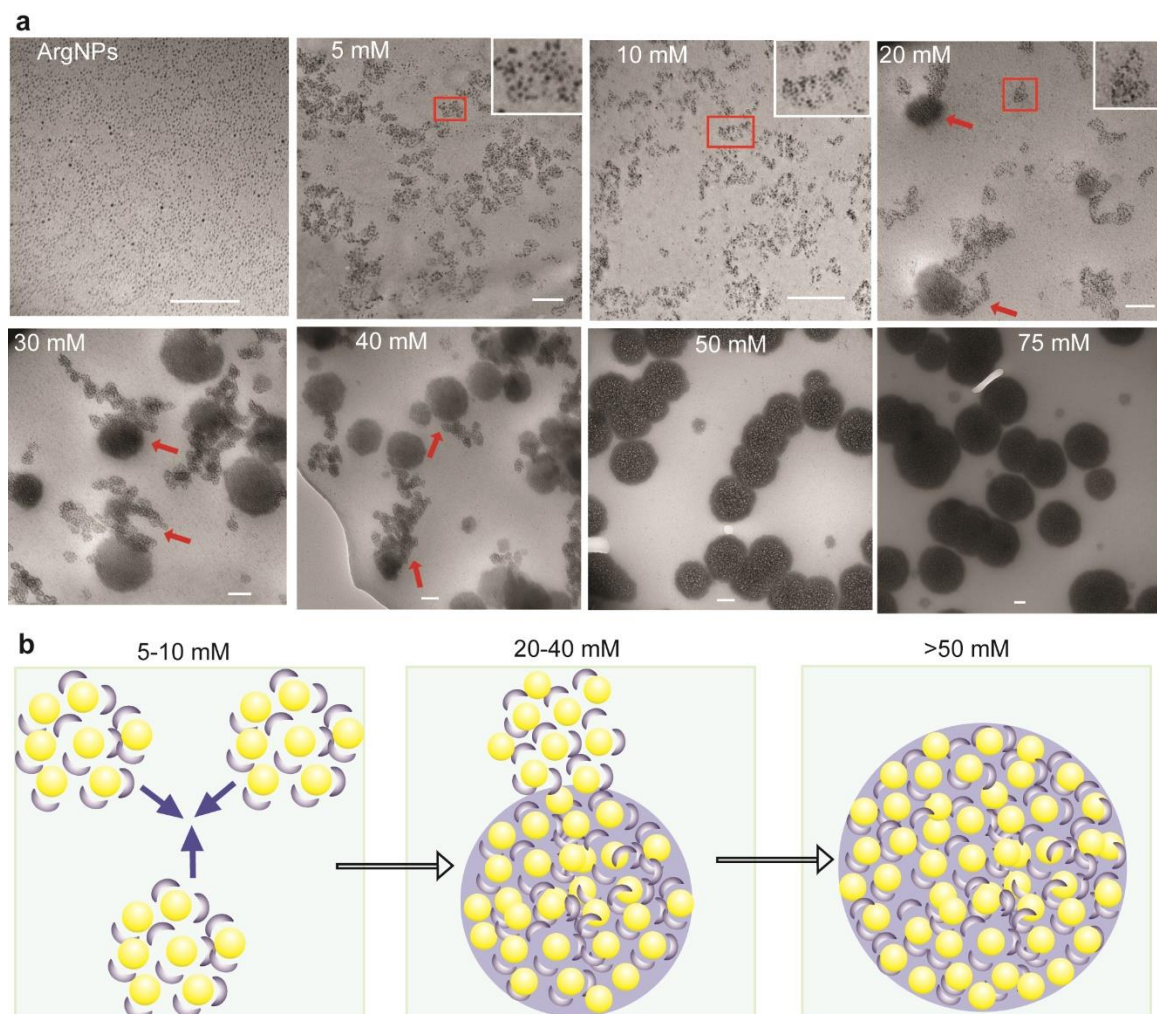


Figure 3. 7. ‘Precursor’ based growth dynamics (evolution) of superstructures. a, At low salt concentration (5–10 mM), GFP-E10 and ArgNPs assembled to form cluster-like precursors (red box) for superstructure growth. However, as salt concentration increased beyond 10 mM, these precursor clusters condensed and continuously evolved (red arrow) to form larger superstructures. b, A model for superstructure evolution. These growth dynamics are similar to the growth of natural minerals such as silicate-1 that was recently reported by Lupulescu *et al.*²⁵

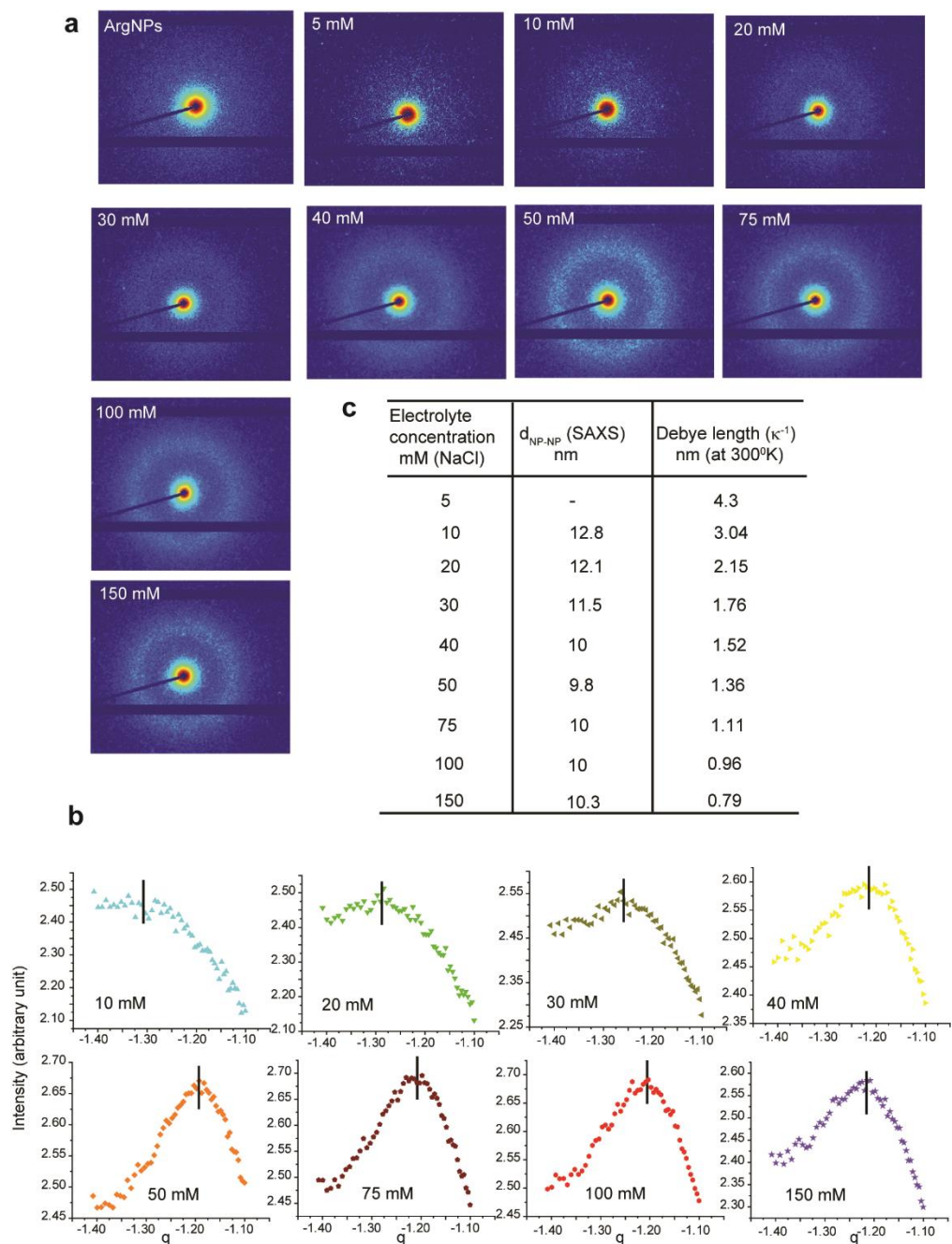


Figure 3. 8. Small angle X-ray scattering (SAXS) investigation of superstructure formation. **a**, SAXS 2D-scattering data showing gradual GFP-E10:ArgNPs superstructure formation with increasing salt concentration indicated by a ring arising from the spacing of particles in the superstructure. **b**, 1D-scattering peak corresponding to the ring in (a). The peaks indicate the interparticle center-to-center distance (d_{NP-NP}). **c**, Comparison of d_{NP-NP} with Debye screening length (κ^{-1}) at different salt concentrations.

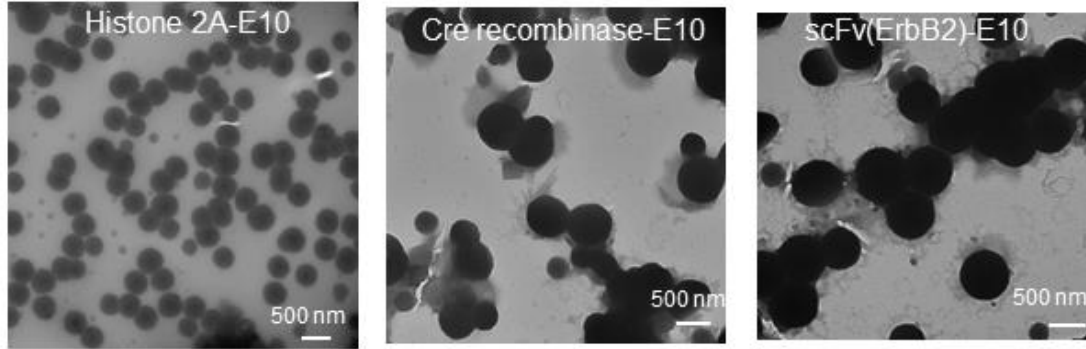


Figure 3. 9. Superstructure formation by different E-tagged proteins, featuring similar structure and dynamic properties as of GFP-E10. An E10 tag was attached to proteins having different pI and molecular weight [Histone 2A (native pI=10.9, MW=14.1 kDa); Cre recombinase (native pI=9.6, MW=38.5 kDa); and a single chain antibody fragment scFv(ErbB2) (native pI=8.4, MW=32.3 kDa)]. Superstructures were fabricated similar to that of GFP-E10 and was investigated by TEM.

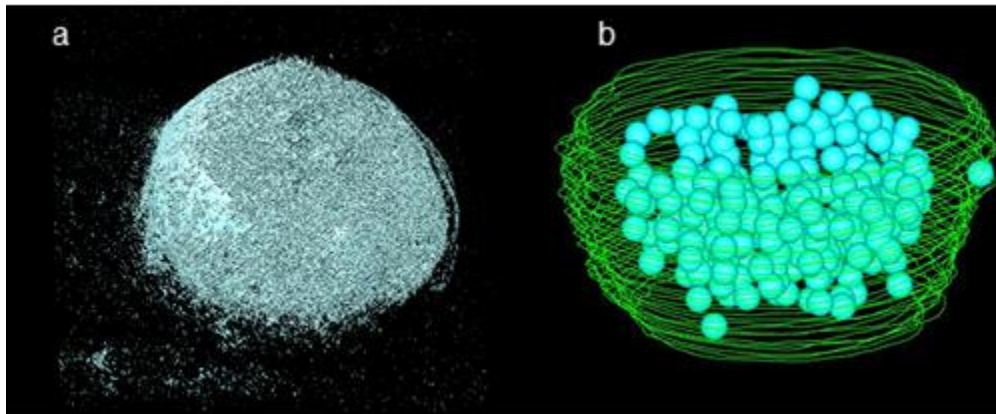


Figure 3. 10. 3D visualization of the GFP-E10:ArgNPs superstructures. a, 3D density map showing the surface structure of the superstructure. b, Front view of a reconstructed superstructure, showing the surface (green) and the inner granules (blue).

3.7. References

- (1) Karsenti, E. Self-Organization in Cell Biology: A Brief History. *Nat. Rev. Mol. Cell Biol.* **2008**, *9*, 255-262.
- (2) Whitesides, G. M.; Grzybowski, B. Self-Assembly at all Scales. *Science* **2002**, *295*, 2418-2421.
- (3) Chung, W. J.; Oh, J. W.; Kwak, K.; Lee, B. Y.; Meyer, J.; Wang, E.; Hexemer, A.; Lee, S. W. Biomimetic Self-Templating Supramolecular Structures. *Nature* **2011**, *478*, 364-368.
- (4) Campbell, N. A.; Reece, J. B. *Biology*, 6th edition, Benjamin Cummings, **2002**.
- (5) Gröschel, A. H.; Walther, A.; Löbbling, T. I.; Schacher, F. H.; Schmalz, H.; Müller, A. H. Guided Hierarchical Co-Assembly of Soft Patchy Nanoparticles. *Nature* **2013**, *503*, 247-251.
- (6) Keber, F. C.; Loiseau, E.; Sanchez, T.; DeCamp, S. J.; Giomi, L.; Bowick, M. J.; Marchetti, M. C.; Dogic, Z.; Bausch, A. R. Topology and Dynamics of Active Nematic Vesicles. *Science* **2014**, *345*, 1135-1139.
- (7) Macfarlane, R. J.; Lee, B.; Jones, M. R.; Harris, N.; Schatz, G. C.; Mirkin, C. A. Nanoparticle Superlattice Engineering with DNA. *Science* **2011**, *334*, 204-208.
- (8) King, N. P.; Bale, J. B.; Sheffler, W.; McNamara, D. E.; Gonen, S.; Gonen, T.; Yeates, T. O.; Baker, D. Accurate Design of Co-Assembling Multi-Component Protein Nanomaterials. *Nature* **2014**, *510*, 103-108.
- (9) Gonen, S.; DiMaio, F.; Gonen, T.; Baker, D. Design of Ordered Two-Dimensional Arrays Mediated by Noncovalent Protein-Protein Interfaces. *Science* **2015**, *348*, 1365-1368.
- (10) Mou, Y.; Yu, J. Y.; Wannier, T. M.; Guo, C. L.; Mayo, S. L. Computational Design of Co-Assembling Protein-DNA Nanowires. *Nature* **2015**, *525*, 230-233.
- (11) Boal, A. K.; Ilhan, F.; DeRouchey, J. E.; Thurn-Albrecht, T.; Russell, T. P.; Rotello, V. M. Self-Assembly of Nanoparticles into Structured Spherical and Network Aggregates. *Nature* **2000**, *404*, 746-748.
- (12) Erb, R. M.; Son, H. S.; Samanta, B.; Rotello, V. M.; Yellen, B. B. Magnetic Assembly of Colloidal Superstructures with Multipole Symmetry. *Nature* **2009**, *457*, 999-1002.

- (13) Singh, G.; Chan, H.; Baskin, A.; Gelman, E.; Reppin, N.; Král, P.; Klajn, R. Self-Assembly of Magnetite Nanocubes into Helical Superstructures. *Science* **2014**, *345*, 1149-1153.
- (14) Qiu, H.; Hudson, Z. M.; Winnik, M. A.; Manners, I. Multidimensional Hierarchical Self-Assembly of Amphiphilic Cylindrical Block Comicelles. *Science* **2015**, *347*, 1329-1332.
- (15) Tan, K. W.; Jung, B.; Werner, J. G.; Rhoades, E. R.; Thompson, M. O.; Wiesner, U. Transient Laser Heating Induced Hierarchical Porous Structures from Block Copolymer-Directed Self-Assembly. *Science* **2015**, *349*, 54-58.
- (16) Kostiaainen, M. A.; Hiekkataipale, P.; Laiho, A.; Lemieux, V.; Seitsonen, J.; Ruokolainen, J.; Ceci, P. Electrostatic Assembly of Binary Nanoparticle Superlattices Using Protein Cages. *Nat. Nanotechnol.* **2013**, *8*, 52-56.
- (17) Park, J. I.; Nguyen, T. D.; de Queirós Silveira, G.; Bahng, J. H.; Srivastava, S.; Zhao, G.; Sun, K.; Zhang, P.; Glotzer, S. C.; Kotov, N. A. Terminal Supraparticle Assemblies from Similarly Charged Protein Molecules and Nanoparticles. *Nat. Commun.* **2014**, *5*, 3593.
- (18) Bayraktar, H.; You, C. C.; Rotello, V. M.; Knapp, M. J. Facial Control of Nanoparticle Binding to Cytochrome C. *J. Am. Chem. Soc.* **2007**, *129*, 2732-2733.
- (19) Douglas, T.; Young, M. Viruses: Making Friends with Old Foes. *Science* **2006**, *312*, 873-875.
- (20) Yang, X. C.; Samanta, B.; Agasti, S. S.; Jeong, Y.; Zhu, Z. J.; Rana, S.; Miranda, O. R.; Rotello, V. M. Drug Delivery Using Nanoparticle-Stabilized Nanocapsules. *Angew. Chem. Int. Ed.* **2011**, *50*, 477-481.
- (21) Wiskur, S. L.; Lavigne, J. J.; Metzger, A.; Tobey, S. L.; Lynch, V.; Anslyn, E. V. Thermodynamic Analysis of Receptors Based on Guanidinium/boronic Acid Groups for the Complexation of Carboxylates, Alpha-Hydroxycarboxylates, and Diols: Driving Force for Binding and Cooperativity. *Chemistry* **2004**, *10*, 3792-804.
- (22) Li, P.; Banjade, S.; Cheng, H. C.; Kim, S.; Chen, B.; Guo, L.; Llaguno, M.; Hollingsworth, J. V.; King, D. S.; Banani, S. F.; Russo, P. S.; Jiang, Q. X.; Nixon, B. T.; Rosen, M. K. Phase Transitions in the Assembly of Multivalent Signalling Proteins. *Nature* **2012**, *483*, 336-340.
- (23) Wang, F.; Sampogna, R. V.; Ware, B. R. pH Dependence of Actin Self-Assembly. *Biophys. J.* **1989**, *55*, 293-298.

- (24) Scott, C.C.; Gruenberg, J. Ion Flux and the Function of Endosomes and Lysosomes: pH is Just the Start: The Flux of Ions Across Endosomal Membranes Influences Endosome Function not only Through Regulation of the Luminal pH. *Bioessays* **2011**, *33*, 103-110.
- (25) Lupulescu, A. I.; Rimer, J. D. *In Situ* Imaging of Silicalite-1 Surface Growth Reveals the Mechanism of Crystallization. *Science* **2014**, *344*, 729-732.
- (26) Van Driessche, A. E.; Benning, L. G.; Rodriguez-Blanco, J. D.; Ossorio, M.; Bots, P.; García-Ruiz, J. M. The Role and Implications of Bassanite as a Stable Precursor Phase to Gypsum Precipitation. *Science* **2012**, *336*, 69-72.
- (27) Kalsin, A. M.; Fialkowski, M.; Paszewski, M.; Smoukov, S. K.; Bishop, K. J.; Grzybowski, B. A. Electrostatic Self-assembly of Binary Nanoparticle Crystals with a Diamond-Like Lattice. *Science* **2006**, *312*, 420-424.
- (28) Batista, C. A.; Larson, R. G.; Kotov, N. A. Nonadditivity of Nanoparticle Interactions. *Science* **2015**, *350*, 1242477.
- (29) Lyklema, J. Coagulation by Multivalent Counterions and the Schulze-Hardy Rule. *J. Colloid Interface Sci.* **2013**, *392*, 102-104.
- (30) Mout, R.; Ray, M.; Tonga, G. Y.; Lee, Y.-W.; Tay, T.; Sasaki, K.; Rotello, V. M. Direct Cytosolic Delivery of CRISPR/Cas9-Ribonucleoprotein for Efficient Gene Editing. *ACS Nano*, **2017**, *11*, 2452-2458.
- (31) Mout, R.; Moyano, D. F.; Rana, S.; Rotello, V. M. Surface Functionalization of Nanoparticles for Nanomedicine. *Chem. Soc. Rev.* **2012**, *41*, 2539-2544.
- (32) Verwey, E.J.; Overbeek, J.T.G. Theory of the Stability of Lyophobic Colloids. Elsevier, Amsterdam, **1948**.
- (33) Boström, M.; Deniz, V.; Franks, G. V.; Ninham, B. W. Extended DLVO Theory: Electrostatic and Non-Electrostatic Forces in Oxide Suspensions. *Adv. Colloid. Interface Sci.* **2006**, *123-126*, 5-15.
- (34) Eichmann, S. L.; Anekal, S. G.; Bevan, M. A. Electrostatically Confined Nanoparticle Interactions and Dynamics. *Langmuir* **2008**, *24*, 714-721.
- (35) Ducker, W. A.; Senden, T. J.; Pashley, R. M. Direct Measurement of Colloidal Forces Using an Atomic Force Microscope. *Nature* **1991**, *353*, 239-241.
- (36) Ambrosetti, A.; Ferri, N.; DiStasio, R. A. Jr.; Tkatchenko, A. Wave-Like Charge Density Fluctuations and van der Waals Interactions at the Nanoscale. *Science* **2016**, *351*, 1171-1176.

(37) Bishop, K. J.; Wilmer, C. E.; Soh, S.; Grzybowski, B. A. Nanoscale Forces and their uses in Self-Assembly. *Small* **2009**, *5*, 1600-1630.

(38) Mout, R.; Tonga, G. Y.; Ray, M.; Moyano, D. F.; Xing, Y.; Rotello, V. M. Environmentally Responsive Histidine-Carboxylate Zipper Formation Between Proteins and Nanoparticles. *Nanoscale* **2014**, *6*, 8873-8877.

(39) You, C. C., De, M.; Han, G.; Rotello, V. M. Tunable Inhibition and Denaturation of Alpha- Chymotrypsin with Amino Acid-Functionalized Gold Nanoparticles. *J. Am. Chem. Soc.*, **2005**, *127*, 12873.

(40) Pettersen, E. F.; Goddard, T. D.; Huang, C. C.; Couch, G. S.; Greenblatt, D. M.; Meng, E. C.; Ferrin, T. E. UCSF Chimera—a Visualization System for Exploratory Research and Analysis. *J. Comput. Chem.* **2004**, *25*, 1605-1612.

CHAPTER 4

A GENERAL STRATEGY FOR DIRECT CYTOPLASMIC PROTEIN DELIVERY VIA PROTEIN-NANOPARTICLE COENGINEERING

4.1. Introduction

Intracellular delivery of proteins into cells is crucial for therapeutic development,¹ cellular imaging and diagnosis,² genome engineering,^{3,4} and synthetic biology applications.⁵ Native enzymes and transcription factors are particularly attractive ‘biologics’ for intracellular enzyme replacement therapy,^{6,7} however effective delivery of these potential therapeutics remains elusive.⁷ Endosomal entrapment is a key hurdle: nanocarrier-based delivery methods result in only a fraction of the entrapped cargo (often ~1%) escaping into the cytosol.⁸ Protease-mediated degradation and exocytosis of the remaining entrapped cargo make these strategies ultimately highly inefficient.⁸⁻¹⁰ Delivery through membrane disruption methods can provide efficient cytosolic protein delivery, however, these methods require additional osmolytic surfactants,¹¹ hypertonic agents,¹² or mechanical distortion techniques¹³ that are harmful for the cells and have challenges for *in vivo* enzyme applications.

Recently, our laboratory has developed a nanocapsule-based¹⁴ strategy for cytosolic protein delivery.¹⁵⁻¹⁷ This method, however, is limited to proteins whose pI values are below ~7. More recently, we developed an engineering strategy to form spherical hierarchical self-assemblies between proteins and nanoparticles.¹⁸ In our approach, proteins tagged with recombinantly attached oligo-glutamic acid (E-tagged proteins) self-assemble with positively charged gold nanoparticles (2 nm core diameter) that carry arginine functionality on their surface (ArgNP).^{14,19} We report here the use of these

assemblies as a general strategy for direct cytosolic delivery of proteins into mammalian cells, with versatility demonstrated using five different proteins with diverse charge, size, and function (Figure 4.1).

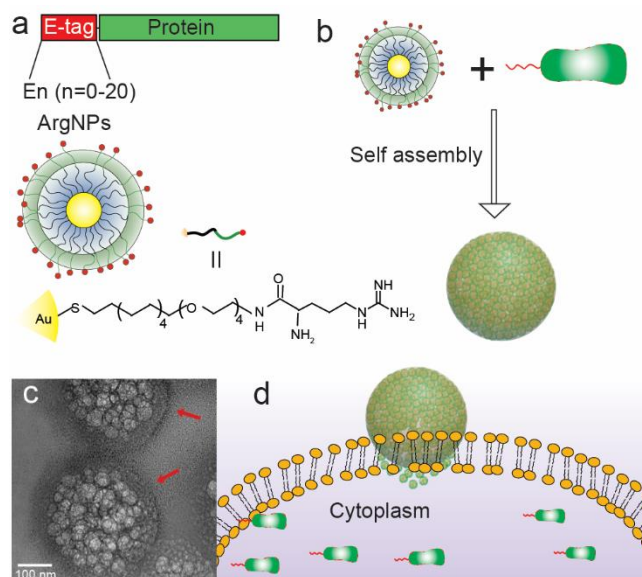


Figure 4. 1. Co-engineering of E-tagged proteins and nanoparticles for direct cytoplasmic protein delivery. a) Strategy for protein engineering, and the chemical structure of arginine functionalized gold nanoparticles (ArgNPs). b) Simple mixing of E-tagged proteins and ArgNPs resulted hierarchical nanoassembly formation. c) Representative transmission electron micrograph (TEM) of GFP-E10:ArgNPs assemblies. Red arrow indicates access nanoparticle coating on the nanoassembly surface. d) Proposed fusion-like mechanism for direct cytosolic protein delivery.

4.2. Results

Engineering E-tagged green fluorescent proteins (GFP) for direct cytoplasmic delivery. For imaging purposes, we began our studies using GFP. We expressed a series of GFPs carrying different lengths of E-tags at the C-terminus and self-assembled them with Arg-NP particles.¹⁸ The assemblies were then screened for delivery efficiency in cultured HeLa cells. After incubating GFP-En:ArgNPs assemblies with HeLa cells for 3 h, the cellular uptake of GFP-En was monitored using confocal laser scanning microscopy (CLSM) and flow cytometry. GFP delivery efficiency increased as the length of E-tag

increased with maximum delivery at GFP-E10 (Figure 4.2e, Figure 4.8), consistent with our prior self-assembly studies.¹⁸ The highest GFP delivery intensity observed at a ratio of 1: 3 ArgNP to GFP-E10 (750 nM), as determined by flow cytometry analysis (Figure 4.9).

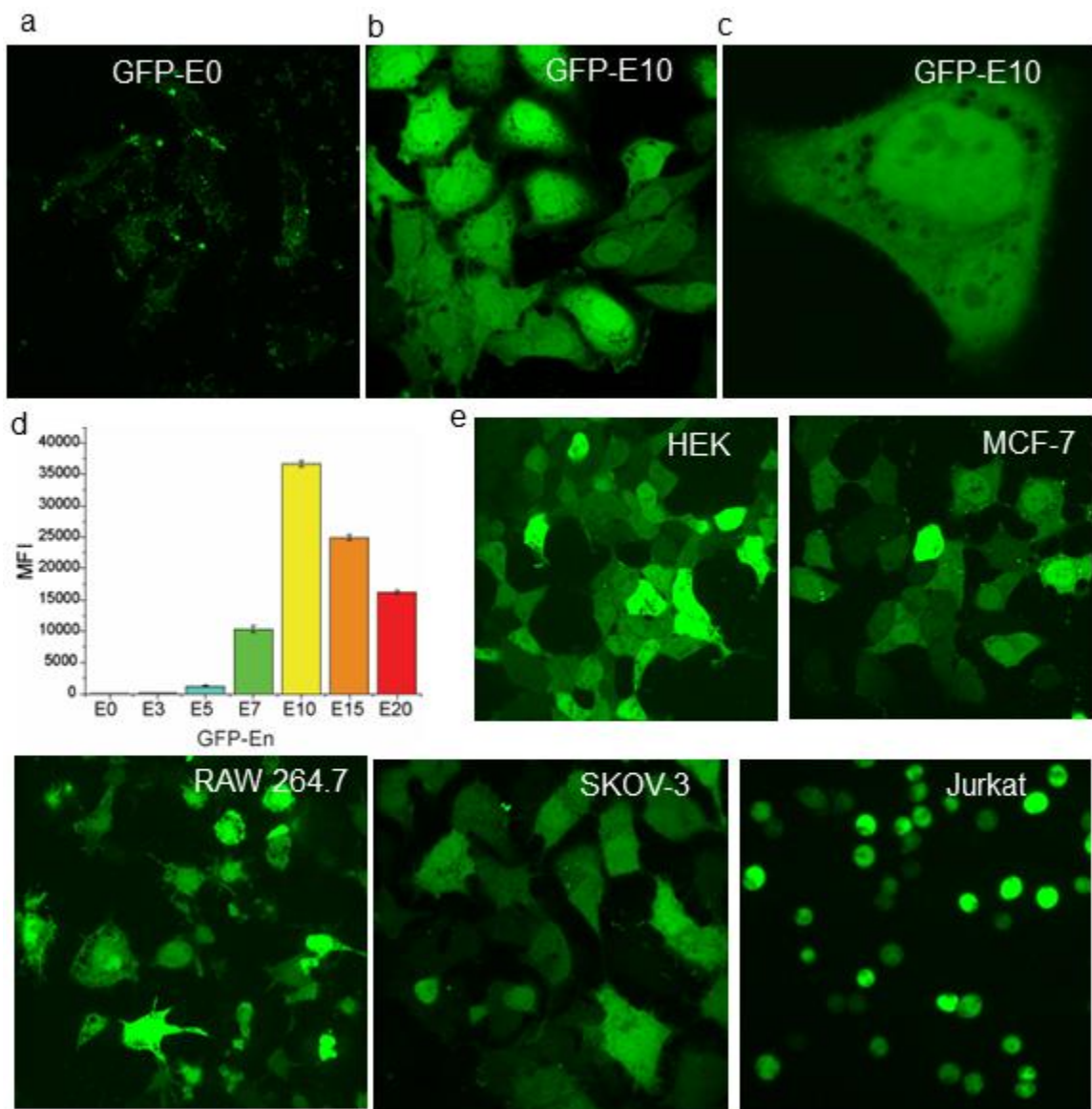


Figure 4. 2. Nanoassembly mediated cytoplasmic delivery of E-tagged GFP in HeLa (a-d) and other cell lines (e). GFP-E10 is delivered into cytosol in HeLa cells (b), but not unmodified GFP (GFP-E0) (a). c) Enlarged image of a GFP-E10 delivered cell, indicating thorough distribution of delivered protein in the cytoplasm and nucleus. d) Flow cytometry data showing GFP-En delivery efficiency increases as the E-tag length increases, reaching maximum at GFP-E10. Delivery efficiency dropped after E-tag length more than E10 due to inefficient assembly formation. e). GFP-E10 delivery in different cell lines.

Confocal microscopy investigation revealed that the delivered GFP-E10 was evenly distributed throughout the cytoplasm (Figure 4.2b-c; Figure 4.10 for z-stacking images), without the punctate fluorescence seen with delivery vehicles with endosomal uptake (Figure 4.11).^{20,21} We also observed fluorescence in the nucleus, consistent with the ability of small proteins like GFP to diffuse across the nuclear pore (Figure 4.2b-c).²² Direct cytoplasmic delivery of GFP-E10 is also evident from live cell video imaging. As shown in Figure 4.3b, the release of GFP-E10 was observed at ~15 min post-incubation, with complete protein delivery obtained in as little as 40 min. We chose five additional mammalian cell lines to demonstrate the generality of the delivery process: human embryonic kidney cells (HEK), mammary epithelial cells (MCF-7), mouse macrophage (RAW 264.7), human ovarian cancer cells (SKOV-3), and T-lymphocyte cells (Jurkat). As shown in Figure 4.2e and Figure 4.12, efficient cytosolic delivery of nanoassembly-mediated GFP-E10 was evident in all of these cell lines, indicating the broad delivery capabilities of our system.

A fusion-like process facilitates direct cytosolic protein delivery. Insight into the delivery process was obtained using time-lapse confocal microscopy. After contact of a nanoassembly with the cell membrane (Figure 4.3a), encapsulated GFP-E10 was quickly released into the cytosol (Figure 4.3c), reaching the opposite end of the cell in less than 30s and visible in the nucleus after 90s (Figure 4.3c). Significantly, free mCherry protein in the media did not enter the cell during nanoassembly mediated GFP-E10 delivery (Figure 4.14), indicating that delivery does not occur through a “hole punching” process.²³ Mechanistic insight was obtained through cholesterol depletion assays, where complete

inhibition of protein delivery (Figure 4.13) was observed. This shut-down suggests that the delivery process occurs through a lipid raft mediated process.²⁴

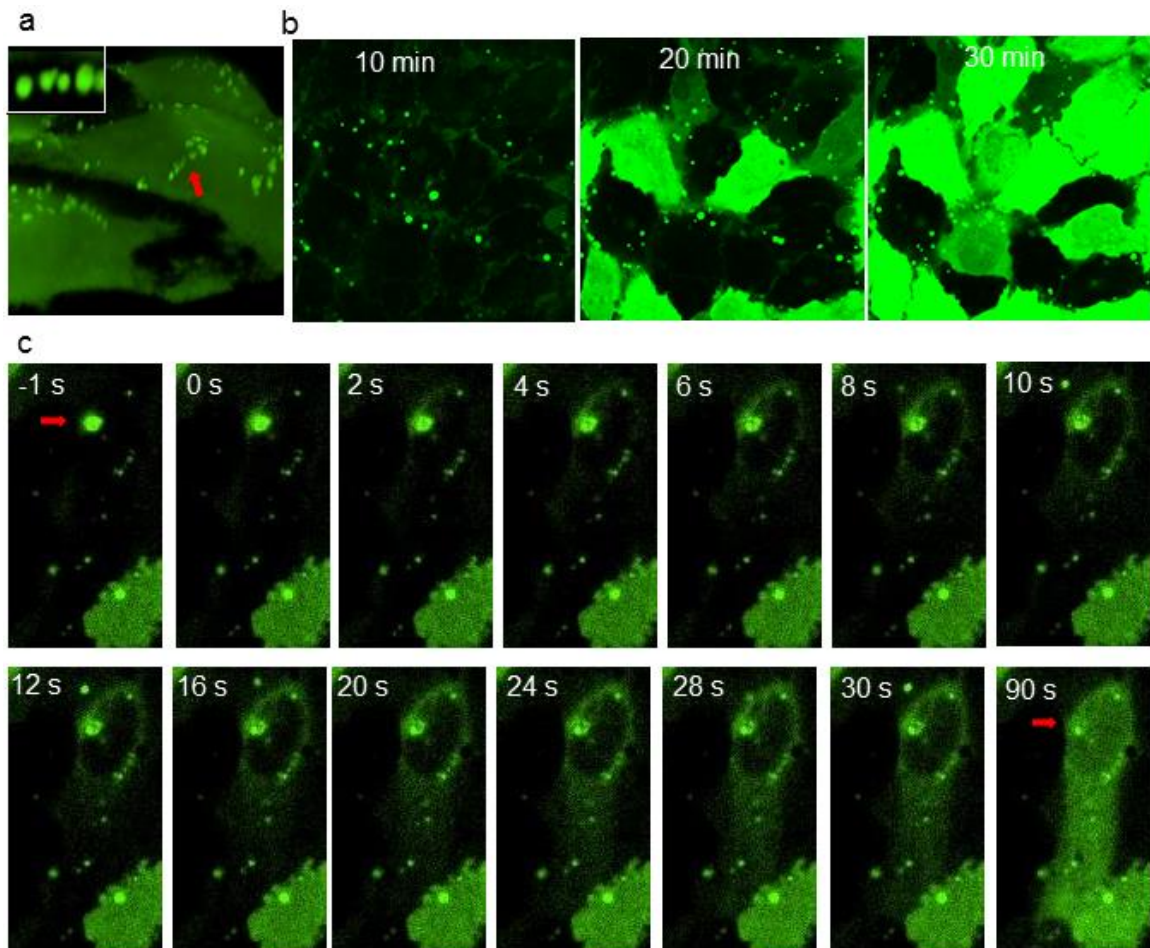


Figure 4. 3. A fusion-like mechanism for nanoassembly-mediated direct cytosolic protein delivery. a) Confocal microscopy images showing nanoassemblies bound to the cell membrane (indicated by red arrow) in SKOV-3 cells that may eventually deliver the protein content to the cytosol. Inset—enlarged image of nanoassemblies. 3D image was reconstructed from z-stacking images. b) Time-lapse confocal microscopy imaging revealed the direct cytosolic delivery of GFP-E10 in HeLa cells. Representative still-images showing at 10, 20, and 30 min after nanoassemblies were added to the cell culture dish. c) A single nanoassembly (red arrow) was fused to the cell membrane (at -1s), which then rapidly released encapsulated GFP-E10 into the cytosol. Delivered GFP-E10 was distributed thorough the cytosol (after 30s), and the nucleus (90s).

A general strategy for direct cytosolic protein delivery. We selected five different proteins with a range of charge (pI), size, and function: Prothymosin- α (pI= 3.71, MW= 11.8 kDa, chromatin remodeling protein);²⁵ GFP (pI= 5.9, MW= 27 kDa, imaging

protein);²⁶ Granzyme A (GzmA) (pI= 9.14, MW= 29.0, cytolytic protein secreted by T-cells);²⁷ Cre recombinase (Cre) (pI= 9.60, MW= 38.5, DNA recombinase);²⁸ Histone 2A (H2A) (pI= 10.60, MW= 13.5, DNA packaging protein in the nucleosome) (Figure 4.4a).²⁹

We attached an E10-tag to these proteins similar to GFP, at either the N- or C-terminus (Experimental section). For imaging studies, these proteins (except GFP) were labeled with fluorescein isothiocyanate (FITC) and assembled with ArgNPs at the appropriate molar ratios (Experimental section). These nanoassemblies were incubated with HeLa cells at 37°C and 5% CO₂ for 3 h. As shown in Figure 4.4b, all E10-tagged proteins were evenly distributed in the cytosol as well as the nucleus, establishing the generality of the protocol.

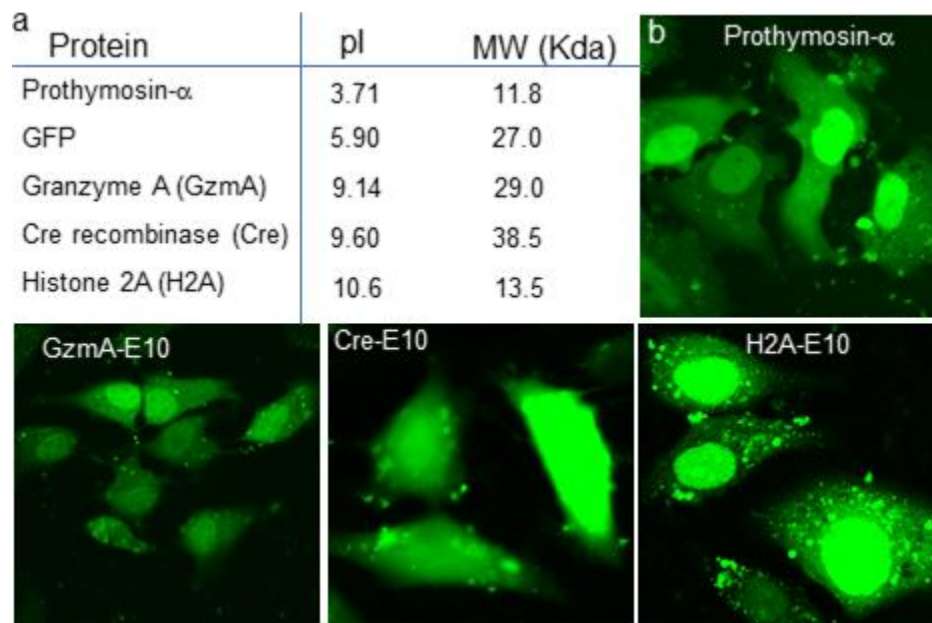


Figure 4. 4. Direct cytoplasmic delivery of multiple E-tagged proteins with diverse size/charge, and functions. a) List of proteins delivered here with their respective charge (pI) and size (MW). b) Nanoassembly mediated delivery of these E-tagged proteins (FITC-labelled) indicated the even distribution in the cytoplasm and nucleus as shown through confocal microscopy images. Note that, except Cre recombinase, these proteins have inherent nuclear signal, which is also reflected by their preferential accumulation in the nucleus.

Functional delivery of Cre recombinase provides efficient gene recombination. Cre recombinase delivery provides an attractive tool for cellular engineering and synthetic biology applications. After achieving successful delivery of FITC-tagged Cre-E10, we tested its activity and function in the delivered cells. Cre excises out (delete) genes flanked by a recognition sequence ‘loxP’.³⁰ To generate a simple readout of Cre activity, we generated a plasmid (loxP-dsRedSTOP-loxP-GFP) and delivered it into human embryonic kidney cells (HEK) for transient expression of the cassette. These cells exhibit red fluorescence, but will turn green after delivery of active Cre. When Cre-E10 was delivered into these reporter cells, red-to-green fluorescence conversion was observed using confocal microscopy and flow cytometry (Figure 4.5). Prominent expression of GFP was observed after 48 h of delivery, indicating that Cre-E10 was delivered in active form.

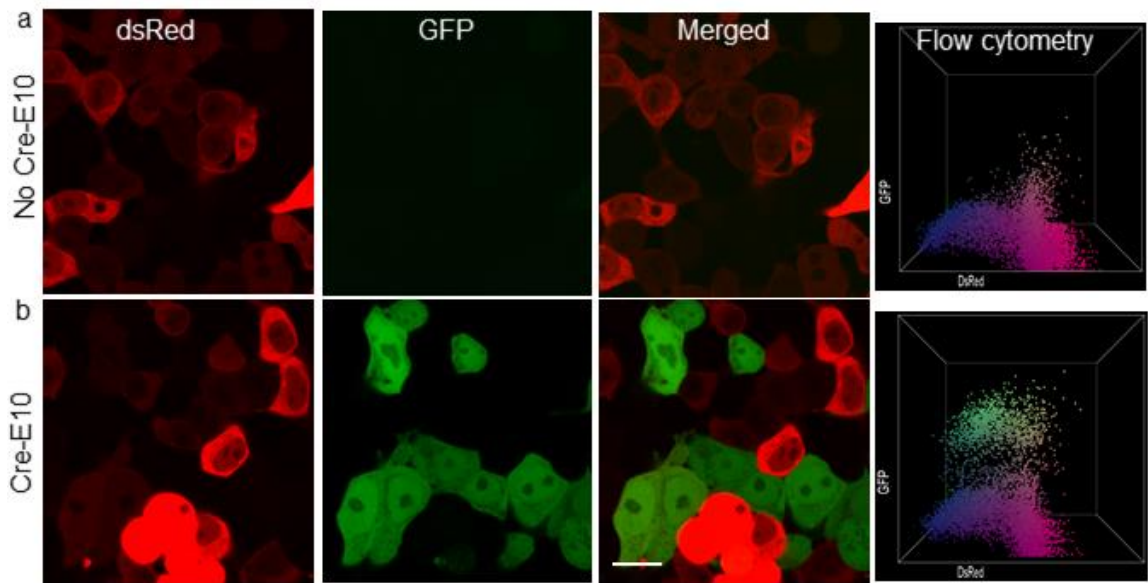


Figure 4. 5. Nanoassembly mediated Cre-E10 delivery resulted efficient gene recombination. Confocal micrograph and flow cytometry data before (a), and after (b) Cre-E10 delivery in HEK cells. Delivery of Cre-E10 efficiently floxed dsRed gene, thus turning on GFP expression (b).

Functional delivery of Granzyme A efficiently kills cancer cells. GzmA delivery provides a direct therapeutic application of intracellular protein delivery. Granzymes are

cytolytic enzymes that are produced by cytotoxic T-cells and released into target cells to kill them,³¹ a process used in adoptive cancer immunotherapy.³² The killing efficiency of delivered GzmA-E10 in HeLa cells was evaluated by incubating nanoassemblies containing GzmA-E10 with HeLa cells at 37°C and 5% CO₂ for 3 h followed by washing. Cell death was assessed immediately or 24 h after, using confocal microscopy, phosphatidylserine staining, and caspase 3/7 staining. As shown in Figure 4.6, GzmA-E10 mediated cell death was observed 24 h after the delivery, but not after 3 h. Staining of phosphatidylserine, which is expressed on granzyme-mediated dead cells, confirmed that the slow cell death was indeed caused by delivered GzmA-E10 activity (Figure 4.6).³³ On the other hand, GFP-E10 delivery did not cause cell death, indicating the specificity of delivered GzmA-E10 (Figure 4.6, bottom panel). Further, delivered GzmA-E10 killed the cells through a caspase 3/7 independent pathway (Figure 4.15), another hallmark of granzyme-A mediated cell death.³⁴ Taken together, nanoassembly-mediated GzmA-E10 delivery may provide an efficient means for intracellular protein therapy for cancer treatment.

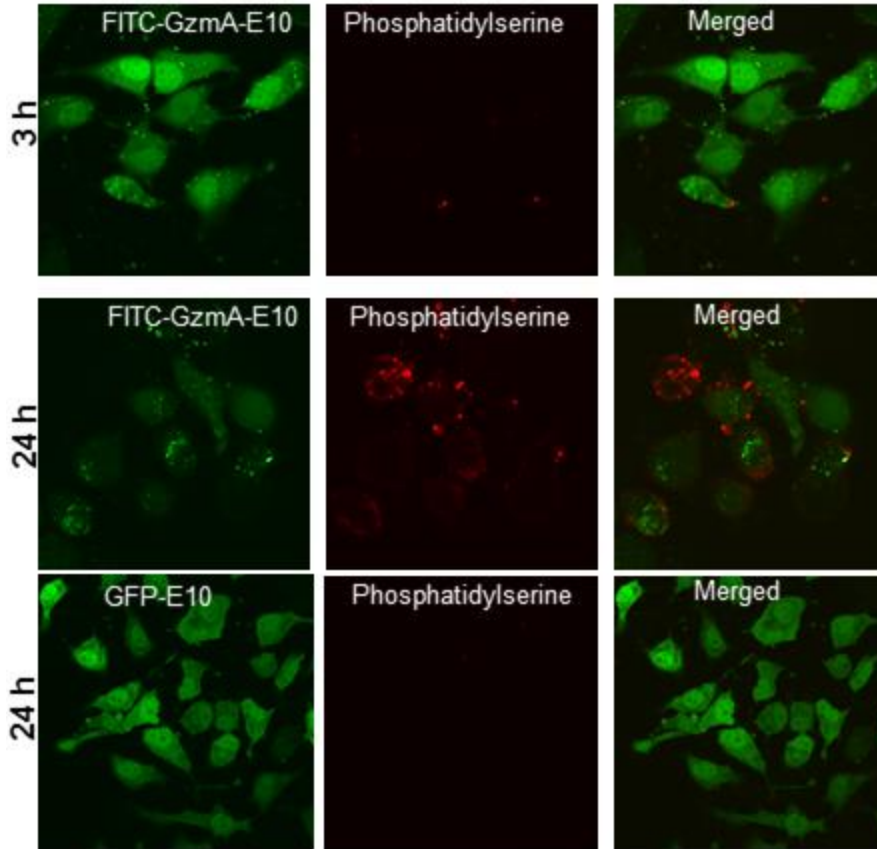


Figure 4. 6. Nanoassembly-mediated delivery of functional Granzyme A-E10 (GzmA-E10) effectively killed HeLa cells. Confocal microscopy images showing FITC-GzmA-E10 or GFP-E10 delivered cells along with phosphatidylserine staining. a) 3, and 24 h after GzmA-E10 delivery. b) 24 h after GFP-E10 delivery. Note that 24 h after GzmA-E10 delivery cells died, which also showed phosphatidylserine staining, confirming the GzmA-E10 mediated cell death.

4.3. Conclusions

In summary, we present here a general method for direct cytoplasmic protein delivery through co-engineering of proteins (E-tagged) and functionalized nanoparticles. The versatility of our method was established by delivering five proteins with diverse sizes, charges, and functions. This system provides a useful tool for cell biology applications *in vitro*, and the potential for new intracellular enzyme replacement therapies for *in vivo* systems. Additionally, our technology may offer new ways for imaging intracellular protein trafficking and dynamics for understanding cellular protein function. Further, we

envision that our method can be applied for many desired proteins for applications including in synthetic biology and genome engineering.

4.4. Experimental section

Engineering E-tagged protein. A series of glutamic acid tags (E-tag) with different length was inserted to the C-terminus of GFP according to our previous method. Similarly, a E10 tag was inserted to Cre recombinase (N-term), Granzyme A (N-term), Histone 2A (C-term), through restriction cloning.

Recombinant proteins were expressed in *E. coli* BL21 Rosetta strain using standard protein expression protocol. Briefly, protein expression was carried out in 2xYT media with an induction condition of 1 mM IPTG and 18/25 °C for 16 hours. At this point, the cells were harvested and the pellets were lysed by using 1% Triton-X-100 (30 min, 37 °C) /DNase-I treatment (10 min). Proteins were purified using HisPur cobalt columns. Note that except GFP-En, proteins were eluted using high salt concentration buffer (2 M NaCl, 300 mM Imidazole) due to the high positive charge of the proteins. Proteins were finally preserved in PBS buffer containing 300 mM salt, (Histone 2A, 750 mM salt). The purity of native proteins was determined using 12% SDS-PAGE gel.

Nanoparticle synthesis and characterization. Arginine-functionalized gold nanoparticles (ArgNPs) were synthesized according to our previous protocol.¹⁴ Briefly, after synthesizing the arginine-functionalized thiol ligand, ArgNPs were prepared by conventional place-exchange reaction of 2-nm sized 1-pentanethiol-protected gold nanoparticles (Au-C5) with HS-C11-TEG-NH-Arginine. The resultant ArgNPs products

were dissolved in distilled water, and purified by dialysis in 5 mM phosphate buffer (PB) (Figure 4.7).

Nanoassembly fabrication. Nanoassemblies of ArgNPs with various E-tagged proteins were fabricated through a simple mixing method, according to our previous method.¹⁸ ArgNPs (50 μ M stock in 5 mM PB, pH 7.4) were first added to 100 μ L of 1 \times PBS in a vial, followed by adding the E-tagged protein at appropriate molar ratio: GFP-En (1:3; 250:750 nM ArgNPs/GFP-En); Cre-E10 (2:1; 250:125 nM ArgNPs/Cre-E10); GzmA-E10 (1:2 250:500 nM ArgNPs/GzmA-E10); H2A-E10 (1:3; 250:750 nM ArgNPs/H2A-E10), Prothymosin- α (1:3; 250:750 nM ArgNPs/PTMA). The assemblies were incubated at room temperature for another 10 min. Following the incubation, DMEM was added to the assemblies to make the final volume up to 1000 μ L. The nanoassemblies were then immediately added to cells grown overnight in round bottom confocal dish plates for delivery experiments.

Cell culture. 80-100k cells were grown in a 24-well plate in low glucose DMEM (with 10% FBS, and 1% antibiotics) for overnight at 37 $^{\circ}$ C under 5% CO₂. Cells were washed with 1 \times PBS (twice) before incubation with nanoassemblies. For confocal studies, ~240,000 cells were seeded per dish.

Delivery. Assembled E-tagged protein:ArgNPs nanoassemblies (preassembled in 100 μ L PBS for 10 min, plus 400 μ L media for 24 well plate or 900 μ L media for confocal dish) were immediately transferred to confluent grown cells. Cells were then incubated with nanoassemblies at 37 $^{\circ}$ C and 5% CO₂ for 3 h. Delivery efficiency was determined by Confocal microscopy or flow cytometry when necessary.

Confocal microscopy and Time-lapse imaging. Confocal microscopy imaging was performed using either Zeiss 510 Meta laser scanning microscope or Nikon spinning disc microscope. Time-lapse real time video imaging was performed in the Nikon spinning disc microscope.

Cre-lox system generation. Briefly, the plasmid was constructed by placing a dsRed-STOP fluorescent protein sequence between loxP recognition sites, and a GFP sequences downstream of it [loxP-dsRed(STOP)-loxP-GFP]. Active Cre can excise out the loxP genes which will turn the color to GFP.

Assessing Cre recombinase activity. Human embryonic kidney (HEK) cells were transiently transfected with Retroviral loxP-DsRed-STOP-loxP-GFP system to create a testbed for Cre recombinase activity. 48 h after the transfection, Cre-E10 was delivered into these cells using nanoassemblies. Cells were let grow for another 72 h, then used confocal microscopy or flow cytometry to assess the Cre activity by checking GFP positive cells.

Assessing GzmA activity. After GzmA-E10 delivery, cells were incubated for another 3, 12, 24, or 48 h. Phosphatidylserine (PS) staining was performed in these cells according to standard manufacturer's protocol. Further, caspase 3/7 activity assay was performed to assess GzmA-E10 activity in the delivered cells according to manufacturer's protocol.

Cholesterol depletion. To investigate the delivery mechanism, endocytic and membrane fusion inhibitors were used. Cells were pretreated with endocytic inhibitor [wortmannin (100ng/mL), chlorpromazine (1 μ g/mL)], and membrane fusion inhibitor [methyl- β -cyclodextrin (MBCD, 5mg/mL)] for 1 h, as reported previously.³⁵ At the same

time nanoassemblies were prepared and kept ready. Inhibitor-treated cells were washed with 1×PBS twice, then the nanoassembly solutions were immediately applied to the cells for protein delivery. Confocal microscopy or flow cytometry experiments were performed after 3 h of nanoassembly incubation.

4.5. Supporting figures

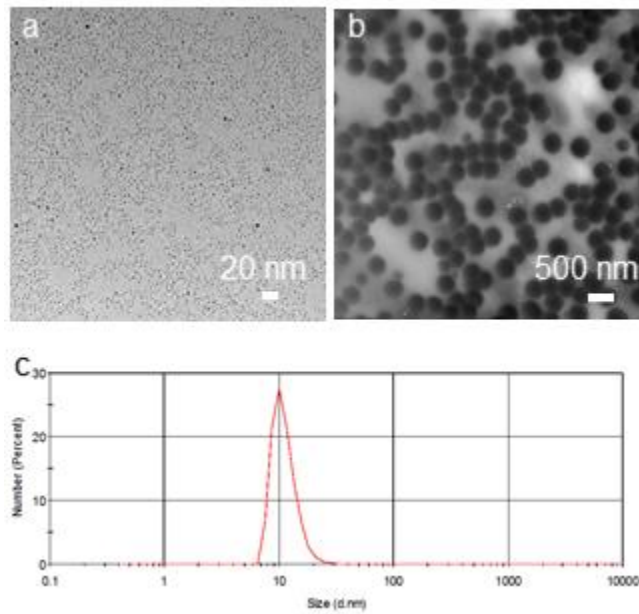


Figure 4. 7. Characterization of nanoassemblies. TEM image of a) ArgNPs, and b) GFP-E10:ArgNPs assemblies. c) DLS size measurement of ArgNPs, indicating the hydrodynamic size (~10 nm in diameter).

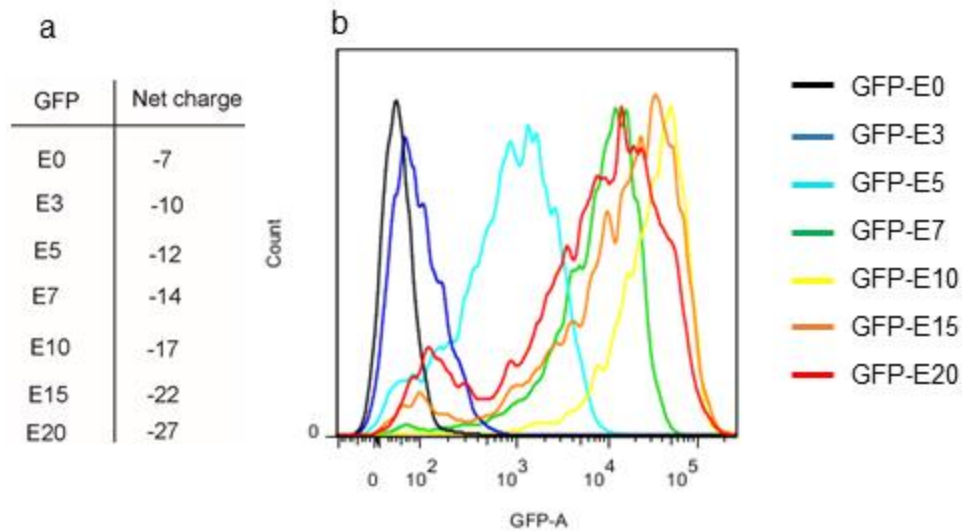


Figure 4. 8. E-tag length determines GFP-En delivery efficiency. a) Addition of appropriate En to GFP and their net negative charge. b) Flow cytometric assessment showing the GFP-En delivery efficiency as the length of E-tag was changed (also see Figure 4.2d for quantification).

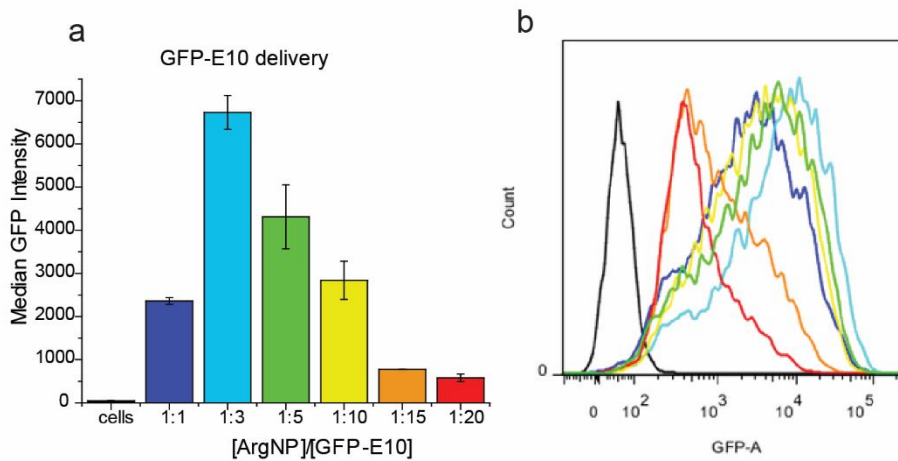


Figure 4. 9. [ArgNP]/[GFP-E10] ratio determines delivery efficiency. Flow cytometry data showing the ratio dependent GFP-E10 delivery efficiency.

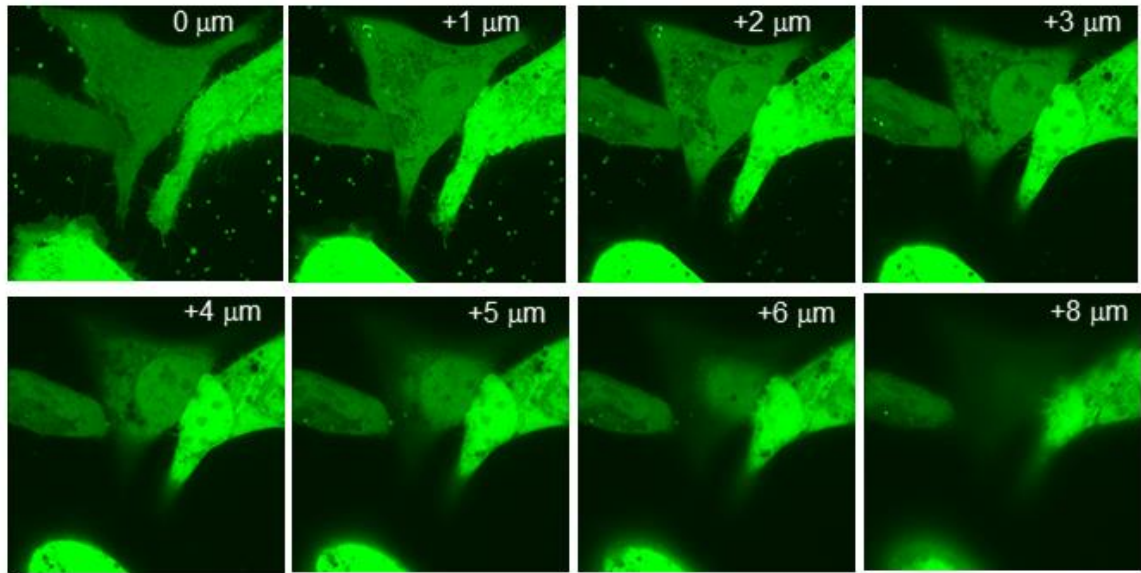


Figure 4. 10. Confocal microscopy Z-stacking images showing through cytosolic and nuclear delivery of GFP-E10. Images were taken at every 1 micron interval. '0' μm indicates the bottom of the cell (at the dish surface).

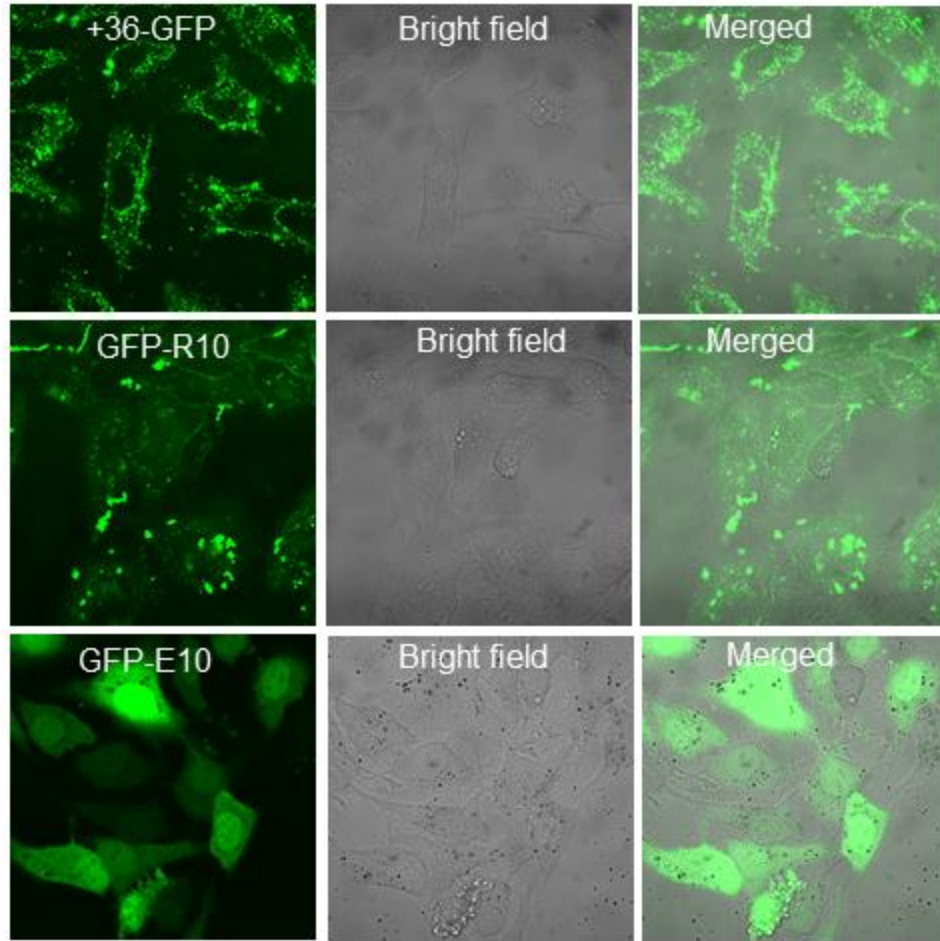


Figure 4. 11. Comparison of protein delivery using various delivery strategies. While supercharged GFP and cell penetrating peptide (CPP) based protein-delivery suffer from endosomal entrapment, our E-tag based nanoassembly method delivers proteins directly to the cytosol.

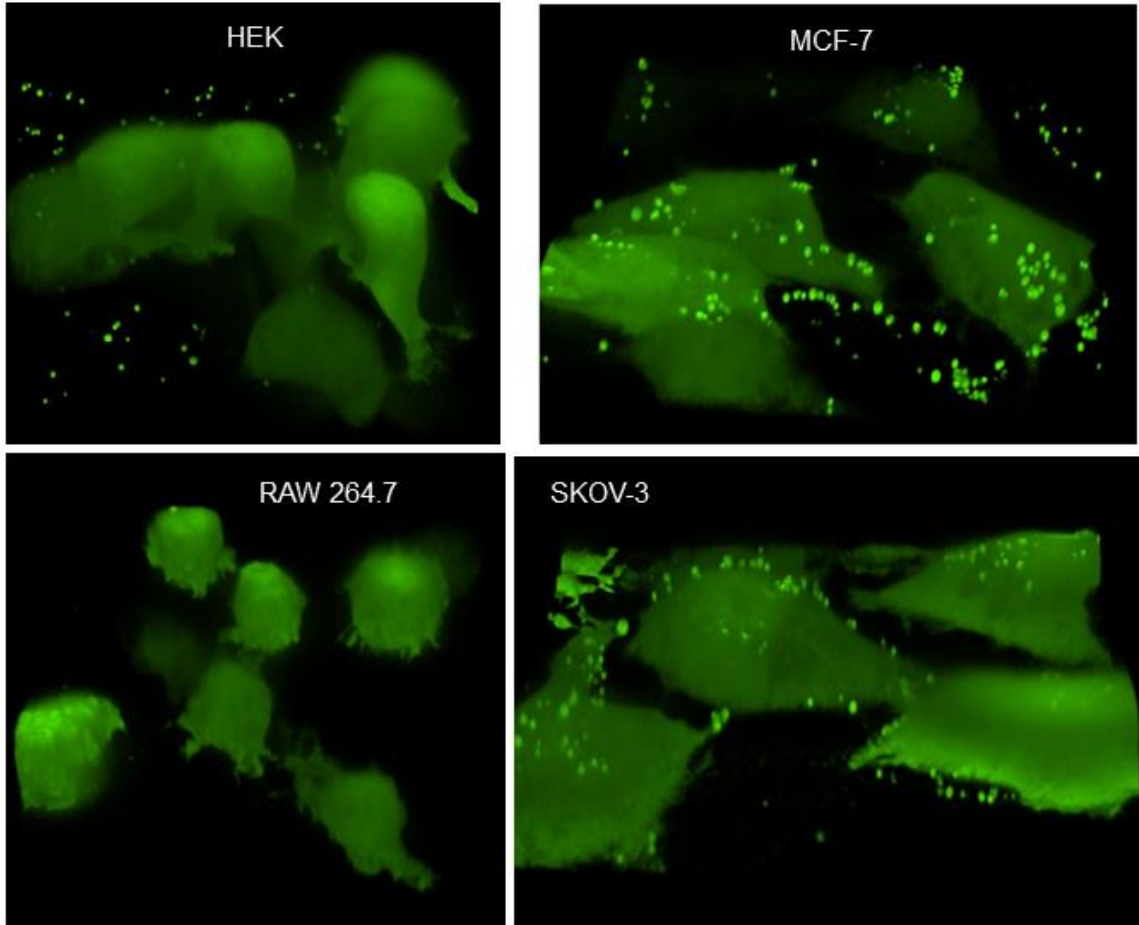


Figure 4. 12. 3D reconstruction of cells from z-stacking confocal images showing GFP-E10 delivery into the whole cell in different cell lines. Note that individual z-stacking images showed thorough cytosolic distribution of GFP-E10 (data not shown here).

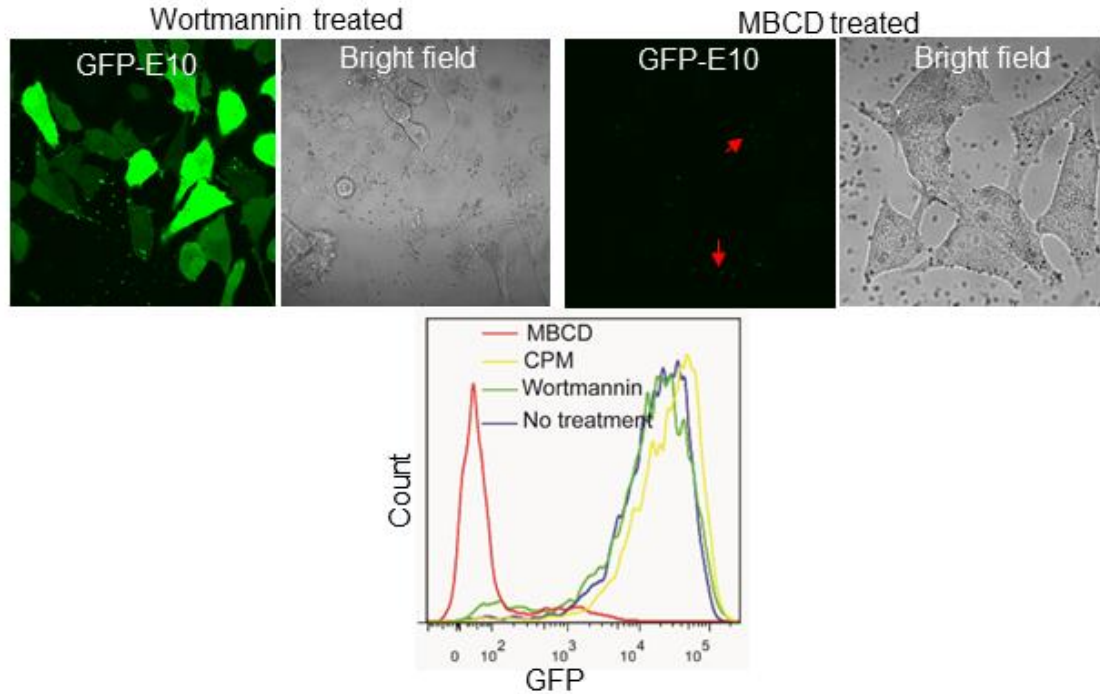


Figure 4. 13. A membrane fusion like mechanism is involved in protein delivery. Confocal microscopy and flow cytometry show that endocytic inhibitors (wortmannin) did not block GFP-E10 delivery, whereas membrane fusion inhibitor (MBCD) completely blocked delivery.

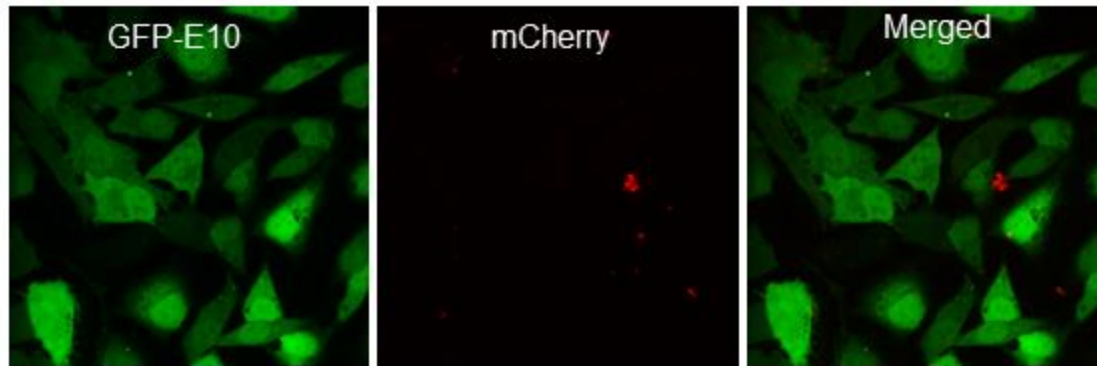


Figure 4. 14. Membrane fusion, but not membrane puncture is involved in nanoassembly-mediated protein delivery. Assembled GFP-E10 was delivered into cells in the presence of free mCherry protein in the media. Free mCherry protein did not enter the cell, while GFP-E10 was delivered into the cell through nanoassembly fusion.

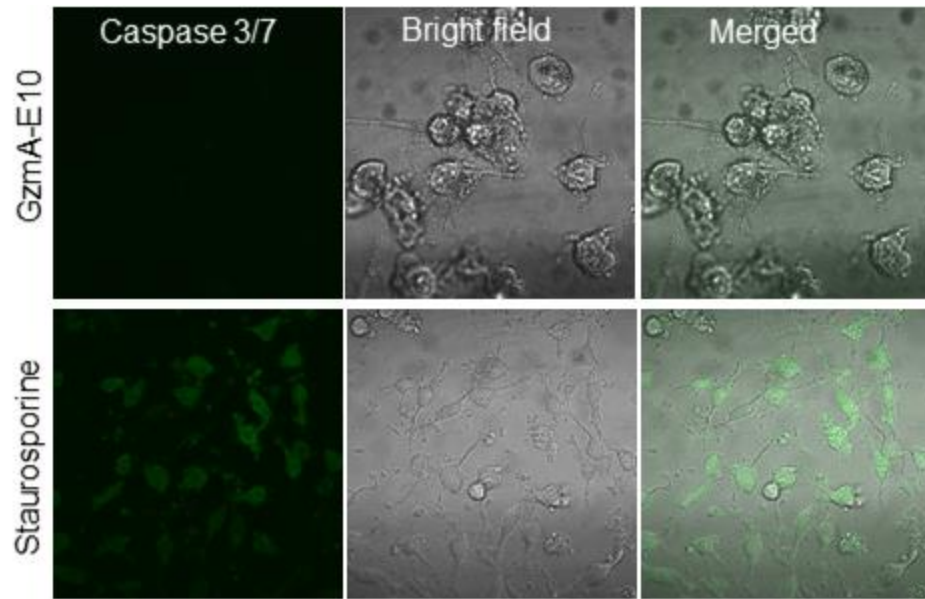


Figure 4. 15. Delivered GzmA-E10 kills cells in a caspase 3/7 independent manner. Although GzmA-E10 delivery resulted in efficient cell death 24 h after delivery, the mechanism of cell death was caspase 3/7 independent; whereas, staurosporine caused caspase 3/7 dependent cell death in less than 3 h. Caspase 3/7 activation was measured using a standard fluorogenic peptide substrate.

4.6. References

- (1) Mitragotri, S.; Burke, P. A.; Langer, R. Overcoming the Challenges in Administering Biopharmaceuticals: Formulation and Delivery Strategies. *Nat. Rev. Drug. Discov.* **2014**, *13*, 655-672.
- (2) Gu, Z.; Biswas, A.; Zhao, M.; Tang, Y. Tailoring Nanocarriers for Intracellular Protein Delivery. *Chem. Soc. Rev.* **2011**, *40*, 3638-3655.
- (3) Komor, A. C.; Badran, A. H.; Liu, D. R. CRISPR-Based Technologies for the Manipulation of Eukaryotic Genomes. *Cell* **2017**, *168*, 20-36.
- (4) Mout, R.; Ray, M.; Lee, Y.W.; Scaletti, F.; Rotello, V. M. *In Vivo* Delivery of CRISPR/Cas9 for Therapeutic Gene Editing: Progress and Challenges. *Bioconjug. Chem.* **2017**, *28*, 880-884.
- (5) Khalil, A. S.; Collins, J. J. Synthetic Biology: Applications Come of Age. *Nat. Rev. Genet.* **2010**, *11*, 367-379.
- (6) Leader, B.; Baca, Q. J.; Golan, D. E. Protein Therapeutics: A Summary and Pharmacological Classification. *Nat. Rev. Drug. Discov.* **2008**, *7*, 21-39.
- (7) Walsh, G. Biopharmaceutical Benchmarks 2014. *Nat. Biotechnol.* **2014**, *32*, 992-1000.
- (8) Stewart, M. P.; Sharei, A.; Ding, X.; Sahay, G.; Langer, R.; Jensen, K. F. *In Vitro* and *Ex Vivo* Strategies for Intracellular Delivery. *Nature* **2016**, *538*, 183-192.
- (9) Gilleron, J.; Querbes, W.; Zeigerer, A.; Borodovsky, A.; Marsico, G.; Schubert, U.; Manygoats, K.; Seifert, S.; Andree, C.; Stöter, M.; Epstein-Barash, H.; Zhang, L.; Kotliansky, V.; Fitzgerald, K.; Fava, E.; Bickle, M.; Kalaidzidis, Y.; Akinc, A.; Maier, M.; Zerial, M. Image-Based Analysis of Lipid Nanoparticle-Mediated siRNA Delivery, Intracellular Trafficking and Endosomal Escape. *Nat. Biotechnol.* **2013**, *31*, 638-646.
- (10) Fu, A.; Tang, R.; Hardie, J.; Farkas, M. E.; Rotello, V. M. Promises and Pitfalls of Intracellular Delivery of Proteins. *Bioconjug. Chem.* **2014**, *25*, 1602-1608.
- (11) Erazo-Oliveras, A.; Najjar, K.; Dayani, L.; Wang, T. Y.; Johnson, G. A.; Pellois, J. P. Protein Delivery into Live Cells by Incubation with an Endosomolytic Agent. *Nat. Methods.* **2014**, *11*, 861-867.
- (12) D'Astolfo, D. S.; Pagliero, R. J.; Pras, A.; Karthaus, W. R.; Clevers, H.; Prasad, V.; Lebbink, R. J.; Rehmann, H.; Geijsen, N. Efficient Intracellular Delivery of Native Proteins. *Cell* **2015** *161*, 674-690.
- (13) Han, X.; Liu, Z.; Jo, M. c.; Zhang, K.; Li, Y.; Zeng, Z.; Li, N.; Zu, Y.; Qin, L. CRISPR-Cas9 Delivery to Hard-to-Transfect Cells *via* Membrane Deformation. *Sci. Adv.* **2015**, *1*, e1500454.

- (14) Yang, X. C.; Samanta, B.; Agasti, S. S.; Jeong, Y.; Zhu, Z. J.; Rana, S.; Miranda, O. R.; Rotello, V. M. Drug Delivery Using Nanoparticle-Stabilized Nanocapsules. *Angew. Chem. Int. Ed.* **2011**, *50*, 477-481.
- (15) Tang, R.; Kim, C. S.; Solfiell, D. J.; Rana, S.; Mout, R.; Velázquez-Delgado, E. M.; Chompoosor, A.; Jeong, Y.; Yan, B.; Zhu, Z. J.; Kim, C.; Hardy, J. A.; Rotello, V. M. Direct Delivery of Functional Proteins and Enzymes to the Cytosol using Nanoparticle-Stabilized Nanocapsules. *ACS Nano* **2013**, *7*, 6667-6673.
- (16) Ray, M.; Tang, R.; Jiang, Z.; Rotello, V. M. Quantitative Tracking of Protein Trafficking to the Nucleus using Cytosolic Protein Delivery by Nanoparticle-Stabilized Nanocapsules. *Bioconjug. Chem.* **2015**, *26*, 1004-1007.
- (17) Tang, R.; Jiang, Z.; Ray, M.; Hou, S.; Rotello, V. M. Cytosolic Delivery of Large Proteins using Nanoparticle-Stabilized Nanocapsules. *Nanoscale* **2016**, *8*, 18038-18041.
- (18) Mout, R.; Tonga, G. Y.; Wang, L.-S.; Ray, M.; Roy, T.; Rotello, V. M. Programmed Self-Assembly of Hierarchical Nanostructures through Protein-Nanoparticle Co-Engineering. *ACS Nano* **2017**, *11*, 3456-3462.
- (19) Mout, R.; Ray, M.; Tonga, G. Y.; Lee, Y.-W.; Tay, T.; Sasaki, K.; Rotello, V. M. Direct Cytosolic Delivery of CRISPR/Cas9-Ribonucleoprotein for Efficient Gene Editing. *ACS Nano*, **2017**, *11*, 2452-2458.
- (20) Cronican, J. J.; Thompson, D. B.; Beier, K. T.; McNaughton, B. R.; Cepko, C. L.; Liu, D. R. Potent Delivery of Functional Proteins into Mammalian Cells *In Vitro* and *In Vivo* using a Supercharged Protein. *ACS Chem. Biol.* **2010**, *5*, 747-752.
- (21) González-Toro, D. C.; Ryu, J. H.; Chacko, R. T.; Zhuang, J.; Thayumanavan, S. Concurrent Binding and Delivery of Proteins and Lipophilic Small Molecules Using Polymeric Nanogels. *J. Am. Chem. Soc.* **2012**, *134*, 6964-6967.
- (22) Dingwall, C.; Laskey, R. A. Protein Import into the Cell Nucleus. *Annu. Rev. Cell Biol.* **1986**, *2*, 367-390.
- (23) Jamur, M. C.; Oliver, C. Permeabilization of Cell Membranes. *Methods Mol. Biol.* **2010**, *588*, 63-66.
- (24) Jiang, Y.; Tang, R.; Duncan, B.; Jiang, Z.; Yan, B.; Mout, R.; Rotello, V. M. Direct Cytosolic Delivery of siRNA Using Nanoparticle-Stabilized Nanocapsules. *Angew. Chem. Int. Ed. Engl.* **2015**, *54*, 506-510.
- (25) Gomez-Marquez, J.; Rodríguez, P. Prothymosin Alpha is a Chromatin-Remodelling Protein in Mammalian Cells. *Biochem. J.* **1998**, *333*, 1-3.
- (26) Tsien, R. Y. The Green Fluorescent Protein. *Annu. Rev. Biochem.* **1998**, *67*, 509-544.
- (27) Lieberman, J. The ABCs of Granule-Mediated Cytotoxicity: New Weapons in the Arsenal. *Nat. Rev. Immunol.* **2003**, *3*, 361-370.

- (28) Nagy, A. Cre Recombinase: The Universal Reagent for Genome Tailoring. *Genesis* **2000**, *26*, 99-109.
- (29) Bönisch, C.; Hake, S. B. Histone H2A Variants in Nucleosomes and Chromatin: More or Less Stable. *Nucleic Acids Res.* **2012**, *40*, 10719-10741.
- (30) Koo, B. K.; Stange, D. E.; Sato, T.; Karthaus, W.; Farin, H. F.; Huch, M.; van Es, J. H.; Clevers, H. Controlled Gene Expression in Primary Lgr5 Organoid Cultures. *Nat. Methods* **2011**, *9*, 81-83.
- (31) Martinvalet, D.; Dykxhoorn, D. M.; Ferrini, R.; Lieberman, J. Granzyme A Cleaves a Mitochondrial Complex I Protein to Initiate Caspase-Independent Cell Death. *Cell* **2008**, *133*, 681-692.
- (32) Restifo, N. P.; Dudley, M. E.; Rosenberg, S. A. Adoptive Immunotherapy for Cancer: Harnessing the T Cell Response. *Nat. Rev. Immunol.* **2012**, *12*, 269-281.
- (33) Lieberman, J. Granzyme A Activates Another Way to Die. *Immunol. Rev.* **2010**, *235*, 93-104.
- (34) Chowdhury, D.; Lieberman, J. Death by a Thousand Cuts: Granzyme Pathways of Programmed Cell Death. *Annu. Rev. Immunol.* **2008**, *26*, 389-420.
- (35) Saha, K.; Kim, S. T.; Yan, B.; Miranda, O. R.; Alfonso, F. S.; Shlosman, D.; Rotello, V. M. Surface Functionality of Nanoparticles Determines Cellular Uptake Mechanisms in Mammalian Cells. *Small* **2013**, *9*, 300-305.

CHAPTER 5

DIRECT CYTOSOLIC DELIVERY OF CRISPR/CAS9- RIBONUCLEOPROTEIN FOR EFFICIENT GENE EDITING

5.1. Introduction

Bacterially derived CRISPR system (Clustered Regularly Interspaced Short Palindromic Repeat) is a versatile tool for genome editing,^{1,2} transcriptional control of genes,^{3,4} and visualizing genome dynamics.⁵ Due to its genome editing efficiency, CRISPR/Cas9 system holds promises for curing human genetic diseases, as demonstrated through correction of a variety of disease-causing mutations in cultured cells⁶ and in animal models.⁷ These studies used gene delivery strategies to generate Cas9 inside cells. However, the required CRISPR genes stay in the host cells once delivered, causing unwanted gene editing and thus posing a major concern for CRISPR/Cas9 based gene therapy.⁸⁻¹⁰ Additionally, the constitutive expression of Cas9 gene in the host may elicit immunogenic response, making CRISPR gene therapy less practical for therapy.^{9,11}

Delivery of Cas9 protein along with a guide RNA (sgRNA) (Cas9-ribonucleoprotein, or Cas9-RNP) provides an alternative strategy for CRISPR process, offering a transient way of editing genes. Although a few strategies for Cas9 protein delivery have been reported,¹²⁻¹⁵ these strategies suffer from endosomal entrapment of both Cas9 and sgRNA. Mechanical methods including electroporation^{16,17} and membrane deformation¹⁸ provide direct delivery, however they require specialized processing and are generally impractical for *in vivo* therapeutic applications.

Here, we report a highly efficient editing strategy based on co-delivery of Cas9 protein and sgRNA into cells. This approach uses gold nanoparticles to co-assemble with engineered Cas9 protein and sgRNA into nanoassemblies. These vectors deliver protein and nucleic acid efficiently to the cytoplasm, with concomitant transport to the nucleus. Using this approach we achieved up to ~90% delivery efficiency in a range of cell types, with subsequent gene editing efficiency up to 30%.

5.2. Results

Co-engineering of Cas9 protein and gold nanoparticles. We first engineered Cas9 protein for self-assembly with the cationic arginine gold nanoparticles (ArgNPs) (Figure 5.1).¹⁹ Cas9 is a highly positively charged protein, so a glutamate peptide tag (E-tag)²⁰ was inserted at the N-terminus of *Streptococcus pyogenes* (*Sp*) Cas9 protein. We engineered a series of Cas9 proteins having a variable E-tag (En) length, where n= 0, 5, 10, 15, and 20. Notably, a Cas9 protein with no modification (Cas9E0) possesses a net 20 positive charges, however, insertion of the E-tag provided a patch of local negative charges that presumably enabled interaction with the positively charged ArgNPs.²¹ In addition, a nuclear localization signal (NLS) was inserted to the C-terminus to provide nuclear targeting of Cas9.

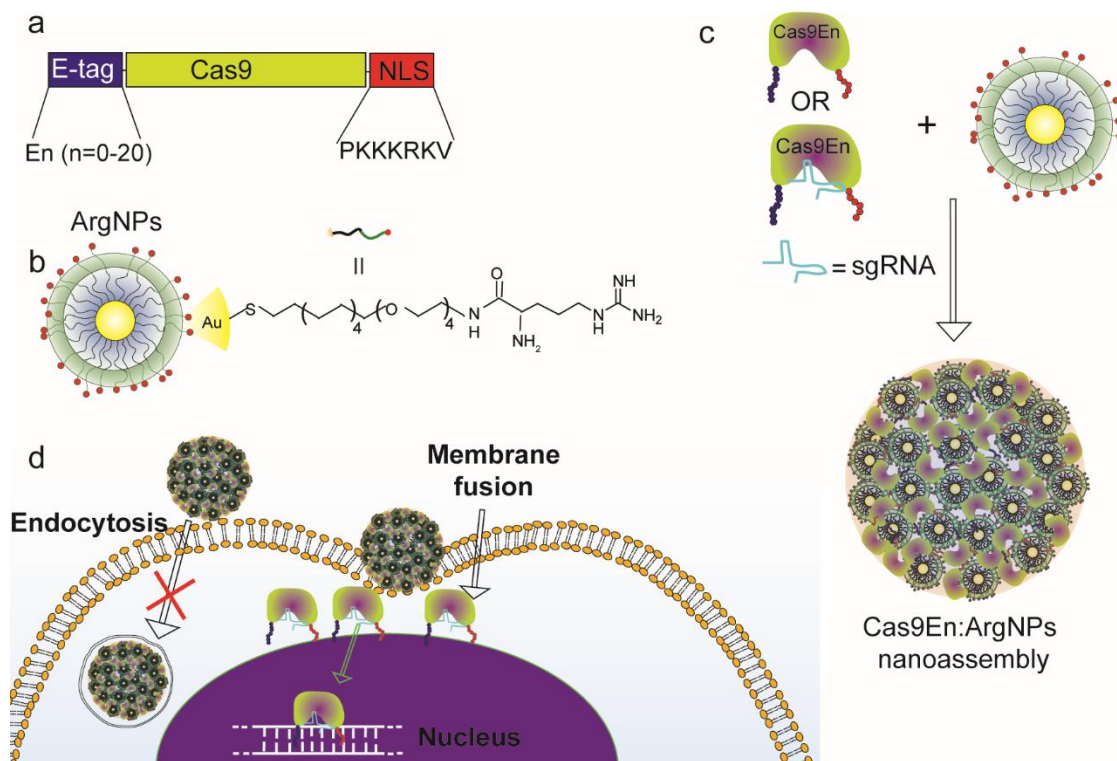


Figure 5. 1. Rational engineering of Cas9 protein and arginine nanoparticles (ArgNPs) for intracellular delivery of Cas9 protein or Cas9-RNP *via* membrane fusion. (a) Engineering Cas9 to carry an N-terminus E-tag and a C-terminus nuclear localization signal (NLS). (b) Chemical structure of ArgNPs. (c) Schematic showing nanoassembly formation by Cas9En-RNP and ArgNPs. (d) Delivery of Cas9En via membrane fusion mechanism. Fusion of nanoassemblies to the cell membrane may facilitate direct release of the protein payload into cytoplasm, bypassing endosomes.

Fabrication of Cas9En-ArgNP nanoassemblies. Having engineered and purified Cas9En proteins, we focused on fabricating self-assemblies between Cas9En and ArgNPs. When the E-tagged Cas9En protein or Cas9En-RNP were mixed with ArgNPs, they formed self-assembled nanoassemblies (Figure 5.1). These nanoassemblies are designed to fuse to cell membranes upon contact, releasing encapsulated Cas9En or Cas9En-RNPs directly into the cell cytoplasm (Figure 5.1), and eventually to the nucleus. The desired self-assemblies were fabricated by mixing Cas9En or Cas9En-RNPs and ArgNPs at varying molar ratio in cell culture DMEM media.²⁰ Following this step, we characterized the assemblies after incubating the mixture at room temperature for 10 min. Transmission

electron microscopic (TEM) results indicated the formation of nanoassemblies. As the length of E-tag increased, larger sized assemblies were observed reaching 475 (± 60) nm in diameter (Figure 5.2). The resulting large size of the assemblies compared to the individual ArgNPs (~ 10 nm hydrodynamic diameter), Cas9En (~ 7.5 nm hydrodynamic diameter), and sgRNA (5.5 nm) (Figure 5.6) indicated the incorporation of a large number of nanoparticles and proteins into the self-assembled structures. Interestingly, high resolution TEM image indicated the dense packing of granular proteins into the nanoassemblies (Figure 5.2b). Cas9E20-RNPs also formed similar nanoassemblies with ArgNPs, however, additional aggregates were observed (Figure 5.2a). The optimal working molar ratio for assembly fabrication was found to be 2:1 (ArgNP:Cas9En), as determined from subsequent delivery experiments. These results collectively indicated that the length of E-tag, hence the multivalency, plays a crucial role in the self-assembly formation between engineered Cas9En and ArgNPs.

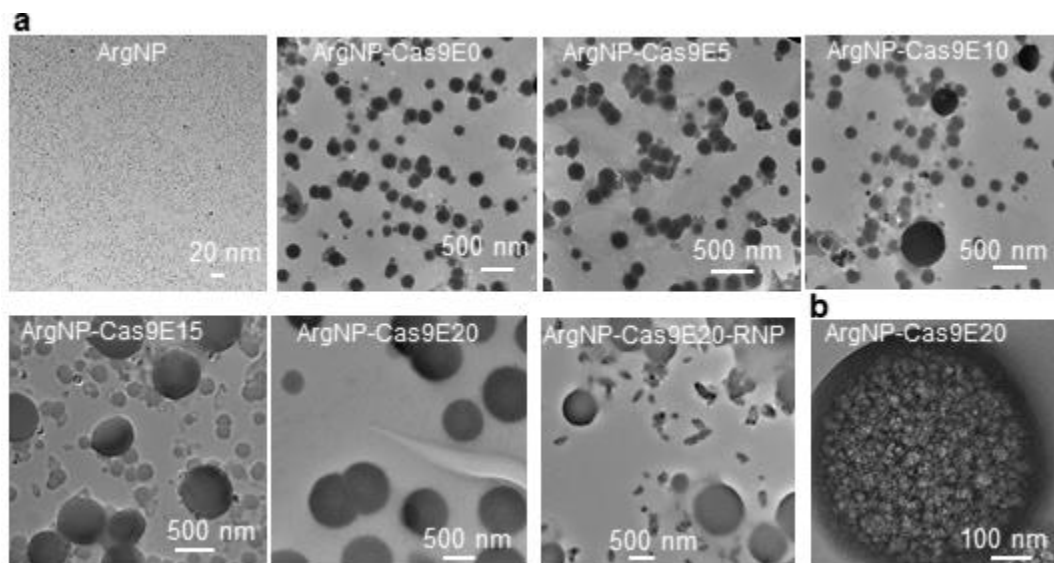


Figure 5. 2. Nanoassembly formation between ArgNPs and Cas9En or Cas9En-RNP is dictated by E-tag length. (a) TEM images of nanoassemblies. As the length of E-tag increased, larger nanoassemblies formed that are favorable for intracellular delivery of Cas9En (Figure 5.3). (b) High magnification image of nanoassemblies showing the inner structure containing protein and nanoparticle granules.

Direct cytoplasmic delivery of Cas9En protein using nanoassemblies. We next investigated the protein delivery capability of these nanoassemblies. We fabricated assemblies of ArgNPs with Cas9En or Cas9En-RNPs and incubated with HeLa cells in cultured media. Cas9En were labelled with fluorescein isothiocyanate (FITC) to monitor the cellular uptake efficiency. Delivery efficiency was evaluated after 3 h of incubation using confocal laser scanning microscopy (CLSM). Cytoplasmic delivery efficiency of Cas9En gradually increased as the E-tag length increased from E0 to E20, achieving up to Cas9E20 delivery in 90% of the cells (Figure 5.3a, b; Figure 5.7). Delivered Cas9En readily dispersed into cytoplasm, and reached the nucleus, a requirement for gene editing (Figure 5.3c). Confocal microscopy Z-stacking further supported the cytoplasmic and nuclear localization of the delivered payload (Figure 5.8). Additionally, delivered Cas9En proteins stayed in the cells for at least 30h, without hampering the cell growth and viability (Figure 5.9). It is possible that poor cytoplasmic delivery of Cas9En with shorter length of E-tag, *i.e.* Cas9E0, Cas9E5, and Cas9E10, may be attributed to their inadequate nanoassembly formation with ArgNPs (Figure 5.2a). Likewise, Cas9E20-RNP was also delivered into cells, although to a lesser extent compared to Cas9E20 alone (Figure 5.3a). Interestingly, Cas9En with a shorter E-tag (E0 and E5) was found to bind the cell membrane, presumably due to the presence of unbound positively charged Cas9 protein in the assembly solution, which alone is capable of binding to the cell membrane (Figure 5.10). The delivery was further validated in other cell lines including human embryonic kidney cells (HEK-293T), and mouse macrophage (Raw 264.7) cells (Figure 5.11). Collectively, these results demonstrated the importance of co-engineering of the protein and ArgNPs for effective Cas9 delivery.

We performed time lapse video imaging to study the intracellular release-dynamics of Cas9En. We recorded the video at 30s intervals 1h after the addition of the nanoassemblies into HeLa cells. Cas9E20 delivery was nearly complete in cultured cells after 3h of post incubation (Figure 5.12). Real time tracking of a delivery event revealed a remarkably fast intracellular delivery, requiring only minutes for complete cytoplasmic/nuclear delivery after the initial contact by a nanoassembly (Figure 5.3d). Notably, a slight delay (1-2 min) in Cas9E20 transport into the nucleus from the cytosol was observed, presumably due to active nuclear transport of NLS-tagged Cas9En (Figure 5.3d). The instantaneous release of Cas9E20 into the whole cell further suggested that the payload may be directly released from the cell membrane and did not go through endocytosis.

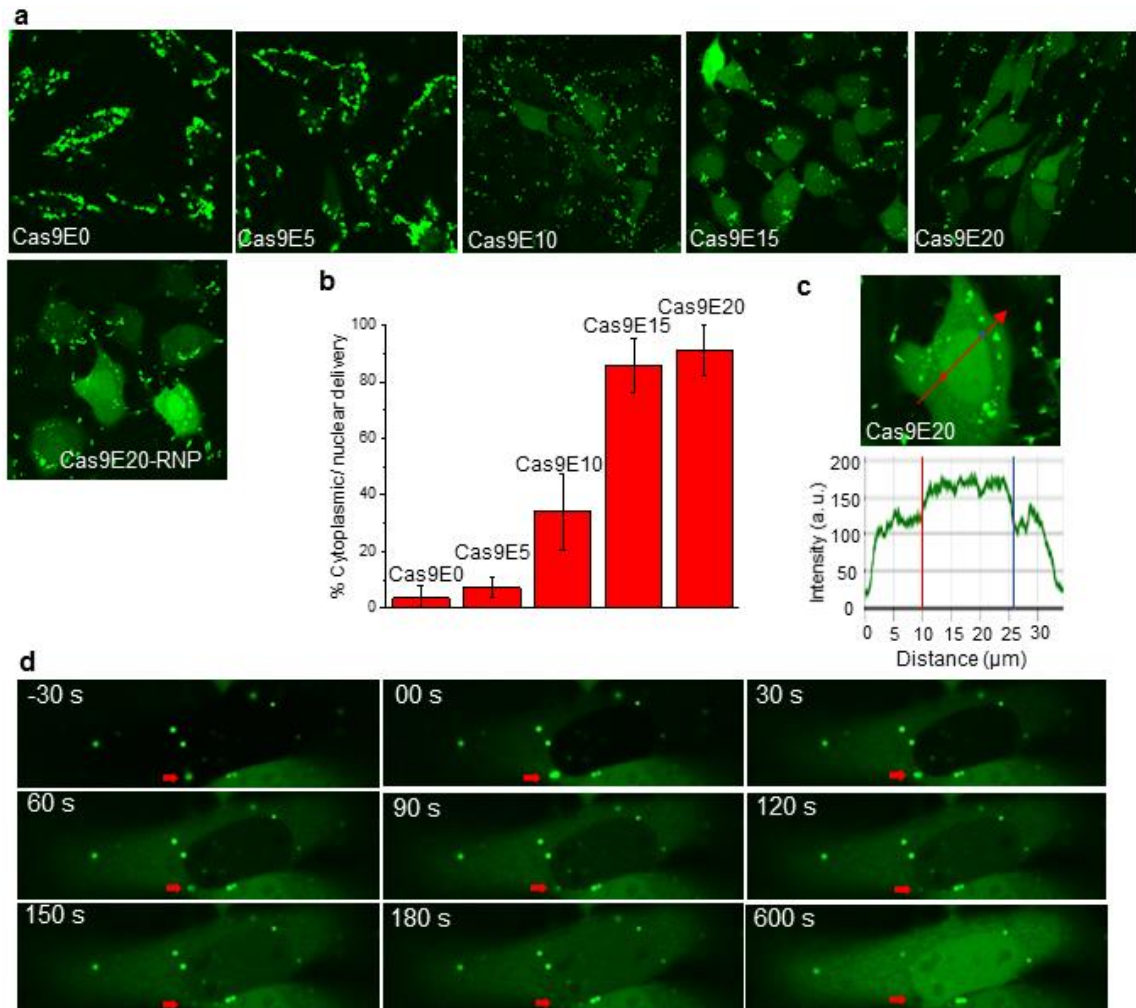


Figure 5.3. Endosomal entrapment-free direct cytoplasmic/nuclear delivery of engineered Cas9En or Cas9En-RNP is dictated by E-tag length. (a) Cytoplasmic/nuclear delivery of FITC labelled Cas9En increased as the length of E-tag increased, reaching maximum at E20. (b) Percentage cytoplasmic/nuclear delivery efficiency of Cas9En as measured by confocal microscopy. (c) Distribution of delivered Cas9E20 protein inside the cell, showing preferential accumulation of the protein in the cytoplasm and nucleus. (d) Real time tracking of a delivery event. Time lapse imaging of Cas9En delivery showed Cas9E20 was rapidly released into the cytosol and subsequently to the nucleus following a nanoassembly (red arrow) made contact with the cell surface. Zero second (00 s) represents the beginning of the delivery event.

Mechanism of CRISPR/Cas9 delivery. We investigated the mechanistic details of nanoassembly mediated Cas9-ribonucleoproteins delivery into cells. Nanoparticle mediated biomolecular delivery can occur through either an endocytic or a membrane fusion mechanisms (Figure 5.1d).²² We pretreated HeLa cells with inhibitors of

endocytosis (chlorpromazine and wortmannin) or cholesterol-dependent membrane fusion (methyl-beta-cyclodextrin (MBCD)),²³ to investigate whether similar mechanisms are involved in Cas9En-RNP delivery. After the inhibitor treatment, HeLa cells were incubated with the nanoassemblies, and monitored the delivery by CLSM. As shown in Figure 5.4, MBCD treatment inhibited FITC-Cas9E20 delivery into cells (2% delivery), compared to chlorpromazine (CPM) (83%) and wortmannin (79%), and untreated controls (90%). These studies collectively suggested that the nanoassembly-mediated Cas9En-RNP delivery occurred preferably through a cholesterol dependent membrane fusion-like process, but not *via* cellular endocytosis. Thus, our approach provided a direct transfer of Cas9En-RNP across the cell membrane into the cytoplasm resulting in a remarkably high delivery efficiency.

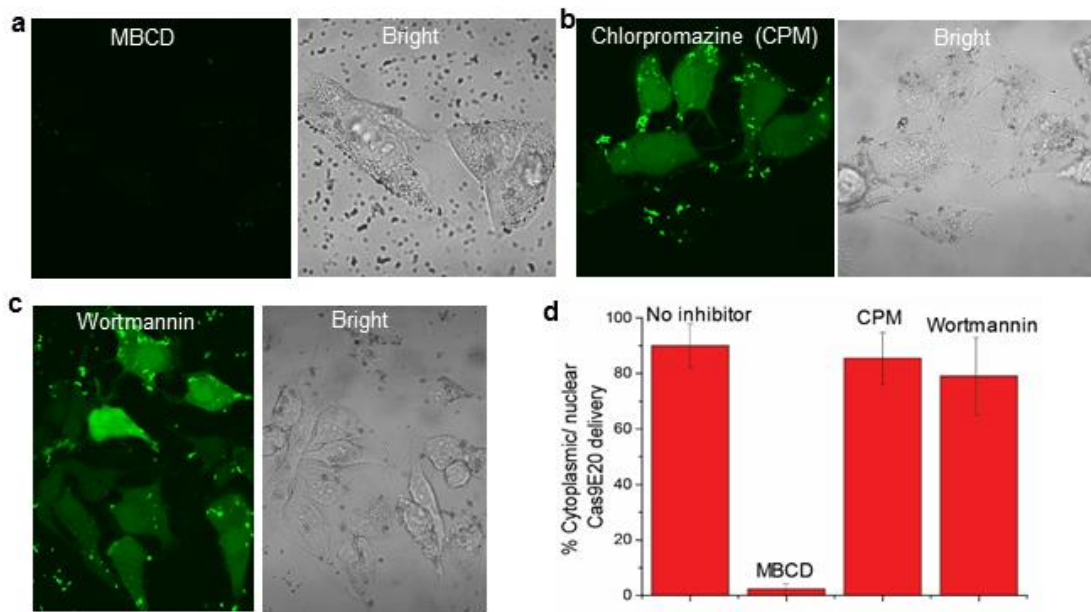


Figure 5. 4. A cholesterol dependent membrane fusion-like delivery mechanism is involved in nanoassembly-mediated Cas9En-RNP delivery. (a) cholesterol depletion (MBCD treatment) completely inhibited FITC-Cas9E20 delivery, whereas endocytic inhibitors (b) chlorpromazine (CPM) and (c) wortmannin did not block the delivery significantly. (d) Percentage of Cas9E20 cytoplasmic/nuclear delivery after various inhibitors treatment.

Gene editing in CRISPR/Cas9 delivered cells. Having efficiently delivered engineered Cas9En protein or Cas9En-RNP into cells, we evaluated the gene editing capability of this construct. We assembled Cas9E15-RNP with ArgNPs targeting human *AAVS1* gene and delivered these nanoassemblies into the HeLa cells.²⁴ In these experiments, the nanoassemblies were incubated with the cells for 3 h. in serum-free media; suitable conditions for *in vitro* and *ex vivo* applications. Genome editing efficiency was evaluated after 48 h, using indel (insertion and deletion) analysis.²⁷ As evident from Figure 5.5, targeting *AAVS1* gene resulted up to 29% of indel efficiency. As expected, delivering Cas9E15-RNP alone, or the untreated controls did not result in gene editing. To validate the usability of our method for any gene, we further targeted the human *PTEN* gene with an appropriate sgRNA.²⁵ Likewise, targeting *PTEN* gene resulted up to 30% of indel efficiency. The gene editing was further validated in HEK-293T and Raw 264.7 cell lines (Figure 5.13). These results collectively showed the efficient genome editing capability of our methodology.

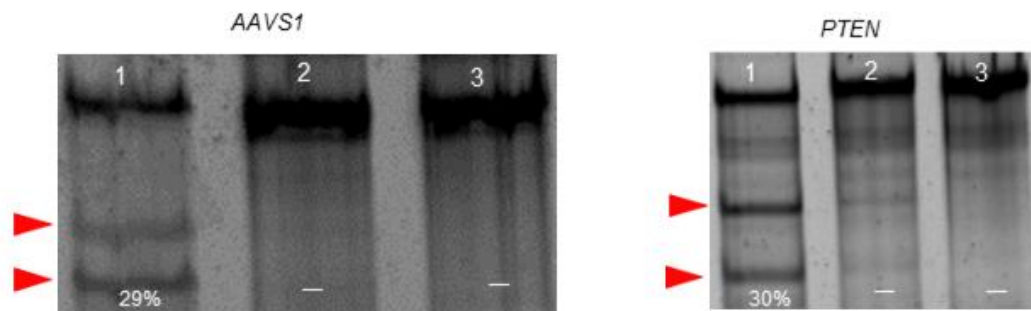


Figure 5. 5. Efficient gene editing resulted from Cas9En-RNP delivery. (a) Delivery of Cas9E15-RNP to target *AAVS1* and *PTEN* gene in HeLa cells resulted efficient gene editing, as determined by indel (insertion and deletion) assay: Lane 1: Cas9E15-RNP:ArgNPs, 2: Cas9E15-RNP, and 3: cells only. Indel efficiency is given in percentage.

5.3. Conclusions

In summary, we present here an engineering approach to drastically enhance the cytoplasmic/nuclear delivery of Cas9-RNPs, with concomitantly effective gene editing. This system provides a direct platform for multiple *in vitro* applications, and will greatly facilitate research in many other areas of rapidly growing genome engineering including spatiotemporal control of gene transcription and imaging chromatin dynamics. Additionally, this system provides a starting point for the creation of transient gene editing therapeutics without the requirement for gene delivery.

5.4. Experimental section

Engineering E-tagged Cas9En. Glutamic acid tag (E-tag) was inserted to N-terminus of SpCas9 through site directed mutagenesis (SDM). Briefly, following primers were used for the insertion of E-tag (inserted nucleotides are underlined in the primers) into the N-terminus Cas9 using pET28b-Cas9 expression vector (Addgene plasmid id=47327)²⁶ as the template. Note that the C-terminus of Cas9 contained a nuclear localization signal (NLS) and a 6xHis tag.

Cas9E0- F: ATGGACAAGAAGTACTCCATTGGGCTCGATATCGGC

Cas9E0- R: GGTATATCTCCTTCTTAAAGTTAAACAAAATTATTTCTAGAGGGG

Cas9E5- F: ATGGACAAGAAGTACTCCATTGGGCTCGATATCGGC

Cas9E5- R:

CTCTTCCTCCTCCTCCATGGTATATCTCCTTCTTAAAGTTAAACAAAATTATTT
CTAGAGGGG

Cas9E10- F:

ATGGAGGAAGAAGAGGAAGAGGAGGAGGAAGAGATGGACAAGAAGTACTC
CATTGGGCTCGAT

Cas9E10- R: GGTATATCTCCTTCTTAAAGTTAAACAAAATTATTTCTAGAGGGG

Cas9E15- F: (Cas9E10 as template)

ATGGAAGAGGAGGAAGAAGAGGAAGAAGAGGAAGAGGAGGAGGAAGAGAT
GGAC

Cas9E15- R: GGTATATCTCCTTCTTAAAGTTAAACAAAATTATTTCTAGAGGGG

Cas9E20- F: (Cas9E15 as template)

ATGGAAGAAGAGGAGGAAGAAGAGGAGGAAGAAGAGGAAGAAGAGGAAGA
GGAGGAG

Cas9E20- R: GGTATATCTCCTTCTTAAAGTTAAACAAAATTATTTCTAGAGGGG

Recombinant proteins (Cas9En) were expressed in *E. coli* BL21 Rosetta strain using standard protein expression protocol. Briefly, protein expression was carried out in 2xYT media with an induction condition of 0.75 mM IPTG and 18 °C for 16 hours. At this point, the cells were harvested and the pellets were lysed by using 1% Triton-X-100/DNase-I treatment. Triton-X-100 treatment was performed for ~30 min followed by DNase-I treatment for 15 min. Lysed cells were then spun down at 14,000 rpm for 30 min. The supernatant was collected and to it an additional 150 mM salt was added.²⁰ Proteins were purified using HisPur cobalt columns. Proteins were finally preserved in PBS buffer containing 300 mM salt. The purity of native proteins was determined using 8% SDS-PAGE gel.

sgRNA design and synthesis. sgRNAs were *in vitro* transcribed from dsDNA template (containing the protospacer and the tracrRNA sequence) using AmpliScribe-T7-Flash Transcription kit according to manufacturer's protocol. dsDNA was PCR amplified from a template plasmid carrying the tracrRNA sequence.²⁷ The following primers were used for the PCR amplification.

sgRNA-R: AAAAAAGCACCGACTCGGTGCCACT (common for all)

sgAAVSI-F:

GAAATTAATACGACTCACTATAGGctccctcccaggatcctctcGTTTTAGAGCTAGAA
ATAGCA

sgPTEN-F:

GAAATTAATACGACTCACTATAGGgagatcgtagcagaaacaaaGTTTTAGAGCTAGA
AATAGCA

In vitro transcribed sgRNAs were purified using RNA purification kit (Zymo research RNA Clean & Concentrator).

Nanoparticle synthesis and characterization. Arginine-functionalized gold nanoparticles (ArgNPs) were prepared according to our previous methods.¹⁹ The arginine-functionalized thiol ligand was synthesized first. Following this, ArgNPs were prepared by conventional place-exchange reaction of 2-nm sized 1-pentanethiol-protected gold nanoparticles (Au-C5) with HS-C11-TEG-NH-Arginine. The resultant ArgNPs were dissolved in distilled water, purified by dialysis, and whose characterization was reported previously.^{19,20} Complete synthesis of a batch of ArgNPs takes around 1-2 weeks, however can be synthesized in large batches that may be stable and used for years for delivery

purpose. The manufacturing cost of our gold nanoparticle is roughly ~10-20 cents (USA) per sample of 'delivery'.

Nanoassembly fabrication. Cas9En-RNP:ArgNPs nanoassemblies were prepared through a simple mixing procedure. Cas9En and sgRNAs (1:1 molar ratio)²⁸ were assembled in 1×PBS for 30 min at room temperature first, then ArgNPs (50 μM stock in 5 mM PB, pH 7.4) were added to 100 μL of 1×PBS in another vial, followed by adding the preassembled Cas9En-RNP at appropriate working molar ratio [usually at 2:1 ratio (ArgNP, 125 nM)/(Cas9En-RNP, 62 nM), which corresponds to ~10 μg of Cas9En protein and ~2 μg of sgRNA per cultured dish]. The working molar ratio was determined by screening different ratios in the subsequent delivery experiments. The nanoassemblies were incubated at room temperature for another 10 min. DMEM was added to the nanoassemblies to make the final volume up to 1000 μL. The nanoassemblies were then incubated either at 37 °C for 30 min for TEM, or directly added to cells grown overnight in confocal dish for delivery experiments.

Cell culture. 240,000-300,000 cells were grown in a confocal dish (glass bottom culture dishes, MatTek) in DMEM (with 10% FBS, and 1% antibiotics) for overnight at 37 °C under 5% CO₂. Cells were washed with 1×PBS (twice) before incubation with nanoassemblies.

Delivery. Assembled Cas9En-RNP:ArgNPs nanoassemblies (preassembled in 100 μL PBS for 10 min, plus 900 μL DMEM media) were immediately transferred to each dish of confluent grown cells. Cells were then incubated at 37 °C and 5% CO₂ for 3h. At this point cells were washed with 1xPBS buffer and immediately processed for investigating delivery efficiency that was determined by Confocal microscopy (Zeiss LSM 510 Meta

microscope, or Nikon A1 laser scanning microscope). Z-stacking was performed using Nikon A1, at every 125 nm interval.

It is noteworthy that the nanoassemblies can be incubated with cells for a longer period of time (~24h) without affecting cell growth/viability, an important issue for *in vitro* and *ex vivo* editing.

Estimation of cytoplasmic/nuclear delivery efficiency. Since flow cytometry cannot distinguish between cytoplasmic/nuclear delivery and endosomally-entrapped delivery, we used confocal microscopy to estimate the delivery efficiency. Around 400 cells were counted for each Cas9En, 3h after the delivery as described above.

Time lapse video imaging. Live-delivery imaging was performed using confocal microscope. Briefly, 1h after the nanoassemblies were added to the cultured HeLa cells in a live-cell imaging chamber containing humidified 5% CO₂ at 37 °C, the images were acquired at every 30s interval for 2h using 60x oil immersion lens.

Cholesterol depletion. Endocytic and membrane fusion inhibitors were used to block the Cas9En-RNP delivery. Cells were pretreated with wortmannin (150ng/mL), chlorpromazine (1.5µg/mL), and methyl-β-cyclodextrin (MBCD, 7.5mg/mL) in DMEM media for 1 h at 37 °C and 5% CO₂.²³ In the meantime, nanoassemblies were prepared. Inhibitor-treated cells were washed with 1×PBS twice, then the nanoassembly solutions were applied for Cas9En delivery. Confocal microscopy experiments were performed after 3h of nanoassembly incubation to image and estimate cytoplasmic/nuclear delivery.

Indel analysis. After Cas9E15-RNP delivery for 3h, cells were washed and replaced with DMEM media (with 10% FBS, and 1% antibiotics), then allowed to grow for another 48 h. At this point cells were harvested to extract genomic DNA using QuickExtract

genomic DNA isolation kit (Epicentre biotechnologies). Indel assays were performed using T7 endonuclease-I according to standard protocol.²⁷

Cas9En protein sequence. (En at the N-terminus represents E-tag, where n = 0, 5, 10, 15, and 20; NLS is underlined at the C-terminus)

MEnMDKKYSIGLDIGTNSVGWAVITDEYKVPSSKKFKVLGNTDRHSIKKNLIGAL
LFDSGETAEATRLKRTARRRYTRRKNRICYLQEIFSNEMAKVDDSSFFHRLEESFL
VEEDKKHERHPIFGNIVDEVAYHEKYPTIYHLRKKLVDSTDKADLRLIYLALAH
MIKFRGHFLIEGDLNPDNSDVDKLFIQLVQTYNQLFEENPINASGVDAKAILSARL
SKSRLENLIAQLPGEKKNGLFGNLIASLGLTPNFKSNFDLAEDAQLQSKDTY
DDDLDNLLAQIGDQYADLFLAAKNLSDAILLSDILRVNTEITKAPLSASMIKRYDE
HHQDLTLLKALVRQQLPEKYKEIFFDQSKNGYAGYIDGGASQEEFYKFIKPILEK
MDGTEELLVVLNREDLLRKQRTFDNGSIPHQIHLGELHAILRRQEDFYPPFLKDNR
EKIEKILTRIPYYVGPLARGNSRFAWMTRKSEETITPWNFEEVVDKGASAQSFIE
RMTNFDKNLPNEKVLPHSLLYEYFTVYNELTKVKYVTEGMRKPAFLSGEQKK
AIVDLLFKTRNKVTVKQLKEDYFKKIECFDSVEISGVEDRFNASLGTYHDLLKIIK
DKDFLDNEENEDILEDIVLTLTLFEDREMIEERLKYAHLFDDKVMKQLKRRRYT
GWGRLSRKLINGIRDKQSGKTILDFLKSDFANRNFMLIHDDSLTFKEDIQKAQ
VSGQGDSLHEHIANLAGSPAIKKILQTVKVVDELVKVMGRHKPENIVIEMARE
NQTQKGQKNSRERMKRIEIGIKELGSQILKEHPVENTQLQNEKLYLYYLQNGR
DMYVDQELDINRLSDYDVDHIVPQSFLKDDSIDNKVLTRSDKNRGKSDNVPSEE
VVKKMKNYWRQLLNAKLITQRKFDNLTKAERGGSELKAGFIKRQLVETRQIT
KHVAQILDSRMNTKYDENDKLIREVKVITLKSCLVSDFRKDFQFYKVREINNYH
HAHDAYLNAVVGTAIIKKYPKLESEFVYGDYKVYDVRKMIKSEQEIGKATAK
YFFYSNIMNFFKTEITLANGEIRKRPLIETNGETGEIVWDKGRDFATVRKVLSPMPQ
VNIVKKTEVQTGGFSKESILPKRNSDKLIARKKDWDPKKYGGFDSPTVAYSVLV
VAKVEKGKSKKLKSVKELLGITIMERSSEKPNIDFLEAKGYKEVKKDLIILPKY
SLFELENGRKRMLASAGELQKGNELALPSKYVNFLYLASHYEKLGSPEDNEQK
QLFVEQHKHYLDEIIEQISEFSKR VILADANLKVLSAYNKHRDKPIREQAENIIHL
FTLTNLGAPAAFKYFDTTIDRKRYTSTKEVLDA TLIHQSITGLYETRIDLSQLGGD
SRADPKKKRVAAALEHHHHHH

5.5. Supporting figures

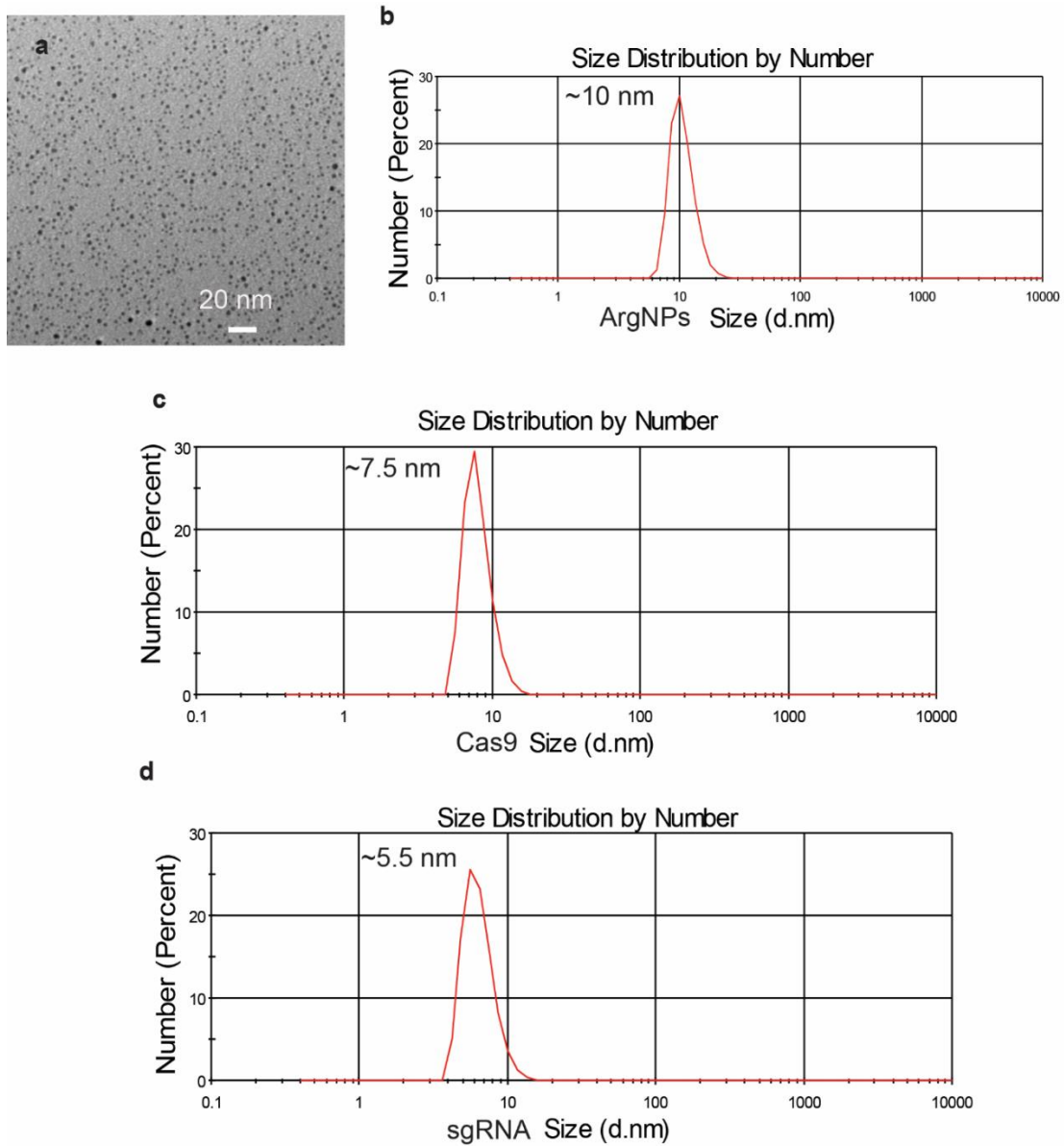


Figure 5. 6. TEM and DLS characterization of nanoparticles, Cas9 and sgRNA. (a) TEM of ArgNPs. Hydrodynamic size of ArgNPs (b), Cas9 (c), and sgRNA (d).

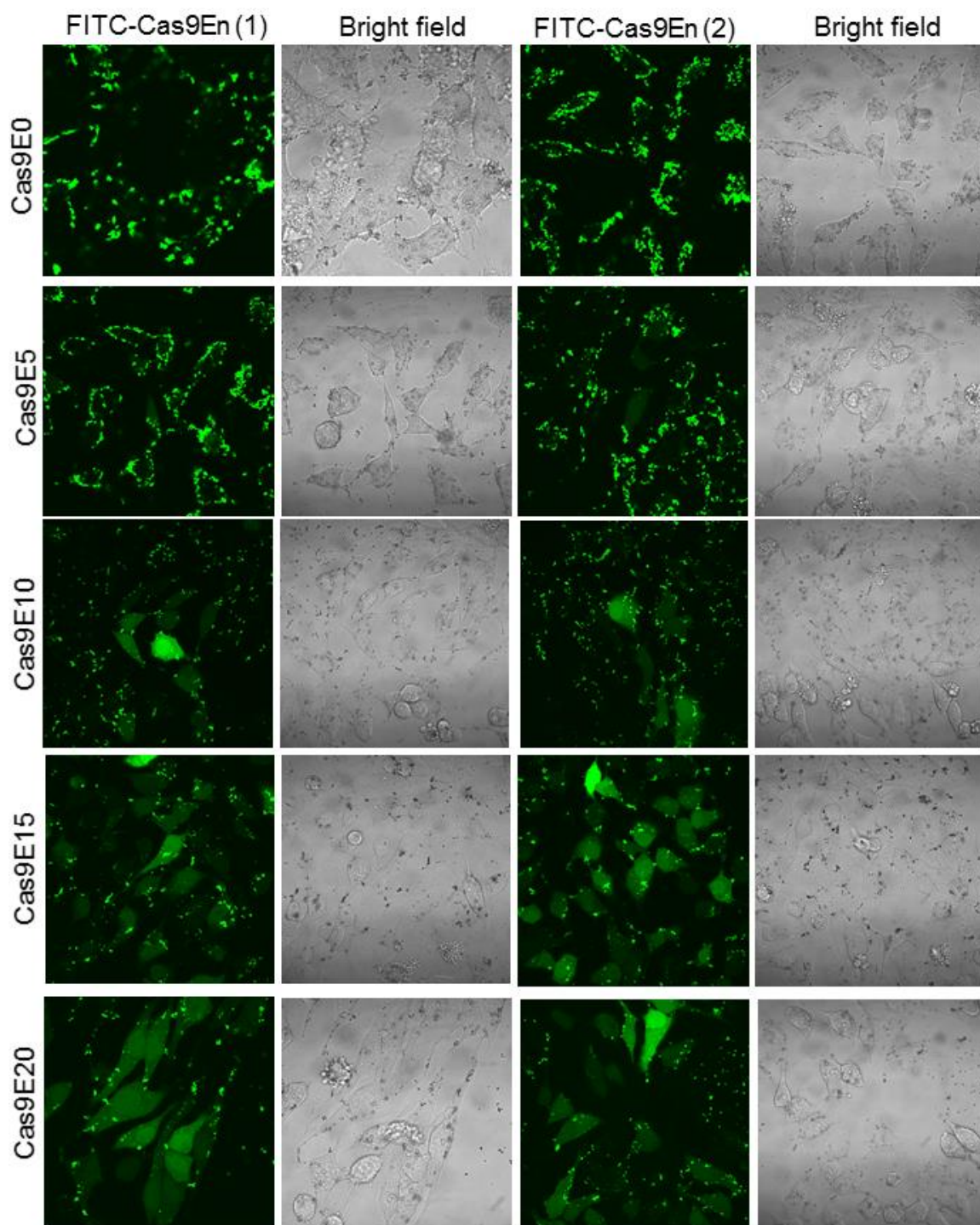


Figure 5. 7. E-tag length determines cytoplasmic/nuclear delivery of Cas9En. Laser scanning confocal microscopy (LSCM) images of delivered FITC labelled Cas9En proteins using nanoassemblies. Two representative slides are provided here for each Cas9En delivery. For quantitative estimation of cytoplasmic/nuclear delivery a large number of slides were considered, and at least ~400 cells were counted. Images were taken 3h post-incubation of the nanoassemblies with HeLa cells.

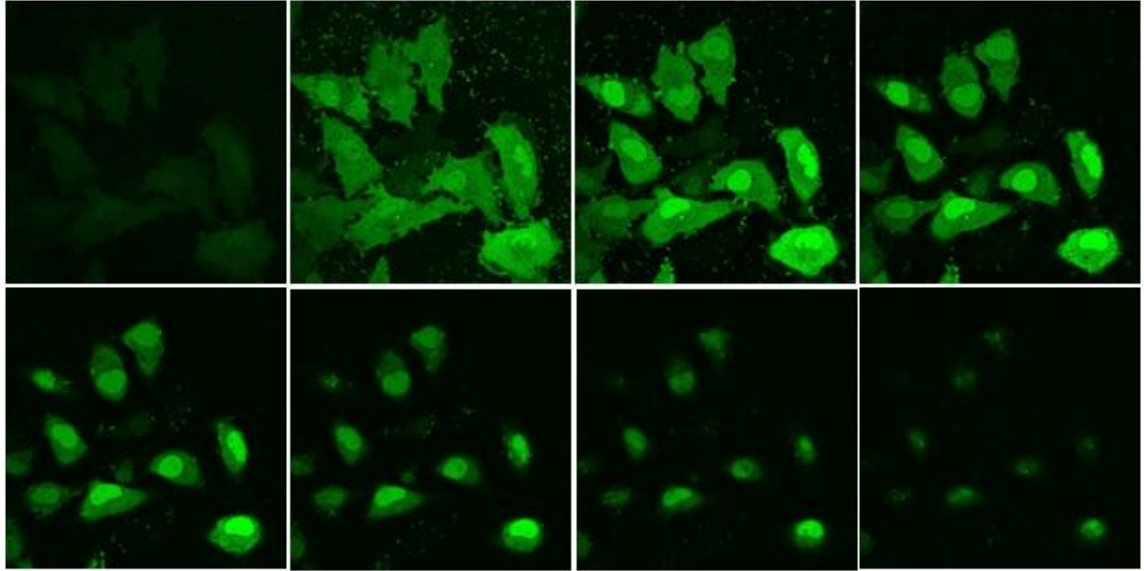


Figure 5. 8. Confocal z-stacking images of delivered FITC labelled Cas9E20 revealing cytoplasmic/nuclear distribution of delivered Cas9. Above images were taken from every 1.25 micron apart.

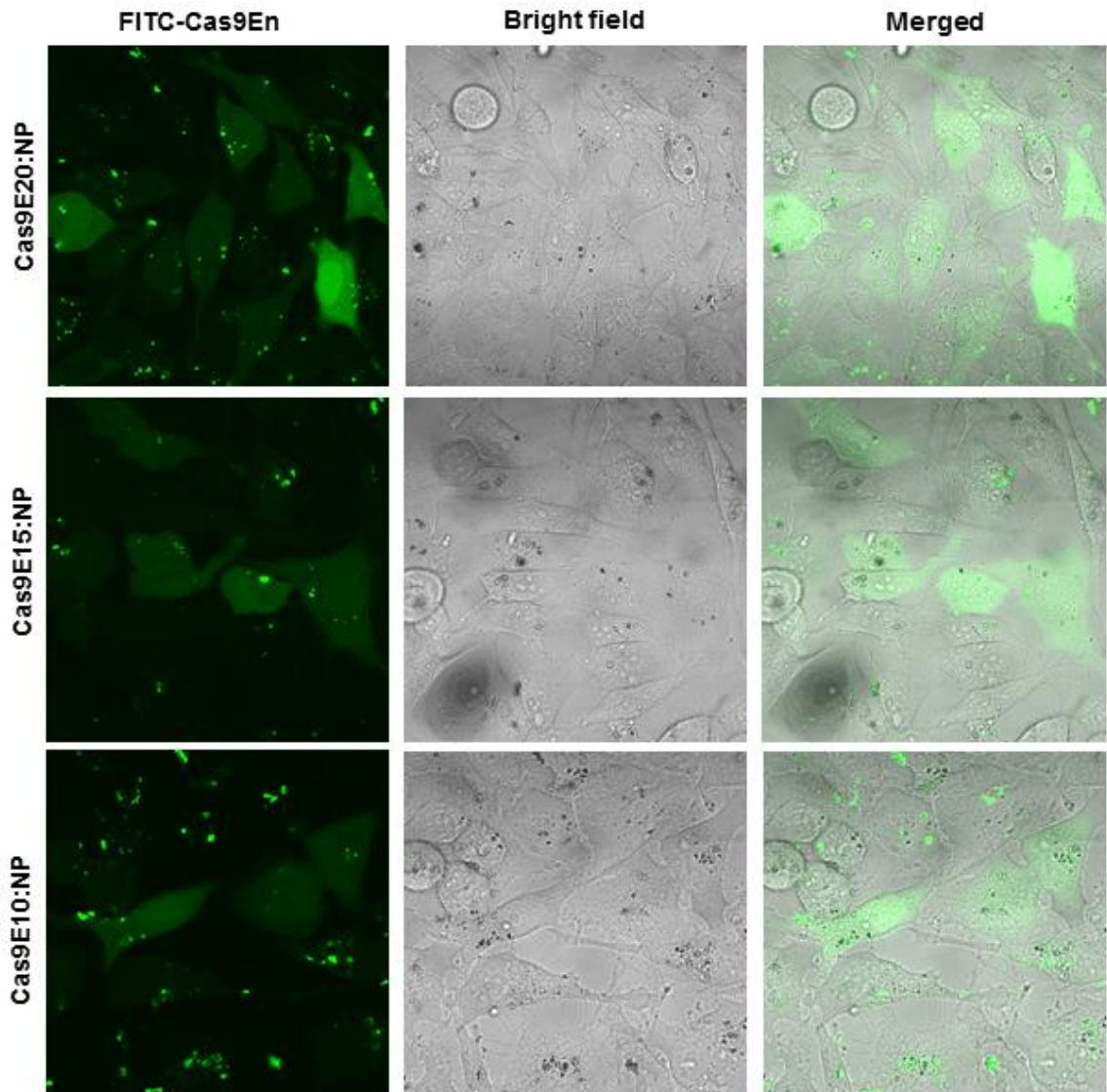


Figure 5. 9. Lifetime of delivered Cas9En. Delivered Cas9En remains in the cell for a long period (at least over a day), without affecting cell viability and growth. Confocal microscopy images showing delivered FITC-labelled Cas9En proteins after 30 h of delivery. Delivered Cas9En did not hamper the cell viability, as can be seen from the regular cell morphology in the bright field image.

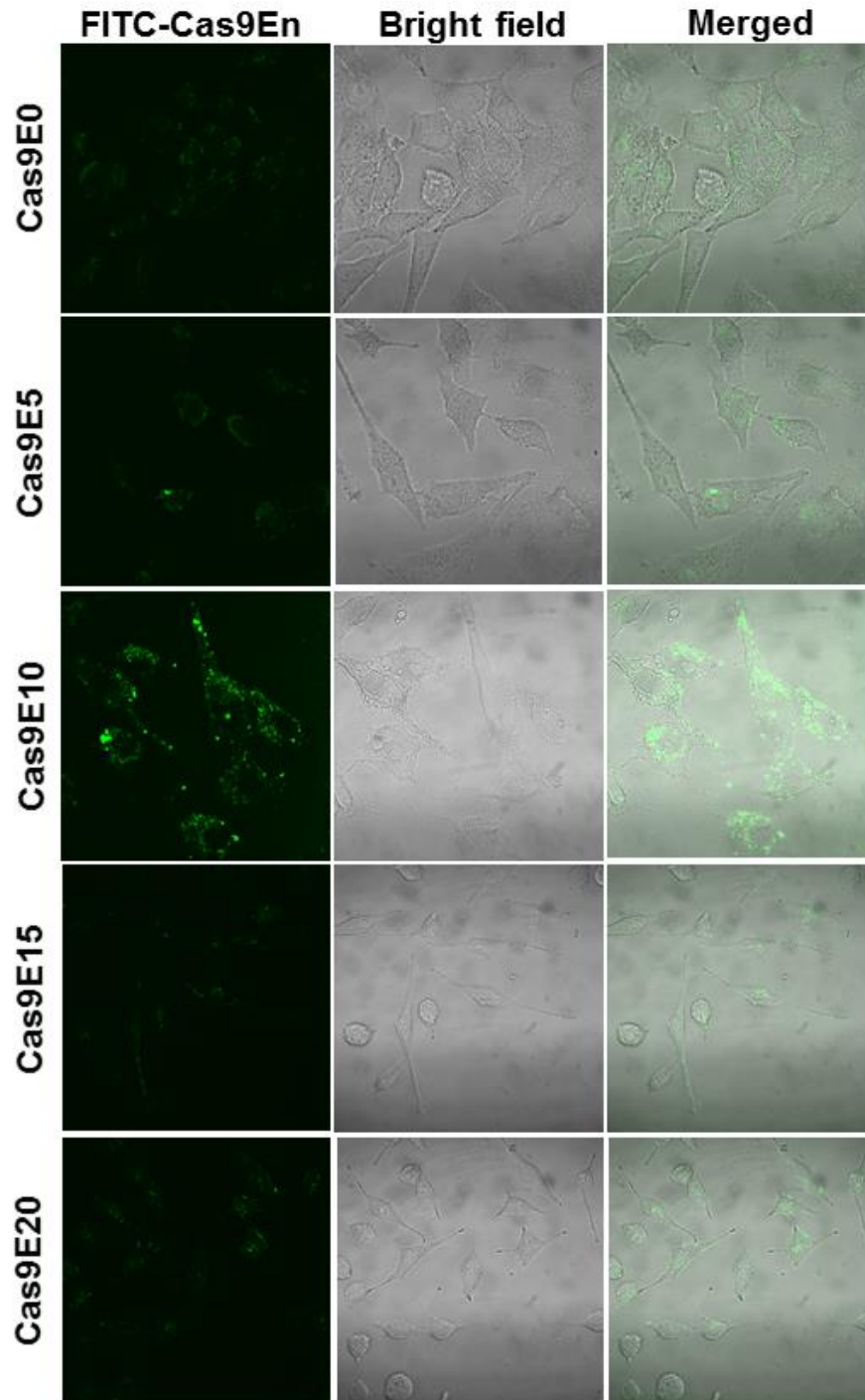


Figure 5. 10. Cas9En protein alone get trapped in the endosomes. Confocal microscopy images showing Cas9En proteins, either attached to the cell membrane or trapped in the endosomes, after 3 h incubation of the cells with Cas9En protein alone.

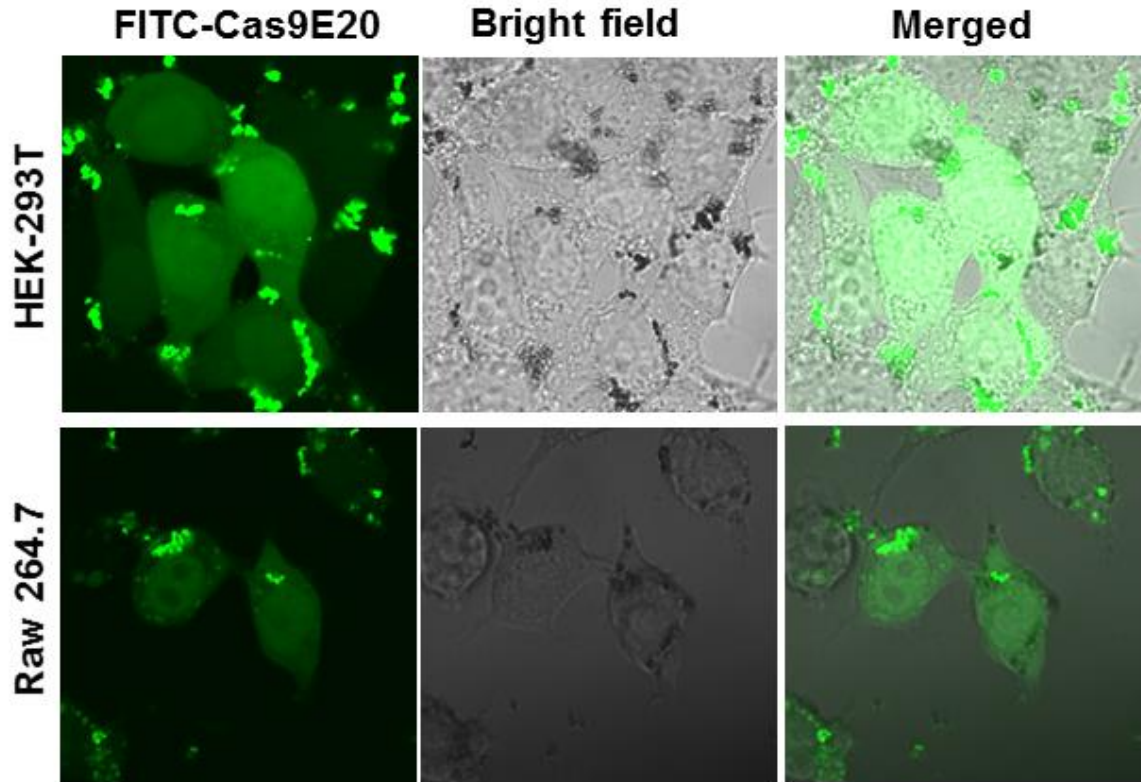


Figure 5. 11. Delivery of Cas9E20 into cultured cells. Confocal microscopy images showing delivered FITC-Cas9E20 after 3 h of incubation in human embryonic kidney cells (HEK-293T), and mouse macrophage (Raw 264.7).

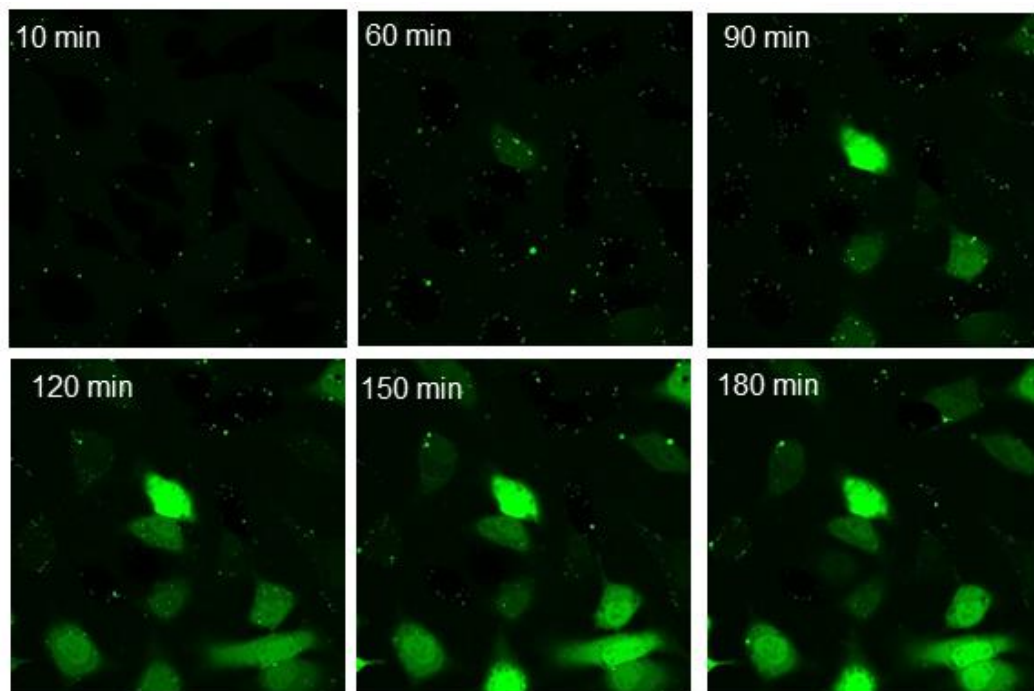


Figure 5. 12. Time-lapse video imaging of Cas9E20 delivery process. Alexa fluor 488 labeled Cas9E20 delivery was nearly completed in 3h.

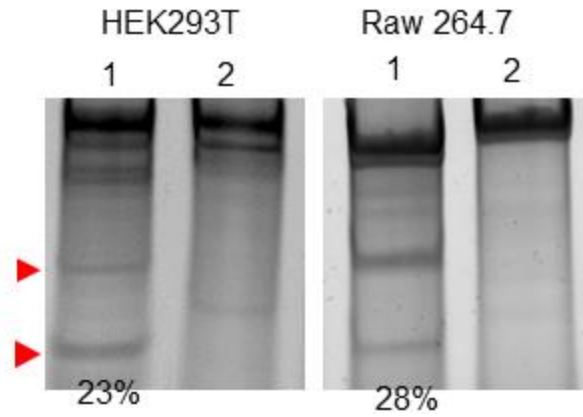


Figure 5. 13. Gene editing in HEK-293T and Raw 264.7 cells. PTEN gene was targeted using Cas9E15-RNP with appropriate sgRNA in HEK293T and Raw 264.7 cells. 48h after delivery indel analysis was performed using standard procedure. (1) Cas9E15-RNP, and (2) cells only. Indel efficiency is given in percentage.

5.6. References

- (1) Doudna, J. A.; Charpentier, E. The New Frontier of Genome Engineering with CRISPR-Cas9. *Science* **2014**, *346*, 1258096.
- (2) Cox, D. B. T.; Platt, R. J.; Zhang, F. Therapeutic Genome Editing: Prospects and Challenges. *Nat. Med.* **2015**, *21*, 121-131.
- (3) Konermann, S.; Brigham, M. D.; Trevino, A. E.; Joung, J.; Abudayyeh, O. O.; Barcena, C.; Hsu, P. D.; Habib, N.; Gootenberg, J. S.; Nishimasu, H. Nureki, O.; Zhang, F. Genome-Scale Transcriptional Activation by an Engineered CRISPR-Cas9 Complex. *Nature* **2015**, *517*, 583-588.
- (4) Kiani, S.; Chavez, A.; Tuttle, M.; Hall, R. N.; Chari, R.; Ter-Ovanesyan, D.; Qian, J.; Pruitt, B. W.; Beal, J.; Vora, S.; Buchthal, J.; Kowal, E. J.; Ebrahimkhani, M. R.; Collins, J. J.; Weiss, R.; Church, G. Cas9 gRNA Engineering for Genome Editing, Activation and Repression. *Nat. Methods* **2015**, *12*, 1051-1054.
- (5) Chen, B.; Gilbert, Luke A.; Cimini, Beth A.; Schnitzbauer, J.; Zhang, W.; Li, G.-W.; Park, J.; Blackburn, Elizabeth H.; Weissman, Jonathan S.; Qi, Lei S.; Huang, B. Dynamic Imaging of Genomic Loci in Living Human Cells by an Optimized CRISPR/Cas System. *Cell* **2013**, *155*, 1479-1491.
- (6) Schwank, G.; Koo, B.-K.; Sasselli, V.; Dekkers, Johanna F.; Heo, I.; Demircan, T.; Sasaki, N.; Boymans, S.; Cuppen, E.; van der Ent, C. K.; Nieuwenhuis, E. E.; Beekman, J. M.; Clevers, H. Functional Repair of CFTR by CRISPR/Cas9 in Intestinal Stem Cell Organoids of Cystic Fibrosis Patients. *Cell Stem Cell* **2013**, *13*, 653-658.
- (7) Yin, H.; Xue, W.; Chen, S.; Bogorad, R. L.; Benedetti, E.; Grompe, M.; Kotliansky, V.; Sharp, P. A.; Jacks, T.; Anderson, D. G. Genome Editing with Cas9 in Adult Mice Corrects a Disease Mutation and Phenotype. *Nat. Biotechnol.* **2014**, *32*, 551-553.
- (8) Nelson, C. E.; Gersbach, C. A. Engineering Delivery Vehicles for Genome Editing. *Annu. Rev. Chem. Biomol. Eng.* **2016**, *7*, 637-662.
- (9) Hsu, P. D.; Lander, E. S.; Zhang, F. Development and Applications of CRISPR-Cas9 for Genome Engineering. *Cell* **2014**, *157*, 1262-1278.
- (10) Oude Blenke, E.; Evers, M. J.; Mastrobattista, E.; van der Oost, J. CRISPR-Cas9 Gene Editing: Delivery Aspects and Therapeutic Potential. *J. Control Release* **2016**, *244*, 139-148.

- (11) Li, L.; He, Z. Y.; Wei, X. W.; Gao, G. P.; Wei, Y. Q. Challenges in CRISPR/Cas9 Delivery: Potential Roles of Nonviral Vectors. *Hum. Gene Ther.* **2015**, *26*, 452-462.
- (12) Zuris, J. A.; Thompson, D. B.; Shu, Y.; Guilinger, J. P.; Bessen, J. L.; Hu, J. H.; Maeder, M. L.; Joung, J. K.; Chen, Z.-Y.; Liu, D. R. Cationic Lipid-Mediated Delivery of Proteins Enables Efficient Protein-Based Genome Editing *in vitro* and *in vivo*. *Nat. Biotechnol.* **2015**, *33*, 73-80.
- (13) Liu, J.; Gaj, T.; Yang, Y.; Wang, N.; Shui, S.; Kim, S.; Kanchiswamy, C. N.; Kim, J.-S.; Barbas Iii, C. F. Efficient Delivery of Nuclease Proteins for Genome Editing in Human Stem Cells and Primary Cells. *Nat. Protoc.* **2015**, *10*, 1842-1859.
- (14) Ramakrishna, S.; Kwaku Dad, A.-B.; Beloor, J.; Gopalappa, R.; Lee, S.-K.; Kim, H. Gene Disruption by Cell-Penetrating Peptide-Mediated Delivery of Cas9 Protein and Guide RNA. *Genome Res.* **2014**, *24*, 1020-1027.
- (15) Sun, W.; Ji, W.; Hall, J. M.; Hu, Q.; Wang, C.; Beisel, C. L.; Gu, Z. Self-Assembled DNA Nanoclews for the Efficient Delivery of CRISPR-Cas9 for Genome Editing. *Angew. Chem. Int. Ed. Engl.* **2015**, *54*, 12029-12033.
- (16) Schumann, K.; Lin, S.; Boyer, E.; Simeonov, D. R.; Subramaniam, M.; Gate, R. E.; Haliburton, G. E.; Ye, C. J.; Bluestone, J. A.; Doudna, J. A.; Marson, A. Generation of Knock-In Primary Human T Cells using Cas9 Ribonucleoproteins. *Proc. Natl. Acad. Sci. U. S. A.* **2015**, *112*, 10437-10442.
- (17) Kim, S.; Kim, D.; Cho, S. W.; Kim, J.; Kim, J.-S. Highly Efficient RNA-Guided Genome Editing in Human Cells *via* Delivery of Purified Cas9 Ribonucleoproteins. *Genome Res.* **2014**, *24*, 1012-1019.
- (18) Han, X.; Liu, Z.; Jo, M. c.; Zhang, K.; Li, Y.; Zeng, Z.; Li, N.; Zu, Y.; Qin, L. CRISPR-Cas9 Delivery to Hard-to-Transfect Cells *via* Membrane Deformation. *Sci. Adv.* **2015**, *1*, e1500454.
- (19) Yang, X. C.; Samanta, B.; Agasti, S. S.; Jeong, Y.; Zhu, Z. J.; Rana, S.; Miranda, O. R.; Rotello, V. M. Drug Delivery using Nanoparticle-Stabilized Nanocapsules *Angew. Chem. Int. Ed.* **2011**, *50*, 477-481.
- (20) Mout, R.; Tonga, G. Y.; Wang, L.S.; Ray, M.; Roy, T.; Rotello, V. M. Programmed Self-Assembly of Hierarchical Nanostructures through Protein-Nanoparticle Co-Engineering. *ACS Nano*, **2017**, *11*, 3456-3462.
- (21) Mout, R.; Tonga, G. Y.; Ray, M.; Moyano, D. F.; Xing, Y.; Rotello, V. M. Environmentally Responsive Histidine-Carboxylate Zipper Formation Between Proteins and Nanoparticles. *Nanoscale* **2014**, *6*, 8873-8877.

- (22) Jiang, Y.; Tang, R.; Duncan, B.; Jiang, Z.; Yan, B.; Mout, R.; Rotello, V. M. Direct Cytosolic Delivery of siRNA using Nanoparticle-Stabilized Nanocapsules. *Angew. Chem. Int. Ed. Engl.* **2015**, *54*, 506-510.
- (23) Saha, K.; Kim, S. T.; Yan, B.; Miranda, O. R.; Alfonso, F. S.; Shlosman, D.; Rotello, V. M. Surface Functionality of Nanoparticles Determines Cellular Uptake Mechanisms in Mammalian Cells. *Small* **2013**, *9*, 300-305.
- (24) Sadelain, M.; Papapetrou, E. P.; Bushman, F. D. Safe Harbours for the Integration of New DNA in the Human Genome. *Nat. Rev. Cancer* **2011**, *12*, 51-58.
- (25) Xue, W.; Chen, S.; Yin, H.; Tammela, T.; Papagiannakopoulos, T.; Joshi, N. S.; Cai, W.; Yang, G.; Bronson, R.; Crowley, D. G. Zhang, F.; Anderson, D. G.; Sharp, P. A.; Jacks, T. CRISPR-Mediated Direct Mutation of Cancer Genes in the Mouse Liver. *Nature* **2014**, *514*, 380-384.
- (26) Gagnon, J. A.; Valen, E.; Thyme, S. B.; Huang, P.; Ahkmetova, L.; Pauli, A.; Montague, T. G.; Zimmerman, S.; Richter, C.; Schier, A. F. Efficient Mutagenesis by Cas9 Protein-Mediated Oligonucleotide Insertion and Large-Scale Assessment of Single-Guide RNAs. *PLoS One* **2014**, *9*, e98186.
- (27) Ran, F. A.; Hsu, P.; Wright, J.; Agarwala, V.; Scott, D. A.; Zhang, F. Genome Engineering Using the CRISPR-Cas9 System. *Nat. Protoc.* **2013**, *8*, 2281-2308.
- (28) Jinek, M.; Chylinski, K.; Fonfara, I.; Hauer, M.; Doudna, J. A.; Charpentier, E. A. Programmable Dual-RNA-Guided DNA Endonuclease in Adaptive Bacterial Immunity. *Science* **2012**, *337*, 816-821.

BIBLIOGRAPHY

Adkins, J. N.; Varnum, S. M.; Auberry, K. J.; Moore, R. J.; Angell, N. H.; Smith, R. D.; Springer, D. L.; Pounds, J. G. Toward a Human Blood Serum Proteome: Analysis by Multidimensional Separation Coupled with Mass Spectrometry. *Mol. Cell Proteomics* **2002**, *1*, 947-955.

Alberts, B.; Johnson, A.; Lewis, J.; et al., Intracellular Vesicular Traffic. *Molecular Biology of the Cell* **2002**, 4th edition, New York: Garland Science.

Ambrosetti, A.; Ferri, N.; DiStasio, R. A. Jr.; Tkatchenko, A. Wave-Like Charge Density Fluctuations and van der Waals Interactions at the Nanoscale. *Science* **2016**, *351*, 1171-1176.

Batista, C. A.; Larson, R. G.; Kotov, N. A. Nonadditivity of Nanoparticle Interactions. *Science* **2015**, *350*, 1242477.

Bayraktar, H.; You, C. C.; Rotello, V. M.; Knapp, M. J. Facial Control of Nanoparticle Binding to Cytochrome C. *J. Am. Chem. Soc.* **2007**, *129*, 2732-2733.

Bishop, K. J.; Wilmer, C. E.; Soh, S.; Grzybowski, B. A. Nanoscale Forces and their uses in Self-Assembly. *Small* **2009**, *5*, 1600-1630.

Boal, A. K.; Ilhan, F.; DeRouchey, J. E.; Thurn-Albrecht, T.; Russell, T. P.; Rotello, V. M. Self-Assembly of Nanoparticles into Structured Spherical and Network Aggregates. *Nature* **2000**, *404*, 746-748.

Bönisch, C.; Hake, S. B. Histone H2A Variants in Nucleosomes and Chromatin: More or Less Stable. *Nucleic Acids Res.* **2012**, *40*, 10719-10741.

Boström, M.; Deniz, V.; Franks, G. V.; Ninham, B. W. Extended DLVO Theory: Electrostatic and Non-Electrostatic Forces in Oxide Suspensions. *Adv. Colloid. Interface Sci.* **2006**, 123-126, 5-15.

Campbell, N. A.; Reece, J. B. *Biology*, 6th edition, Benjamin Cummings, **2002**.

Chen, B.; Gilbert, Luke A.; Cimini, Beth A.; Schnitzbauer, J.; Zhang, W.; Li, G.-W.; Park, J.; Blackburn, Elizabeth H.; Weissman, Jonathan S.; Qi, Lei S.; Huang, B. Dynamic Imaging of Genomic Loci in Living Human Cells by an Optimized CRISPR/Cas System. *Cell* **2013**, *155*, 1479-1491.

Cheng, R.; Peng, J.; Yan, Y.; Cao, P.; Wang, J.; Qiu, C.; Tang, L.; Liu, D.; Tang, L.; Jin, J.; Huang, X.; He, F.; Zhang, P. Efficient Gene Editing in Adult Mouse Livers via Adenoviral Delivery of CRISPR/Cas9. *FEBS Lett.* **2014**, *588*, 3954-3958.

- Chew, W. L.; Tabebordbar, M.; Cheng, J. K.; Mali, P.; Wu, E. Y.; Ng, A. H.; Zhu, K.; Wagers, A. J.; Church, G. M. A Multifunctional AAV-CRISPR-Cas9 and its Host Response. *Nat. Methods* **2016**, *13*, 868-874.
- Cho, S. W.; Kim, S.; Kim, Y.; Kweon, J.; Kim, H. S.; Bae, S.; Kim, J. S. Analysis of Off-Target Effects of CRISPR/Cas-Derived RNA-Guided Endonucleases and Nickases. *Genome Res.* **2014**, *24*, 132-141.
- Cho, S. W.; Kim, S.; Kim, J. M.; Kim, J. S. Targeted Genome Engineering in Human Cells with the Cas9 RNA-Guided Endonuclease. *Nat. Biotechnol.* **2013**, *31*, 230-232.
- Choi, S. O.; Kim, Y. C.; Lee, J. W.; Park, J. H.; Prausnitz, M. R.; Allen, M. G. Intracellular Protein Delivery and Gene Transfection by Electroporation using a Microneedle Electrode Array. *Small* **2012**, *8*, 1081-1091.
- Chowdhury, D.; Lieberman, J. Death by a Thousand Cuts: Granzyme Pathways of Programmed Cell Death. *Annu. Rev. Immunol.* **2008**, *26*, 389-420.
- Chung, W. J.; Oh, J. W.; Kwak, K.; Lee, B. Y.; Meyer, J.; Wang, E.; Hexemer, A.; Lee, S. W. Biomimetic Self-Templating Supramolecular Structures. *Nature* **2011**, *478*, 364-368.
- Cong, L.; Ran, F. A.; Cox, D.; Lin, S.; Barretto, R.; Habib, N.; Hsu, P. D.; Wu, X.; Jiang, W.; Marraffini, L. A.; Zhang, F. Multiplex Genome Engineering Using CRISPR/Cas Systems. *Science* **2013**, *339*, 819-823.
- Cormack, B. P.; Valdivia, R. H.; Falkow, S. FACS-Optimized Mutants of the Green Fluorescent Protein (GFP). *Gene* **1996**, *173*, 33-38.
- Cox, D. B. T.; Platt, R. J.; Zhang, F. Therapeutic Genome Editing: Prospects and Challenges. *Nat. Med.* **2015**, *21*, 121-131.
- Cronican, J. J.; Thompson, D. B.; Beier, K. T.; McNaughton, B. R.; Cepko, C. L.; Liu, D. R. Potent Delivery of Functional Proteins into Mammalian Cells In Vitro and In Vivo using a Supercharged Protein. *ACS Chem. Biol.* **2010**, *5*, 747-752.
- Culik, R. M.; Jo, H.; DeGrado, W. F.; Gai, F. Using Thioamides to Site-Specifically Interrogate the Dynamics of Hydrogen Bond Formation in β -Sheet Folding. *J. Am. Chem. Soc.* **2012**, *134*, 8026-8029.
- D'Astolfo, D. S.; Pagliero, R. J.; Pras, A.; Karthaus, W. R.; Clevers, H.; Prasad, V.; Lebbink, R. J.; Rehmann, H.; Geijsen, N. Efficient Intracellular Delivery of Native Proteins. *Cell* **2015**, *161*, 674-690.
- Daniel, M. C.; Astruc, D. Gold Nanoparticles: Assembly, Supramolecular Chemistry, Quantum-Size-Related Properties, and Applications Toward Biology, Catalysis, and Nanotechnology. *Chem. Rev.* **2004**, *104*, 293-346.

De, M.; Ghosh, P. S.; Rotello, V. M. Applications of Nanoparticles in Biology. *Adv. Mater.* **2008**, *20*, 4225-4241.

De, M.; Rana, S.; Akpinar, H.; Miranda, O. R.; Arvizo, R. R.; Bunz, U. H.; Rotello, V. M. Sensing of Proteins in Human Serum using Conjugates of Nanoparticles and Green Fluorescent Protein. *Nat. Chem.* **2009**, *1*, 461-465.

De, M.; Rana, S.; Rotello, V. M. Nickel-Ion-Mediated Control of the Stoichiometry of His-Tagged Protein/Nanoparticle Interactions. *Macromol. Biosci.* **2009**, *9*, 174-178.

Deora, A. A.; Diaz, F.; Schreiner, R.; Rodriguez-Boulan, E. Efficient Electroporation of DNA and Protein into Confluent and Differentiated Epithelial Cells in Culture. *Traffic* **2007**, *8*, 1304-1312.

Dinca, A.; Chien, W. M.; Chin, M. T. Intracellular Delivery of Proteins with Cell-Penetrating Peptides for Therapeutic Uses in Human Disease. *Int. J. Mol. Sci.* **2016**, *17*, 263.

Ding, Q.; Strong, A.; Patel, K. M.; Ng, S.-L.; Gosis, B. S.; Regan, S. N.; Rader, D. J.; Musunuru, K. Permanent Alteration of PCSK9 with in vivo CRISPR-Cas9 Genome Editing. *Circ. Res.* **2014**, *115*, 488-492.

Dingwall, C.; Laskey, R. A. Protein Import into the Cell Nucleus. *Annu. Rev. Cell Biol.* **1986**, *2*, 367-390.

Diss, M. L.; Kennan, A. J. Simultaneous Directed Assembly of Three Distinct Heterodimeric Coiled Coils. *Org. Lett.* **2008**, *10*, 3797-3800.

Dong, B.; Nakai, H.; Xiao, W. Characterization of Genome Integrity for Oversized Recombinant AAV Vector. *Mol. Ther.* **2010**, *18*, 87-92.

Doudna, J. A.; Charpentier, E. The New Frontier of Genome Engineering with CRISPR-Cas9. *Science* **2014**, *346*, 1258096.

Douglas, T.; Young, M. Viruses: Making Friends with Old Foes. *Science* **2006**, *312*, 873-875.

Drews J. Drug Discovery: A Historical Perspective. *Science* **2000**, *287*, 1960-1964.

Drews, J.; Ryser, S. Classic Drug Targets. *Nat. Biotechnol.* **1997**, *15*, 1350.

Ducker, W. A.; Senden, T. J.; Pashley, R. M. Direct Measurement of Colloidal Forces Using an Atomic Force Microscope. *Nature* **1991**, *353*, 239-241.

Eichmann, S. L.; Anekal, S. G.; Bevan, M. A. Electrostatically Confined Nanoparticle Interactions and Dynamics. *Langmuir* **2008**, *24*, 714-721.

Erazo-Oliveras, A.; Najjar, K.; Dayani, L.; Wang, T. Y.; Johnson, G. A.; Pellois, J. P. Protein Delivery into Live Cells by Incubation with an Endosomolytic Agent. *Nat. Methods*. **2014**, *11*, 861-867.

Erb, R. M.; Son, H. S.; Samanta, B.; Rotello, V. M.; Yellen, B. B. Magnetic Assembly of Colloidal Superstructures with Multipole Symmetry. *Nature* **2009**, *457*, 999-1002.

Fu, A.; Tang, R.; Hardie, J.; Farkas, M. E.; Rotello, V. M. Promises and Pitfalls of Intracellular Delivery of Proteins. *Bioconjug. Chem.* **2014**, *25*, 1602-1608.

Fu, Y.; Foden, J. A.; Khayter, C.; Maeder, M. L.; Reyon, D.; Joung, J. K.; Sander, J. D. High-Frequency Off-Target Mutagenesis Induced by CRISPR-Cas Nucleases in Human Cells. *Nat. Biotechnol.* **2013**, *31*, 822-826.

Gagnon, J. A.; Valen, E.; Thyme, S. B.; Huang, P.; Ahkmetova, L.; Pauli, A.; Montague, T. G.; Zimmerman, S.; Richter, C.; Schier, A. F. Efficient Mutagenesis by Cas9 Protein-Mediated Oligonucleotide Insertion and Large-Scale Assessment of Single-Guide RNAs. *PLoS One* **2014**, *9*, e98186.

Gasiunas, G.; Barrangou, R.; Horvath, P.; Siksnys, V. Cas9-crRNA Ribonucleoprotein Complex Mediates Specific DNA Cleavage for Adaptive Immunity in Bacteria. *Proc. Natl. Acad. Sci. U S A.* **2012**, *109*, E2579-86.

Gilleron, J.; Querbes, W.; Zeigerer, A.; Borodovsky, A.; Marsico, G.; Schubert, U.; Manygoats, K.; Seifert, S.; Andree, C.; Stöter, M.; Epstein-Barash, H.; Zhang, L.; Koteliansky, V.; Fitzgerald, K.; Fava, E.; Bickle, M.; Kalaidzidis, Y.; Akinc, A.; Maier, M.; Zerial, M. Image-Based Analysis of Lipid Nanoparticle-Mediated siRNA Delivery, Intracellular Trafficking and Endosomal Escape. *Nat. Biotechnol.* **2013**, *31*, 638-646.

Gomez-Marquez, J.; Rodríguez, P. Prothymosin Alpha is a Chromatin-Remodelling Protein in Mammalian Cells. *Biochem. J.* **1998**, *333*, 1-3.

Gonen, S.; DiMaio, F.; Gonen, T.; Baker, D. Design of Ordered Two-Dimensional Arrays Mediated by Noncovalent Protein-Protein Interfaces. *Science* **2015**, *348*, 1365-1368.

González-Toro, D. C.; Ryu, J. H.; Chacko, R. T.; Zhuang, J.; Thayumanavan, S. Concurrent Binding and Delivery of Proteins and Lipophilic Small Molecules Using Polymeric Nanogels. *J. Am. Chem. Soc.* **2012**, *134*, 6964-6967.

Gori, J. L.; Hsu, P. D.; Maeder, M. L.; Shen, S.; Welstead, G. G.; Bumcrot, D. Delivery and Specificity of CRISPR/Cas9 Genome Editing Technologies for Human Gene Therapy. *Hum. Gene Ther.* **2015**, *26*, 443-451.

Gröschel, A. H.; Walther, A.; Löblich, T. I.; Schacher, F. H.; Schmalz, H.; Müller, A. H. Guided Hierarchical Co-Assembly of Soft Patchy Nanoparticles. *Nature* **2013**, *503*, 247-251.

Gu, Z.; Biswas, A.; Zhao, M.; Tang, Y. Tailoring Nanocarriers for Intracellular Protein Delivery. *Chem. Soc. Rev.* **2011**, *40*, 3638-3655.

Hacein-Bey-Abina, S.; Garrigue, A.; Wang, G. P.; Soulier, J.; Lim, A.; Morillon, E.; Clappier, E.; Caccavelli, L.; Delabesse, E.; Beldjord, K. et al. Insertional Oncogenesis in 4 Patients After Retrovirus-Mediated Gene Therapy of SCID-X1. *J. Clin. Invest.* **2008**, *118*, 3132-3142.

Han, D.; Pal, S.; Yang, Y.; Jiang, S.; Nangreave, J.; Liu, Y.; Yan, H. DNA Gridiron Nanostructures Based on Four-Arm Junctions. *Science* **2013**, *339*, 1412-1415.

Han, X.; Liu, Z.; Jo, M. c.; Zhang, K.; Li, Y.; Zeng, Z.; Li, N.; Zu, Y.; Qin, L. CRISPR-Cas9 Delivery to Hard-to-Transfect Cells via Membrane Deformation. *Sci. Adv.* **2015**, *1*, e1500454.

Hong, R.; Emrick, T.; Rotello, V. M. Monolayer-Controlled Substrate Selectivity using Noncovalent Enzyme-Nanoparticle Conjugates. *J. Am. Chem. Soc.* **2004**, *126*, 13572-13573.

Hsu, P. D.; Lander, E. S.; Zhang, F. Development and Applications of CRISPR-Cas9 for Genome Engineering. *Cell* **2014**, *157*, 1262-1278.

<https://www.ncbi.nlm.nih.gov/books/NBK7286/>

<https://ncats.nih.gov/files/NCATS-factsheet>

Iinuma, R.; Ke, Y.; Jungmann, R.; Schlichthaerle, T.; Woehrstein, J. B.; Yin, P. Polyhedra Self-Assembled from DNA Tripods and Characterized with 3D DNA-PAINT. *Science* **2014**, *344*, 65-69.

Jamur, M. C.; Oliver, C. Permeabilization of Cell Membranes. *Methods Mol. Biol.* **2010**, *588*, 63-66.

Jiang, Y.; Tang, R.; Duncan, B.; Jiang, Z.; Yan, B.; Mout, R.; Rotello, V. M. Direct Cytosolic Delivery of siRNA Using Nanoparticle-Stabilized Nanocapsules. *Angew. Chem. Int. Ed. Engl.* **2015**, *54*, 506-510.

Jinek, M.; Chylinski, K.; Fonfara, I.; Hauer, M.; Doudna, J. A.; Charpentier, E. A. Programmable Dual-RNA-Guided DNA Endonuclease in Adaptive Bacterial Immunity. *Science* **2012**, *337*, 816-821.

Kalsin, A. M.; Fialkowski, M.; Paszewski, M.; Smoukov, S. K.; Bishop, K. J.; Grzybowski, B. A. Electrostatic Self-assembly of Binary Nanoparticle Crystals with a Diamond-Like Lattice. *Science* **2006**, *312*, 420-424.

Kanaras, A. G.; Kamounah, F. S.; Schaumburg, K.; Kiely, C. J.; Brust, M. Thioalkylated Tetraethylene Glycol: a New Ligand for Water Soluble Monolayer Protected Gold Clusters. *Chem. Commun. (Camb)* **2002**, *20*, 2294-2295.

Karsenti, E. Self-Organization in Cell Biology: A Brief History. *Nat. Rev. Mol. Cell Biol.* **2008**, *9*, 255-262.

Keber, F. C.; Loiseau, E.; Sanchez, T.; DeCamp, S. J.; Giomi, L.; Bowick, M. J.; Marchetti, M. C.; Dogic, Z.; Bausch, A. R. Topology and Dynamics of Active Nematic Vesicles. *Science* **2014**, *345*, 1135-1139.

Khalil, A. S.; Collins, J. J. Synthetic Biology: Applications Come of Age. *Nat. Rev. Genet.* **2010**, *11*, 367-379.

Kiani, S.; Chavez, A.; Tuttle, M.; Hall, R. N.; Chari, R.; Ter-Ovanesyan, D.; Qian, J.; Pruitt, B. W.; Beal, J.; Vora, S.; Buchthal, J.; Kowal, E. J.; Ebrahimkhani, M. R.; Collins, J. J.; Weiss, R.; Church, G. Cas9 gRNA Engineering for Genome Editing, Activation and Repression. *Nat. Methods* **2015**, *12*, 1051-1054.

Kim, H. W.; Jung, J.; Han, M.; Lim, S.; Tamada, K.; Hara, M.; Kawai, M.; Kim, Y.; Kuk, Y. One-Dimensional Molecular Zippers. *J. Am. Chem. Soc.* **2011**, *133*, 9236-9238.

Kim, S.; Kim, D.; Cho, S. W.; Kim, J.; Kim, J.-S. Highly Efficient RNA-Guided Genome Editing in Human Cells via Delivery of Purified Cas9 Ribonucleoproteins. *Genome Res.* **2014**, *24*, 1012-1019.

King, N. P.; Bale, J. B.; Sheffler, W.; McNamara, D. E.; Gonen, S.; Gonen, T.; Yeates, T. O.; Baker, D. Accurate Design of Co-Assembling Multi-Component Protein Nanomaterials. *Nature* **2014**, *510*, 103-108.

Kleinstiver, B. P.; Pattanayak, V.; Prew, M. S.; Tsai, S. Q.; Nguyen, N. T.; Zheng, Z.; Joung, J. K. High-Fidelity CRISPR-Cas9 Nucleases with no Detectable Genome-Wide Off-Target Effects. *Nature* **2016**, *529*, 490-495.

Komor, A. C.; Badran, A. H.; Liu, D. R. CRISPR-Based Technologies for the Manipulation of Eukaryotic Genomes. *Cell* **2017**, *168*, 20-36.

Konermann, S.; Brigham, M. D.; Trevino, A. E.; Joung, J.; Abudayyeh, O. O.; Barcena, C.; Hsu, P. D.; Habib, N.; Gootenberg, J. S.; Nishimasu, H. Nureki, O.; Zhang, F. Genome-Scale Transcriptional Activation by an Engineered CRISPR-Cas9 Complex. *Nature* **2015**, *517*, 583-588.

Koo, B. K.; Stange, D. E.; Sato, T.; Karthaus, W.; Farin, H. F.; Huch, M.; van Es, J. H.; Clevers, H. Controlled Gene Expression in Primary Lgr5 Organoid Cultures. *Nat. Methods* **2011**, *9*, 81-83.

Kostiainen, M. A.; Hiekkataipale, P.; Laiho, A.; Lemieux, V.; Seitsonen, J.; Ruokolainen, J.; Ceci, P. Electrostatic Assembly of Binary Nanoparticle Superlattices using Protein Cages. *Nat. Nanotechnol.* **2013**, *8*, 52-56.

Kushner, D. J. Self-Assembly of Biological Structures. *Bacteriol. Rev.* **1969**, *33*, 302-345.

Leader, B.; Baca, Q. J.; Golan, D. E. Protein Therapeutics: A Summary and Pharmacological Classification. *Nat. Rev. Drug. Discov.* **2008**, *7*, 21-39.

Lehn, J. M. Toward Self-Organization and Complex Matter. *Science* **2002**, *295*, 2400-2403.

Levine, P. M.; Carberry, T. P.; Holub J. M.; Kirshenbaum, K. Crafting Precise Multivalent Architectures. *Med. Chem. Commun.* **2013**, *4*, 493-509.

Li, L.; He, Z. Y.; Wei, X. W.; Gao, G. P.; Wei, Y. Q. Challenges in CRISPR/Cas9 Delivery: Potential Roles of Nonviral Vectors. *Hum. Gene Ther.* **2015**, *26*, 452-462.

Li, P.; Banjade, S.; Cheng, H. C.; Kim, S.; Chen, B.; Guo, L.; Llaguno, M.; Hollingsworth, J. V.; King, D. S.; Banani, S. F.; Russo, P. S.; Jiang, Q. X.; Nixon, B. T.; Rosen, M. K. Phase Transitions in the Assembly of Multivalent Signalling Proteins. *Nature* **2012**, *483*, 336-340.

Lieberman, J. Granzyme A Activates Another Way to Die. *Immunol. Rev.* **2010**, *235*, 93-104.

Lieberman, J. The ABCs of Granule-Mediated Cytotoxicity: New Weapons in the Arsenal. *Nat. Rev. Immunol.* **2003**, *3*, 361-370.

Liu, J.; Gaj, T.; Yang, Y.; Wang, N.; Shui, S.; Kim, S.; Kanchiswamy, C. N.; Kim, J.-S.; Barbas Iii, C. F. Efficient Delivery of Nuclease Proteins for Genome Editing in Human Stem Cells and Primary Cells. *Nat. Protoc.* **2015**, *10*, 1842-1859.

Long, C.; Amoasii, L.; Mireault, A. A.; McAnally, J. R.; Li, H.; Sanchez-Ortiz, E.; Bhattacharyya, S.; Shelton, J. M.; Bassel-Duby, R.; Olson, E. N. Postnatal Genome Editing Partially Restores Dystrophin Expression in a Mouse Model of Muscular Dystrophy. *Science* **2016**, *351*, 400-403.

Lupulescu, A. I.; Rimer, J. D. In Situ Imaging of Silicalite-1 Surface Growth Reveals the Mechanism of Crystallization. *Science* **2014**, *344*, 729-732.

Lyklema, J. Coagulation by Multivalent Counterions and the Schulze-Hardy Rule. *J. Colloid Interface Sci.* **2013**, *392*, 102-104.

Macfarlane, R. J.; Lee, B.; Jones, M. R.; Harris, N.; Schatz, G. C.; Mirkin, C. A. Nanoparticle Superlattice Engineering with DNA. *Science* **2011**, *334*, 204-208.

Mali, P.; Yang, L.; Esvelt, K. M.; Aach, J.; Guell, M.; DiCarlo, J. E.; Norville, J. E.; Church, G. M. RNA-Guided Human Genome Engineering via Cas9. *Science* **2013**, *339*, 823-826.

Marti, D. N.; Bosshard, H. R. Electrostatic Interactions in Leucine Zippers: Thermodynamic Analysis of the Contributions of Glu and His Residues and the Effect of Mutating Salt Bridges. *J. Mol. Biol.* **2003**, *330*, 621-637.

Martinvalet, D.; Dykxhoorn, D. M.; Ferrini, R.; Lieberman, J. Granzyme A Cleaves a Mitochondrial Complex I Protein to Initiate Caspase-Independent Cell Death. *Cell* **2008**, *133*, 681-692.

Mateu, M. G. Assembly, Stability and Dynamics of Virus Capsids. *Arch. Biochem. Biophys.* **2013**, *531*, 65-79.

Mitragotri, S.; Burke, P. A.; Langer, R. Overcoming the Challenges in Administering Biopharmaceuticals: Formulation and Delivery Strategies. *Nat. Rev. Drug. Discov.* **2014**, *13*, 655-672.

Mou, Y.; Yu, J. Y.; Wannier, T. M.; Guo, C. L.; Mayo, S. L. Computational Design of Co-Assembling Protein-DNA Nanowires. *Nature* **2015**, *525*, 230-233.

Mout, R. M.; Moyano, D. F.; Rana S.; Rotello, V. M. Surface Functionalization of Nanoparticles for Nanomedicine. *Chem. Soc. Rev.* **2012**, *41*, 2539-2544.

Mout, R.; Ray, M.; Tonga, G. Y.; Lee, Y.-W.; Tay, T.; Sasaki, K.; Rotello, V. M. Direct Cytosolic Delivery of CRISPR/Cas9-Ribonucleoprotein for Efficient Gene Editing. *ACS Nano*, **2017**, *11*, 2452-2458.

Mout, R.; Ray, M.; Lee, Y.W.; Scaletti, F.; Rotello, V. M. In Vivo Delivery of CRISPR/Cas9 for Therapeutic Gene Editing: Progress and Challenges. *Bioconjug. Chem.* **2017**, *28*, 880-884.

Mout, R.; Ray, M.; Tay, T.; Sasaki, K.; Tonga, G. Y.; Rotello, V. M. A General Strategy for Direct Cytoplasmic Protein Delivery. *Submitted manuscript*.

Mout, R.; Rotello, V. M. Bio and Nano Working Together: Engineering the Protein-Nanoparticle Interface. *Isr. J. Chem.* **2013**, *53*, 521-529.

Mout, R.; Tonga, G. Y.; Wang, L.-S.; Ray, M.; Roy, T.; Rotello, V. M. Programmed Self-Assembly of Hierarchical Nanostructures through Protein-Nanoparticle Co-Engineering. *ACS Nano* **2017**, *11*, 3456-3462.

Mout, R.; Tonga, G. Y.; Ray, M.; Moyano, D. F.; Xing, Y.; Rotello, V. M. Environmentally Responsive Histidine-Carboxylate Zipper Formation Between Proteins and Nanoparticles. *Nanoscale* **2014**, *6*, 8873-8877.

Nagy, A. Cre Recombinase: The Universal Reagent for Genome Tailoring. *Genesis* **2000**, *26*, 99-109.

Neefjes, J.; Jongasma, M. L.; Paul, P.; Bakke, O. Towards a Systems Understanding of MHC Class I and MHC Class II Antigen Presentation. *Nat. Rev. Immunol.* **2011**, *11*, 823-836.

Nelson, C. E.; Gersbach, C. A. Engineering Delivery Vehicles for Genome Editing. *Annu. Rev. Chem. Biomol. Eng.* **2016**, *7*, 637-662.

Nelson, C. E.; Hakim, C. H.; Ousterout, D. G.; Thakore, P. I.; Moreb, E. A.; Rivera, R. M. C.; Madhavan, S.; Pan, X.; Ran, F. A.; Yan, W. X.; Asokan, A.; Zhang, F.; Duan, D.; Gersbach, C. A. In vivo Genome Editing Improves Muscle Function in a Mouse Model of Duchenne Muscular Dystrophy. *Science* **2015**, *351*, 403-407.

Nir, E.; Kleinerhmanns, K.; de Vries, M. S. Pairing of Isolated Nucleic-Acid Bases in the Absence of the DNA Backbone. *Nature* **2000**, *408*, 949-951.

Oude Blenke, E.; Evers, M. J.; Mastrobattista, E.; van der Oost, J. CRISPR-Cas9 Gene Editing: Delivery Aspects and Therapeutic Potential. *J. Control Release* **2016**, *244*, 139-148.

Park, J. I.; Nguyen, T. D.; de Queirós Silveira, G.; Bahng, J. H.; Srivastava, S.; Zhao, G.; Sun, K.; Zhang, P.; Glotzer, S. C.; Kotov, N. A. Terminal Supraparticle Assemblies from Similarly Charged Protein Molecules and Nanoparticles. *Nat. Commun.* **2014**, *5*, 3593.

Peer, D.; Karp, J. M.; Hong, S.; Farokhzad, O. C.; Margalit, R.; Langer, R. Nanocarriers as an Emerging Platform for Cancer Therapy. *Nat. Nanotechnol.* **2007**, *2*, 751-760.

Pettersen, E. F.; Goddard, T. D.; Huang, C. C.; Couch, G. S.; Greenblatt, D. M.; Meng, E. C.; Ferrin, T. E. UCSF Chimera—a Visualization System for Exploratory Research and Analysis. *J. Comput. Chem.* **2004**, *25*, 1605-1612.

Peng, Z. G.; Hidajat, K.; Uddin, M. S. Adsorption of Bovine Serum Albumin on Nanosized Magnetic Particles. *J. Colloid. Interface Sci.* **2004**, *271*, 277-283.

Qiu, H.; Hudson, Z. M.; Winnik, M. A.; Manners, I. Multidimensional Hierarchical Self-Assembly of Amphiphilic Cylindrical Block Comicelles. *Science* **2015**, *347*, 1329-1332.

Quianzon, C. C.; Cheikh, I. History of Insulin. *J. Community Hosp. Intern. Med. Perspect.* **2012**, *2*.

Ramakrishna, S.; Kwaku Dad, A.-B.; Beloor, J.; Gopalappa, R.; Lee, S.-K.; Kim, H. Gene Disruption by Cell-Penetrating Peptide-Mediated Delivery of Cas9 Protein and Guide RNA. *Genome Res.* **2014**, *24*, 1020-1027.

Ran, F. A.; Cong, L.; Yan, W. X.; Scott, D. A.; Gootenberg, J. S.; Kriz, A. J.; Zetsche, B.; Shalem, O.; Wu, X.; Makarova, K. S.; Koonin, E. V.; Sharp, P. A.; Zhang, F. In vivo Genome Editing using *Staphylococcus Aureus* Cas9. *Nature* **2015**, *520*, 186-191.

Ran, F. A.; Hsu, P.; Wright, J.; Agarwala, V.; Scott, D. A.; Zhang, F. Genome Engineering Using the CRISPR-Cas9 System. *Nat. Protoc.* **2013**, *8*, 2281-2308.

Rana, S.; Bajaj, A.; Mout, R.; Rotello, V. M. Monolayer Coated Gold Nanoparticles for Delivery Applications. *Adv. Drug. Deliv. Rev.* **2012**, *64*, 200-216.

Rana, S.; Singla, A. K.; Bajaj, A.; Elci, S. G.; Miranda, O. R.; Mout, R.; Yan, B.; Jirik, F. R.; Rotello, V. M. Array-Based Sensing of Metastatic Cells and Tissues using Nanoparticle-Fluorescent Protein Conjugates. *ACS Nano* **2012**, *6*, 8233-8240.

Ray, M.; Lee, Y.-W.; Scaletti, F.; Yu, R.; Rotello, V. M. Intracellular Delivery of Proteins by Nanocarriers. *Nanomedicine (Lond)*. **2017**, *12*, 941-952.

Ray, M.; Tang, R.; Jiang, Z.; Rotello, V. M. Quantitative Tracking of Protein Trafficking to the Nucleus using Cytosolic Protein Delivery by Nanoparticle-Stabilized Nanocapsules. *Bioconjug. Chem.* **2015**, *26*, 1004-1007.

Restifo, N. P.; Dudley, M. E.; Rosenberg, S. A. Adoptive Immunotherapy for Cancer: Harnessing the T Cell Response. *Nat. Rev. Immunol.* **2012**, *12*, 269-281.

Rosi, N. L.; Mirkin, C. A. Nanostructures in Biodiagnostics. *Chem. Rev.* **2005**, *105*, 1547-1562.

Sadelain, M.; Papapetrou, E. P.; Bushman, F. D. Safe Harbours for the Integration of New DNA in the Human Genome. *Nat. Rev. Cancer* **2011**, *12*, 51-58.

Saha, K. Understanding Structure-Property Relationships at the Nano-Bio Interface for Delivery Applications. *Doctoral Dissertations* **2014**.

Saha, K.; Kim, S. T.; Yan, B.; Miranda, O. R.; Alfonso, F. S.; Shlosman, D.; Rotello, V. M. Surface Functionality of Nanoparticles Determines Cellular Uptake Mechanisms in Mammalian Cells. *Small* **2013**, *9*, 300-305.

Salata, O. V. Applications of Nanoparticles in Biology and Medicine. *J. Nanobiotechnology* **2004**, 2, 3.

Sandblad, L.; Busch, K. E.; Tittmann, P.; Gross, H.; Brunner, D.; Hoenger, A. The Schizosaccharomyces Pombe EB1 Homolog Mal3p Binds and Stabilizes the Microtubule Lattice Seam. *Cell* **2006**, 127, 1415-1424.

Sander, J. D.; Joung, J. K. CRISPR-Cas Systems for Editing, Regulating and Targeting Genomes. *Nat. Biotechnol.* **2014**, 32, 347-355.

Schmaltz, C.; Hardenbergh, P. H.; Wells, A.; Fisher, D. E. Regulation of Proliferation-Survival Decisions During Tumor Cell Hypoxia. *Mol. Cell Biol.* **1998**, 18, 2845-2854.

Schumann, K.; Lin, S.; Boyer, E.; Simeonov, D. R.; Subramaniam, M.; Gate, R. E.; Haliburton, G. E.; Ye, C. J.; Bluestone, J. A.; Doudna, J. A.; Marson, A. Generation of Knock-In Primary Human T Cells using Cas9 Ribonucleoproteins. *Proc. Natl. Acad. Sci. U. S. A.* **2015**, 112, 10437-10442.

Schwank, G.; Koo, B.-K.; Sasselli, V.; Dekkers, Johanna F.; Heo, I.; Demircan, T.; Sasaki, N.; Boymans, S.; Cuppen, E.; van der Ent, C. K.; Nieuwenhuis, E. E.; Beekman, J. M.; Clevers, H. Functional Repair of CFTR by CRISPR/Cas9 in Intestinal Stem Cell Organoids of Cystic Fibrosis Patients. *Cell Stem Cell* **2013**, 13, 653-658.

Scott, C.C.; Gruenberg, J. Ion Flux and the Function of Endosomes and Lysosomes: pH is Just the Start: The Flux of Ions Across Endosomal Membranes Influences Endosome Function not only Through Regulation of the Luminal pH. *Bioessays* **2011**, 33, 103-110.

Senís, E.; Fatouros, C.; Große, S.; Wiedtke, E.; Niopek, D.; Mueller, A. K.; Börner, K.; Grimm, D. CRISPR/Cas9-Mediated Genome Engineering: An Adeno-Associated Viral (AAV) Vector Toolbox. *Biotechnol. J.* **2014**, 9, 1402-1412.

Singh, G.; Chan, H.; Baskin, A.; Gelman, E.; Repnin, N.; Král, P.; Klajn, R. Self-Assembly of Magnetite Nanocubes into Helical Superstructures. *Science* **2014**, 345, 1149-1153.

Slymaker, I. M.; Gao, L.; Zetsche, B.; Scott, D. A.; Yan, W. X.; Zhang, F. Rationally Engineered Cas9 Nucleases with Improved Specificity. *Science* **2016**, 351, 84-88.

Sorkin, A.; Von Zastrow, M. Signal Transduction and Endocytosis: Close Encounters of Many Kinds. *Nat. Rev. Mol. Cell Biol.* **2002**, 3, 600-614.

Spencer, R.; Chen, K. H.; Manuel, G.; Nowick, J. S. Recipe for β -Sheets: Foldamers Containing Amyloidogenic Peptide Sequences. *Eur. J. Org. Chem.* **2013**, 3523-3528.

Stewart, M. P.; Sharei, A.; Ding, X.; Sahay, G.; Langer, R.; Jensen, K. F. In Vitro and Ex Vivo Strategies for Intracellular Delivery. *Nature* **2016**, 538, 183-192.

Sun, W.; Ji, W.; Hall, J. M.; Hu, Q.; Wang, C.; Beisel, C. L.; Gu, Z. Self-Assembled DNA Nanoclews for the Efficient Delivery of CRISPR-Cas9 for Genome Editing. *Angew. Chem. Int. Ed. Engl.* **2015**, *54*, 12029-12033.

Tabebordbar, M.; Zhu, K.; Cheng, J. K. W.; Chew, W. L.; Widrick, J. J.; Yan, W. X.; Maesner, C.; Wu, E. Y.; Xiao, R.; Ran, F. A.; Cong, L.; Zhang, F.; Vandenberghe, L. H.; Church, G. M.; Wagers, A. J. In vivo Gene Editing in Dystrophic Mouse Muscle and Muscle Stem Cells. *Science* **2016**, *351*, 407-411.

Tan, K. W.; Jung, B.; Werner, J. G.; Rhoades, E. R.; Thompson, M. O.; Wiesner, U. Transient Laser Heating Induced Hierarchical Porous Structures from Block Copolymer-Directed Self-Assembly. *Science* **2015**, *349*, 54-58.

Tang, R.; Jiang, Z.; Ray, M.; Hou, S.; Rotello, V. M. Cytosolic Delivery of Large Proteins using Nanoparticle-Stabilized Nanocapsules. *Nanoscale* **2016**, *8*, 18038-18041.

Tang, R.; Kim, C. S.; Solfiell, D. J.; Rana, S.; Mout, R.; Velázquez-Delgado, E. M.; Chompoosor, A.; Jeong, Y.; Yan, B.; Zhu, Z. J.; Kim, C.; Hardy, J. A.; Rotello, V. M. Direct Delivery of Functional Proteins and Enzymes to the Cytosol using Nanoparticle-Stabilized Nanocapsules. *ACS Nano* **2013**, *7*, 6667-6673.

Templeton, A. C.; Wuelfing, W. P.; Murray, R. W. Monolayer-Protected Cluster Molecules. *Acc. Chem. Res.* **2000**, *33*, 27-36.

Torrens, F.; Castellano, G. Protein Negative/Positively Cooperative Binding to Zwitterionic/Anionic Vesicles. *J. Cheminform.* **2010**, *2*(Suppl 1): P12.

Tsien, R. Y. The Green Fluorescent Protein. *Annu. Rev. Biochem.* **1998**, *67*, 509-544.

Van Driessche, A. E.; Benning, L. G.; Rodriguez-Blanco, J. D.; Ossorio, M.; Bots, P.; García-Ruiz, J. M. The Role and Implications of Bassanite as a Stable Precursor Phase to Gypsum Precipitation. *Science* **2012**, *336*, 69-72.

Verwey, E.J.; Overbeek, J.T.G. Theory of the Stability of Lyophobic Colloids. Elsevier, Amsterdam, **1948**.

Vick, J. E.; Johnson, E. T.; Choudhary, S.; Bloch, S. E.; Lopez-Gallego, F.; Srivastava, P.; Tikh, I. B.; Wawrzyn, G. T.; Schmidt-Dannert, C. Optimized Compatible set of BioBrick™ Vectors for Metabolic Pathway Engineering. *Appl. Microbiol. Biotechnol.* **2011**, *92*, 1275-1286.

Walsh, G. Biopharmaceutical Benchmarks 2014. *Nat. Biotechnol.* **2014**, *32*, 992-1000.

Wang, A. Y.; Peng, P. D.; Ehrhardt, A.; Storm, T. A.; Kay, M. A. Comparison of Adenoviral and Adeno-Associated Viral Vectors for Pancreatic Gene Delivery in vivo. *Hum. Gene Ther.* **2004**, *15*, 405-413.

Wang, F.; Sampogna, R. V.; Ware, B. R. pH Dependence of Actin Self-Assembly. *Biophys. J.* **1989**, *55*, 293-298.

Waters, M. L. Aromatic Interactions in Peptides: Impact on Structure and Function. *Biopolymers* **2004**, *76*, 435-445.

Weaver, R. F. *Molecular Biology*, 5th ed; McGraw-Hill, **2011**.

Whitesides, G. M.; Grzybowski, B. Self-Assembly at all Scales. *Science* **2002**, *295*, 2418-2421.

Wiskur, S. L.; Lavigne, J. J.; Metzger, A.; Tobey, S. L.; Lynch, V.; Anslyn, E. V. Thermodynamic Analysis of Receptors Based on Guanidinium/boronic Acid Groups for the Complexation of Carboxylates, Alpha-Hydroxycarboxylates, and Diols: Driving Force for Binding and Cooperativity. *Chemistry* **2004**, *10*, 3792-804.

Wu, Z.; Yang, H.; Colosi, P. Effect of Genome Size on AAV Vector Packaging. *Mol. Ther.* **2010**, *18*, 80-86.

Xue, W.; Chen, S.; Yin, H.; Tammela, T.; Papagiannakopoulos, T.; Joshi, N. S.; Cai, W.; Yang, G.; Bronson, R.; Crowley, D. G. Zhang, F.; Anderson, D. G.; Sharp, P. A.; Jacks, T. CRISPR-Mediated Direct Mutation of Cancer Genes in the Mouse Liver. *Nature* **2014**, *514*, 380-384.

Yang, X. C.; Samanta, B.; Agasti, S. S.; Jeong, Y.; Zhu, Z. J.; Rana, S.; Miranda, O. R.; Rotello, V. M. Drug Delivery Using Nanoparticle-Stabilized Nanocapsules. *Angew. Chem. Int. Ed.* **2011**, *50*, 477-481.

Yin, H.; Xue, W.; Chen, S.; Bogorad, R. L.; Benedetti, E.; Grompe, M.; Kotliansky, V.; Sharp, P. A.; Jacks, T.; Anderson, D. G. Genome Editing with Cas9 in Adult Mice Corrects a Disease Mutation and Phenotype. *Nat. Biotechnol.* **2014**, *32*, 551-553.

You, C. C.; De, M.; Han, G.; Rotello, V. M. Tunable Inhibition and Denaturation of Alpha-Chymotrypsin with Amino Acid-Functionalized Gold Nanoparticles. *J. Am. Chem. Soc.* **2005**, *127*, 12873-12881.

Zincarelli, C.; Soltys, S.; Rengo, G.; Rabinowitz, J. E. Analysis of AAV Serotypes 1-9 Mediated Gene Expression and Tropism in Mice After Systemic Injection. *Mol. Ther.* **2008**, *16*, 1073-1080.

Zuris, J. A.; Thompson, D. B.; Shu, Y.; Guilinger, J. P.; Bessen, J. L.; Hu, J. H.; Maeder, M. L.; Joung, J. K.; Chen, Z.-Y.; Liu, D. R. Cationic Lipid-Mediated Delivery of Proteins Enables Efficient Protein-Based Genome Editing In Vitro and In Vivo. *Nat. Biotechnol.* **2015**, *33*, 73-80.